Vibration of Axially Moving Small-Size Beams Under Non-Uniform Electrostatic Excitation

BY

MUSTAFA TAHIR AL SHAQAQ

A Thesis Presented to the

DEANSHIP OF GRADUATE STUDIES

KING FAHD UNIVERSITY OF PETROLEUM & MINERALS

DHAHRAN, SAUDI ARABIA

In Partial Fulfillment of the

Requirements for the Degree of

MASTER OF SCIENCE

In

MECHANICAL ENGINEERING

May 2018

KING FAHD UNIVERSITY OF PETROLEUM AND MINERALS

DHAHRAN-31261, SAUDI ARABIA

DEANSHIP OF GRADUATE STUDIES

This thesis, written by **MUSTAFA TAHIR ALSHAQAQ** under the direction of his thesis advisor and approved by his thesis committee, has been presented and accepted by the dean of Graduate Studies, in partial fulfillment of the requirements for the degree of **MASTER OF SCIENCE IN MECHANICAL ENGINEERING**

Dr. Zuhair Gasem
Department Chairman

Dr. Muhammad Hawwa
(Advisor)

Dr. Salam A. Zummo
Dean of Graduate Studies

Dr. Jafar Albinmousa
(Member)

25/12/13
Date

Dr. Fadi Al-Badour
(Member)

To my family

Acknowledgements

I would like to thank King Fahd University of Petroleum & Minerals for giving me the opportunity to pursue my master degree. I would like to express sincere gratitude to my advisor Dr. Muhammad Hawwa for the continuous support of my research, for his patience, motivation, enthusiasm, and immense knowledge. Much of my achievements would not have been possible without him and I am deeply grateful for his dedication in my success.

Secondly, I would like to thank my thesis committee: Dr. Jafar Albinmousa and Dr. Fadi Al-Badour, for their genuine comments and advice on my research.

None of this would have been possible without the love and patience of my family. My parents to whom this thesis is dedicated to, have been a constant source of love, concern, support and strength at all times.

Finally, I would like to thank my wife, Kawthar, for her support, encouragement and quite patience. I am truly thankful for having you in my life.

Table of Contents

List of Tables

List of Figures

List of Abbreviations

α	Stretching parameter
β	Fringing field parameter
$\hat{v}$	Dimensionless axial speed of the micro-beam
Ω	Excitation frequency of the applied AC voltage
ϕ	mode shape of the micro-beam
ε	Axial strain
A	Cross sectional area of the micro-beam
b	width of the micro-beam
c	Viscous damping
E	Modulus of elasticity of the micro-beam

g	Gap distance
g_1	Left gap width
g_2	Right gap width
h	Thickness of the micro-beam
I	Mass moment of inertia of the micro-beam
L	Length of the micro-beam
l	Material length scale parameter
m	Slope of the non-uniform electrostatic surface
P	Applied tension
q	Time function for transverse vibration
T	Kinetic energy
U	Strain energy
v	Axial velocity of the micro-beam
V_{AC}	Amplitude of the applied AC voltage
V_{DC}	Applied DC voltage

w Transverse vibration

Abstract

Full Name	: Mustafa Tahir Al Shaqaq
Thesis Tile	: Vibration of Axially Moving Small-Size Beams Under Non-Uniform Electrostatic force
Major Field	: Mechanical Engineering
Date of Degree	: May 2018

This thesis studies the vibration of an axially moving micro-beam over varying electrostatic gaps based on the modified couple-stress theory. The varying electrostatic gaps considered in this study include: linearly increasing electrostatic gap model and linearly decreasing electrostatic gap model. The micro-beam is moving axially over two simple supports. The primary objective of this work is to investigate the effect of the varying electrostatic gap on the vibration of the micro-beam and to examine the effect of different parameters on the dynamic behavior of the system. These parameters include axial speed, applied tension, length scale, fringing field parameter, and quality factor. The Galerkin method with a first mode-shape function of simply supported beams is utilized to develop

a mathematical model that describes the static and dynamic behaviors of the axially moving micro-beam.

Numerical solutions of the developed model are obtained using a fourth-order Runge-Kutta algorithm in the commercial software MATLAB. The natural frequencies are calculated, and the results are compared with those for stationary beam under classical beam theory. Results showed that when the small size effect is considered the natural frequencies became higher than those in the classical beam theory.

Frequency response curves are obtained to study the forced vibration of the axially moving micro-beam over a linearly varying electrostatic gap. When the micro-beam is axially moving numerical solutions showed, in the case of linearly increasing electrostatic gap, that the increase of the angle of the fixed electrode increased the maximum deflection in the frequency response curves. Also, in the case of a linearly decreasing electrostatic gap, the increase in the angle decreased the maximum deflection. However, when the micro-beam is stationary, the effect of increasing or decreasing the angle is negligible.

ملخص الرسالة

الاسم الكامل: مصطفى طاهر محمد الشقاق

عنوان الرسالة: اهتزاز ذراع صغير متحرك افقيا تحت تأثير قهوة كهروستاتيكية غير منتظمة

التخصص: الهندسة الميكانيكية

تاريخ الدرجة العلمية: مايو 2018

تقدم هذه الرسالة دراسة عن اهتزاز ذراع صغيرة متحرك أفقيا على سطح كهروستاتيكي غير منتظم يعتمد على نظرية الإجهاد الزوجي المعدلة. تشمل السطوح الكهروستاتيكية غير المنتظمة التي تم دراستها في هذه الدراسة: السطوح المتباعدة ، والسطوح المتقاربة ، والسطوح المتباينة المتقاربة ، والسطوح المتباينة المتقاربة. يعتبر الذراع الدقيق بمثابة ذراع مدعوم ببساطة يسير أفقيا. الهدف الرئيسي من هذا العمل هو دراسة تأثير السطح الكهروستاتي غير الموحد على اهتزاز الذراع والتحقيق في تأثير عدد من العوامل المختلفة على الاستجابة الديناميكية للنظام. تتضمن هذه العوامل ، السرعة الأفقية ، الشد على الذراع ، مقياس الطول ، معامل حقل التهيج ، وعامل الجودة. تم استخدام طريقة قالركين مع شكل أول لاهتزاز الذراع الدقيق المرتكز على دعامات بسيطة كدوال أساسية لتحقيق نموذج رياضي يصف السلوك الساكن والديناميكي للذراع الدقيق المتحرك أفقيا.

يتم الحصول على الحلول العددية للنموذج المطور باستخدام خوارزمية رنج-كتا من المرتبة الرابعة تحت بيئة ماتلاب. تم حساب الترددات الأساسية وتم مقارنة النتائج مع تلك للذراع الدقيق الثابت تحت نظرية العامود الكلاسيكية.

تم ايجاد منحنيات التردد الزاوي لدراسة الاهتزاز القسري للذراع الدقيق المتحرك أفقيا تحت تأثير القوة الالكتروستاتيكية. أظهرت الحلول العددية أن منحدر السطح الكهروستاتيكي له تأثير تليين في منحنى الاستجابة الترددية. أيضا ، في حالة وجود سطح إلكتروستاتي متباعد ، فإن الزيادة في السرعة الأفقية لها تأثير التخميد على الانحراف الأقصى للذراع الدقيق. ومع ذلك ، فإن هذه الزيادة في السرعة الأفقية لها تأثير معاكس في حالة سطح متقارب ، بحيث يؤدي زيادة السرعة إلى زيادة انحراف أقصى للذراع

Chapter 1

Introduction

1.1 Motivation

With the emerging technologies of the internet of things, smart consumer electronics, and smart cities, the demand for MEMS / NEMS devises is increasing [1–4]. Therefore, high rate production of these small size devices is needed. Roll-based manufacturing techniques have been over years the method of choice for boosting production rates [5]. Under roll-based processing, components move axially while being exposed to mechanical, electrical, magnetic, optical, chemical and thermal effects [6]. Due to this, researchers have recently started to study vibrations of axially moving micro-beams as well as axially moving nano-beams, which consti-

tute the basic building blocks of MEMS / NEMS structures.

The need for accurate simulation tools and models has been recognized by many researchers and engineers in the micro/nano electromechanical systems community. Many challenges face MEMS researchers and engineers when trying to model and simulate the mechanical behavior of MEMS. These challenges can be divided into three main groups: nonlinearities, small-scale phenomena, physical field coupling.

Nonlinearities are present in the macro-scale; however, their presence on the micro-scale is more significant and dominant. Therefore, overlooking these nonlinearities can lead to inaccurate predictions of the mechanical behavior of NEMS. Sources of nonlinearities in NEMS include forcing, damping, and stiffness. Nonlinearities introduced by force can be found in actuation and detection mechanisms. For instance, the parallel-plate electrostatic force is nonlinear by nature – the electrostatic force is a function of the gap width squared between the moving and fixed electrodes. Other nonlinear forces include callipary forces due to humidity and van-der Waals forces due to the proximity of two microstructures.

There are several examples of nonlinearites coming from damping mechanisms. The most common one is squeeze-film damping, which is a function of the gap cubed between two adjacent surfaces. Its influence is evident in large surface area between two close surfaces.

When small-size structures are actuated, they undergo a large deflection in comparison with the other dimensions of the structure. This relatively large deflection amplifies geometric nonlinearities of the structure [7, 8]. In macro-structure, we can apply linear theory because the deflection is small as compared with the other dimensions of the structure. However, in micro/nano structures, the deflection is relatively large and geometric nonlinearities such as mid-plane stretching might be induced which results in significant change in its stiffness and dynamical behavior [9].

Focusing on the nonlinearities due to forcing; more specifically the electrostatic force in the parallel-plate actuators, and since the forcing term depends on the gap width squared – We need to investigate what would happen to the dynamic behavior of micro/nano structures under electrostatic force when the fixed electrode is not uniform. This non-uniformity might be intentionally induced to achieve

certain dynamical behaviors, or to account for the difficulty in accurately manufacture parallel-plate actuators.

1.2 Small-size Beams

Many experiments have shown that classical continuum theory failed in accurately predicting the mechanical behavior of small size structures [10–13]. In order to accurately analyze the dynamical behavior of these small-size structures, size-dependent continuum theories should be utilized. These theories model small-size structures with greater accuracy because they include size-dependent parameters. There are different size-dependent mathematical models for small-size beams. These models include: modified couple stress theory [14], non-local elasticity theory [15] ,and strain gradient elasticity theory [16].

Some researchers in 1960s introduced the couple-stress elastic theory [17, 18] In the constitutive equation of this theory, some higher-order material length scale parameters were introduced in addition to the two classical lame constants. Yang et al. [14] debated that there is another equilibrium equation that should be considered in addition to the classical equilibrium equations of forces and moments of forces. This new equation is the equilibrium of moments of couples. They showed

that the new equilibrium relations stated that the couple stress tensor must be a symmetric tensor. Based on this result, a modified couple-stress theory was developed. In this new modified couple-stress framework, only one material length scale parameter is required.

The other theory is called the nonlocal elasticity theory which was established in 1972 by Eringen and Edelen [15]. Unlike the classical theory, which states that the stress at a point is a function of the strain at that point, nonlocal elasticity theory states that the stress at a point is a function of strains of all points in the continuum. The original theory is defined as an integral nonlocal model which is difficult to solve mathematically. To simplify this integral model, a certain approximation is made [16], and the new model is then defined as a strain gradient. The strain gradient model regards the stress at a point as a function of the strain and strain gradients at that particular point.

1.3 Thesis Objectives

The followings are the main objectives of this thesis:

1. To calculate the natural frequencies of the simply supported axially moving micro-beam and to study the effect of system's parameters like the length

scale, tension, stretching parameter, and critical velocity on the obtained natural frequencies.

2. To investigate the free response of the system. This includes studying the effect of the parameters mentioned above on the free vibration.

3. To study the forced vibration due to applied voltages. This is by determining the pull-in voltage and by examining the effect of the fringing field parameter along with system's parameters on the forced responses.

4. To investigate the forced response of the system for different cases where the electrostatic gap is varying linearly. The varying electrostatic gaps are quantified by the angle formed between a horizontal line parallel to the moving beam.

5. To examine frequency response curves and to point out the non-linearity induced due to each parameter including the fixed electrode's slope.

1.4 Thesis Overview

In Chapter 2 after the introduction, we will present some literature review on the area of small size beams and axially moving beams, and explain our contribution to this field. In Chapter 3, the mathematical model of axially moving micro-beam

used in this thesis will be developed based on Euler-Bernoulli beam theory. In Chapter 4, we will examine the free vibration of the axially moving micro-beam in terms of natural frequencies and critical velocities. In Chapter 5, we will discuss forced vibration of axially moving micro-beam under electrostatic force. We will consider three cases for the electrostatic gap. The first case discusses a constant electrostatic gap, and Chapter 6 discusses the other two different non-uniform electrostatic gaps: linearly increasing and linearly decreasing electrostatic gaps. The results will be given in the form of frequency response curves and phase portrait.

Chapter 2

Literature Review

In this chapter, we will make a review of the work done in the area of nonlinear dynamics of small-size beams. Section 2.1 covers the work done to study the dynamic characteristics and the vibration of beams on the basis of the modified couple-stress theory and nonlocal elasticity theory. Section 2.2 includes studies on the vibration of axially moving macro-beams. More studies on the vibration of axially moving micro-beams and nano-beams are presented in section 2.3 and section 2.4, respectively. Finally, section 2.5 explains the contribution of this thesis in the field.

2.1 Small Size Beams

Park and Gao [19] studied a Bernoulli-Euler cantilever beam under modified couple stress theory consideration. They found that the rigidity of the cantilever beam under small size effect was larger than that predicted by the classical beam model. When the beam thickness was below 10 µm, there was a significant difference of the beam deflection between the two models; the size-dependent model always showed a smaller beam deflection. However, as the beam thickness increased, that difference in the beam deflection diminished. These findings agreed with work observed in experiments [20].

Miandoab et al. [21] examined the static pull-in voltages and natural frequencies for a polysilicon nano-beam on the basis of both modified couple-stress and Eringen's nonlocal elasticity theories. They concluded that the results obtained from the modified couple-stress theory matched experimental results better than the results obtained from Eringen's nonlocal elasticity and classical theories.

Rahaeifard et al. [22] studied the size-dependent dynamic behavior of micro-cantilevers under suddenly applied DC voltage based on the modified couple stress theory. They found that the modified couple stress theory predicted the size-

dependent dynamic behavior of micro-beams unlike the classical theory, which did not account for the small size of micro-beams. In agreement with [19] they showed that when the thickness of the beam was minimal, in order of its material length scale, the difference between the results given in classical theory and the results predicted by the modified couple stress theory was considerable. However, when the thickness increased, the results given by the classical theory and the modified couple stress theory were close to each other. Furthermore, Rahaeifard et al. [23] investigated the static deflection and pull-in of micro-bridges based on the modified couple stress theory to predict the size effects for structures in the micron scale. The results showed that when the beam thickness was small, in order of its internal material length scale, there was a significant difference between the results given by the modified couple stress theory and the classical theory.

Mojahedi [24] studied the non-linear vibration of clamped-clamped micro-beam under an electrostatic force based on Euler-Bernoulli and Timoshenko beams theory. He considered the modified couple stress theory to take care of the beam's small size. He studied the effect of implementing the size-dependent theory on the amplitude frequency response curve. He concluded that considering the small size effect had a decreasing effect on the amplitude of the nonlinear vibration as

well as strengthening the linear frequency response curve, by increasing the length scale parameter the frequency response curve exhibited linear behavior.

Rokni et al. [25] investigated the effect of the material length scale parameter on the static pull-in behavior in electrostatic micro-actuators based on the modified couple stress theory. They found that micro-cantilever beams were more sensitive to the size effect than clamped-clamped micro-beams. Furthermore, they found that the material length scale parameter for silicon and polysilicon was in the order of magnitude of 10^{-1} µm.

Asghari et al. [26] formulated a functionally graded Timoshenko beam on the basis of the modified couple stress theory. They investigated the static and free vibration of a functionally graded cantilever and functionally graded simply supported beams. They found that beams modeled based on the modified couple stress theory had more stiffness than classically modeled beams. Moreover, for small beam thickness, the difference between the results obtained from the modified couple stress theory and the classical theory was significant.

Chen and Meguid [27] studied the non-linear vibration of a clamped-clamped

micro-beam under electrostatic force at different values of DC and AC voltages. They designed a chart in terms of DC and AC voltages that showed whether the resulting frequency response curve exhibited linear, hardening or softening effect. Also, they examined the effect of the fringing field parameter and concluded that there was insignificant effects on the frequency response curves when the fringing field parameter was considered.

Li [28] investigated the vibration characteristics of a micro/nanoscale beam within the framework of the strain gradient nonlocal theory. The nonlocal elastic theory states that the stress at a point is a function of the strain of all points in the continuum. This is called the integral nonlocal elasticity. However, simplifications were made to this original theory to convert it into strain gradient theory which states that the stress at a point is a function of the strain and strain gradients in that particular point. This simplification agrees well with the molecular dynamic simulation, and therefore many researchers adopted the strain gradient nonlocal elasticity theory in their work. They considered different boundary conditions, simply supported, fully clamped, flexible fixed ends and cantilever micro-nano beams. Their work showed that as the small-size parameter increased, the natural frequencies of micro-nano scale beams decreased. Also, as the tension increased,

the natural frequency increased. Furthermore, when comparing the first natural frequency obtained from the classical theory, nonlocal strain gradient theory and molecular dynamic simulation, considering the small-size parameter made the natural frequency higher than that in classical theory and close to molecular dynamics simulation.

Akgoz and Civalek [29] studied the free transverse vibration of axially functionally tapered graded micro-beams on the basis of modified couple stress theory. They examined the effect of material length scale, taper ratio for the width and taper ratio for the height on the natural frequencies. They concluded that natural frequencies obtained within modified couple stress theory were higher than those obtained from classical theory. Also, the increase in the taper ratio for the height and the taper ratio for the width increased the natural frequencies.

Ouakad et al. [30] considered a multilayer actuator. They compared a single micro-beam actuator with a double micro-beam actuator in terms of their static deflection and pull-in voltage. They found that the maximum deflection of the upper beam of the double micro-beam actuator was higher than a single micro-beam actuator. Also, the pull-in voltage was much larger for double micro-beam

actuators than that in single micro-beam actuators.

Reddy [31] studied the bending, buckling, and vibration of nano-beams based on nonlocal differential elasticity theory. He considered Euler-Bernoulli, Timoshenko, Reddy and Levinson beam theories in modeling nano-beams. After incorporating the nonlocal elasticity theory in the four models, he compared these models in terms of the natural frequencies. Also, he concluded that the appearance of the nonlocal effect increased the deflections; however, it decreased the natural frequencies and buckling loads.

Li et al. [32] investigated the nonlocal transverse vibration of nano-beams with a variable axial load based on nonlocal elasticity theory. They concluded that nonlocal nanoscale parameter and axial tension increased the natural frequencies. While the compression load decreased the natural frequencies.

Akgoz and Civalek [33] studied the free vibration of a single-layer graphene sheet within the framework of modified couple stress theory. This graphene sheet is embedded in an elastic matrix. They modeled the graphene sheet using KTPT[1]. They found that the increase in the length scale parameter increased the natural

[1]Kirchhoff thin plate the

frequencies. Moreover, this size-dependency effect was significant when the length and width of SLGS[2] were small. Also, the small-scale effect was considerable for higher modes.

Liu et al. [34] studied bending, buckling and vibration of graphene nanosheets within the context of nonlocal elasticity theory. They modeled graphene sheets as plate using KTPT. They found that the new model they developed gave larger deflection, lower frequencies, amplitude, and buckling load when compared with the classical model.

Naghinejad et al. [35] examined the free vibration of nano-beams on the basis of nonlocal integral elasticity theory. They developed a nonlocal finite element method to study the free vibration of nano-beams. They concluded that the natural frequencies were affected by the length to height ratio. Furthermore, the natural frequencies for clamped boundary condition were larger when compared with those for simply supported and cantilever boundary conditions.

Mobki et al. [36] investigated the nonlinear vibration of nano-beams under MCST[3].

[2]Single-layered graphene sheet
[3]Modified couple stress theory

They found that ignoring the size-dependency would result in an order of magnitude error in static pull-in voltages, i.e., as the length scale parameter increased the pull-in voltage increased.

Bagdatli [37] studied nonlinear transverse vibration of nano-beams under axial tension based on nonlocal elasticity theory. He found that the increase in the axial tension caused the natural frequencies to increase. Also, in frequency response curves, axial tension and stretching parameter of neutral axis induced hardening non-linearity type.

Kivi et al. [38] performed a bifurcation analysis of nano-beams under an electrostatic excitation on the basis of MCST. They concluded that when modified couple stress theory was considered the pull-in voltage increased.

2.2 Axially Moving Beams

In 1990s, Wicker and Mote [39] studied the classical vibration of axially moving continua. First, they modeled roll-to-roll webs as axially moving strings, and then as axially moving beams. They developed the equations of motion under the framework of the linear theory. They found that linear analyses cannot accurately

predict the response for high-speed regime.

Wickert [40] studied the free non-linear vibration of an axially moving, elastic, tensioned beam over sub- and supercritical transport speed ranges. He investigated the longitudinal and transverse vibrations of a beam moving at constant axial speed. He derived two coupled, non-linear differential equations that describe the beam vibration along the longitudinal and transverse directions. He also simplified the transverse equation of motion by suppressing the appearance of the longitudinal displacement in the transverse equation. This is done by approximating the dynamic tension component as a function of time alone. The simplification is based on results from experimental work which showed that longitudinal disturbances propagate significantly faster than transverse ones [41].

2.3 Axially Moving Micro-Beams

Marynowski [42] studied the free vibration of an axially moving micro-scale panel on the basis of modified couple stress theory. He found that the dynamic behavior of the panel in the over critical range of transport speed is mostly affected by the

time histories of lowest frequencies of free flexural vibrations.

Dehrouyeh-Semnani et al. [43] studied the dynamic characteristics of axially moving micro-beam considering the size-dependency based on modified couple stress theory. They investigated the effect of the axial speed on the fundamental frequencies. They found that the critical speed, speed at which instability occurs, and the fundamental frequencies of the micro-beam both increased with the increase of the small size parameter.

All of the aforementioned authors studied the free vibration of micro-beams under constant temperature field. It is known that the change in temperature has significant impact on the bending of beams. Subsequently, vibration characteristics and dynamics of the beam change.

Abouelregal et al. [44] investigated the vibration of a thermoelastic axially moving microbeam under harmonic transverse excitation and harmonic pulse heating. They examined the effect of pulse-width of thermal vibration, axial speed, and harmonic excitation on the transverse vibration, temperature, displacement, and bending moment of the micro-beam. They concluded that, the effect of axial ve-

locity was significant on the amplitude of transverse vibration, displacement and bending moments. However, the effect of axial velocity on the temperature was little pronounced.

2.4 Axially Moving Nano-Beams

Lim et al. [45] studied the free transverse vibration of axially moving nano-beams based on nonlocal elasticity theory. They investigated the effect of nonlocal nanoscale parameter, dimensionless axial velocity and the applied tension on the natural frequencies of nano-beams. They found that each of the aforementioned parameters had significant effects on the dynamic behavior of nano-beams. The increase in the nanoscale parameter increased the stiffness of nano-beams, hence, natural frequencies were increased.

Li et al. [46] investigated the effect of thermal fields on the natural frequencies and critical velocities of an axially moving nano-beam based on nonlocal elasticity theory. They considered nano-beams with simply-supported, clamped, and cantilevered boundary conditions. They concluded that the nanoscale parameter had a significant effect on the dynamic behavior of the nano-beam. Also, the effect of the thermal field appeared to be weak and showed that at low temperature field

the increase of temperature difference caused the natural frequency to increase, while at high temperature fields, the temperature difference caused the natural frequency to decrease.

Li et al. [46] studied the dynamical characteristics of visco-elastic axially accelerating nano-beams on the basis of modified nonlocal theory. They showed that the nanoscale parameter, small visco-elastic damping, and the time-dependent velocity all had significant effect on the unstable zone of the nano-beam.

Liu et al. [47] studied the transverse vibration and stability of axially moving nano-plates based on nonlocal elasticity theory. They investigated the effects of axial speed, nanoscale parameter and boundary conditions using both the complex mode and Galerkin methods. They found that for moving simply supported nano-plates the natural frequencies decreased with the increase of the nanoscale parameter and axial speed in the sub-critical regions, but for fully a clamped case, the natural frequencies decreased with the increase in the nanoscale parameter only when the axial speed exceeded a specific value. Also, the critical speed decreased with the increase of the nanoscale parameter and therefore decreased the sub-critical regions. They reported that the sub-critical regions for fully clamped

nano-plates were larger than those of simply supported.

Li [27] investigated the vibration of axially moving piezoelectric nano-beams with thermo-electro-mechanical coupling within the framework of nonlocal elasticity theory. He studied the natural frequencies for simply supported and fully clamped nano-beams. He concluded that the natural frequency decreased with the increase of the applied positive external voltage, axial compressive force and change of temperature.

Liu et al. [48] studied the dynamical response and stability of axially moving nano-beams with time-dependent velocity based on the nonlocal stress gradient theory. They concluded that natural frequencies of nano-beams decreased with stronger nonlocal effects.

Mukhtari et al. [49] investigated the vibration response of axially moving nano-beams under thermal loads within the framework of modified coupled stress theory. They analyzed the vibration of nano-beams using a wavelet-based spectral method. They studied the effect of axial velocity, tensile force and thermal loads on the vibration and wave characteristics.

Guo et al. [50] investigated the free vibration characteristics analyses of axially moving and rotating nano-beams based on nonlocal strain gradient theory. They found that the natural frequency of axially moving nano-beams decreased with the increase of the axial velocity. However, the natural frequencies of rotating nano-beams are divided into forward and backward frequencies. As the rotating velocity increased, the forward frequency increased, while the backward frequency decreased. Also, the nonlocal parameter decreased natural frequencies of nano-beams, while the strain gradient parameter decreased the natural frequencies.

Razae et al. [51] investigated the nonlocal small-scale effects on the vibration and stability of a nano-beam with a time-dependent axial velocity. They analyzed the system using the multiple scales method. They concluded that instability occurs when the frequency of velocity fluctuation is close to twice that of any natural frequency of nano-beams.

Kiani [52] investigated the longitudinal, transverse and torsional vibrations of axially moving single-walled carbon nanotubes within the framework of nonlocal elasticity theory. He studied the effect of the axial velocity, small-size parame-

ter on the stability and dynamic behavior on the system. He concluded that the presence of the small-size parameter made the occurrence of divergence and flutter instabilities took place at lower values of axial speed. Kiani [53] also examined the longitudinal and transverse vibrations and stabilities of functionally graded nanobeam based on nonlocal elasticity theory. His results showed that the variation of small-size, power-law index and velocity of nano-beam have significantly affected the natural frequencies of the nano-beam. Furthermore, the threshold velocity of divergence and flutter instabilities was reduced as the small-size parameter increased.

Guo et al. [54] studied the torsional vibration of axially moving carbon nanotube based on nonlocal strain gradient theory. They included the velocity gradient effect in the model to account for the small-scale size of the nanotube. They investigated the effect of axial velocity, two small-scale parameters and velocity gradient parameter on the torsional frequencies of the nanotube. Their results showed that the increase in the strain gradient parameter strengthened the stiffness while the nonlocal parameter weakened the stiffness of the nanotube. Furthermore, they concluded that when the strain gradient effect was larger than nonlocal effect, the torsional frequencies obtained were greater than those predicted by the clas-

sical theory. When the strain gradient effect was smaller than nonlocal effect, the torsional frequencies were lower than those obtained by the classical theory. And when the effect of both nonlocal and strain gradient were equal, the torsional frequencies were the same as those predicted by the classical theory. The increase in axial velocity resulted in a decrease in torsional frequencies and the critical velocity increased with the increase of the strain gradient parameter and decreased with the increase of nonlocal parameter.

Other than axially moving nano-beams, Ilkhani et al. [55] studied the transverse vibration of rotating nano/micro-beams on the basis of the modified couple-stress theory. They investigated the effect of angular velocity of the beam, axial load, and the small scale parameter on the dynamic characteristics of the beam. They found that as the rotation of the beam increased, natural frequencies divaricated into forward and backward whirls. As the angular velocity increased, the forward frequencies increased while the backward frequencies decreased. The compressive load tended to decrease both the backward and the forward natural frequencies. Moreover, the small scale parameters increased both the forward and backward natural frequencies.

Shen et al. [56] studied the vibration of axially moving silicon nano-beams considering nonlocal elasticity and surface energy. Numerical results showed that the increase in axial motion decreased the natural frequencies.

2.5 Contribution

In all of the previously covered literature, one can conclude that free vibrating axially moving small-size beams were given most consideration. Comparatively speaking, none was published so far on forced vibration analysis of axially moving small-size beams. This thesis endeavor to shed light on the influence of non-uniform electrostatic force on vibration characteristics of axially moving micro-beams. For this purpose, vibrations of an axially moving micro-beam, which extends between two sets of guiding rolls and is attracted to a stationary electrode, is considered.

Chapter 3

Analytical Model

In this chapter, we derive the equation of motion for an axially moving micro-beam using Hamilton's principle. Also, we utilize Galerkin methods to solve the equation of motion.

3.1 Mathematical Modeling of Simply Supported Micro-Beam

Using Cartesian frame of reference $(x - z)$, Figure 3.1 shows a micro-beam travelling with a constant velocity v in the x direction. This beam has a flexural rigidity of EI and axial stiffness of EA where E is Young's modulus, A is the

cross-sectional area, and I is the second area moment of inertia. This micro-beam is assumed as simply supported at both ends. The longitudinal displacement of the micro-beam is given as $u(x,t)$ and transverse displacement is given as $w(x,t)$. The model is simplified such that [40] the beam is modeled using Euler-Bernoulli theory in which rotary inertia and shear deformation are neglected, the axial stiffness is sufficiently large in which the longitudinal deformation resulting from the pretension is negligible, cross-sectional area is considered constant during vibration, the longitudinal displacement is sufficiently small so that the non-linear strain derived from u is negligible and the small-size effect is captured using the modified couple stress theory [14].

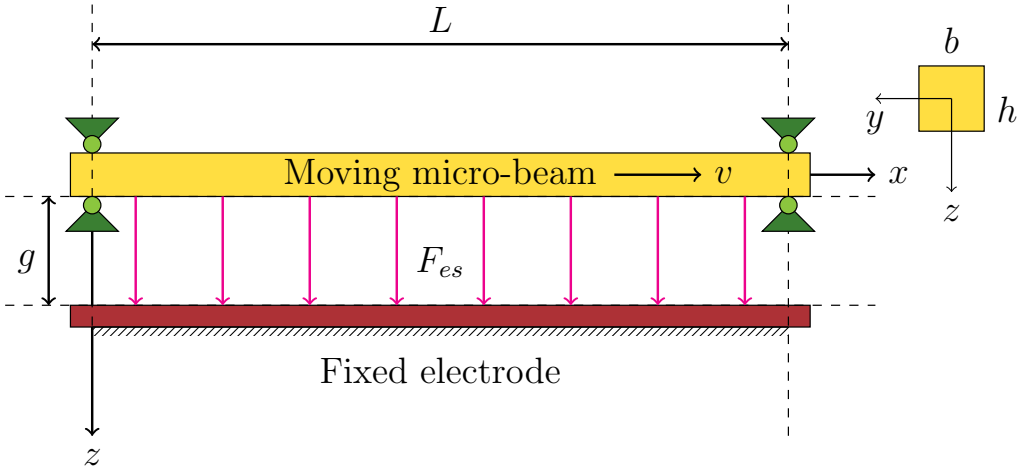

Figure 3.1 Simply supported axially moving micro-beam under an electrostatic force

The boundary conditions are

$$u(0,t) = u(L,t) = 0 \tag{3.1}$$

$$w(0,t) = w(L,t) = \frac{\partial w^2}{dx^2}(0,t) = \frac{\partial w^2}{dx^2}(L,t) = 0 \tag{3.2}$$

3.2 Strain

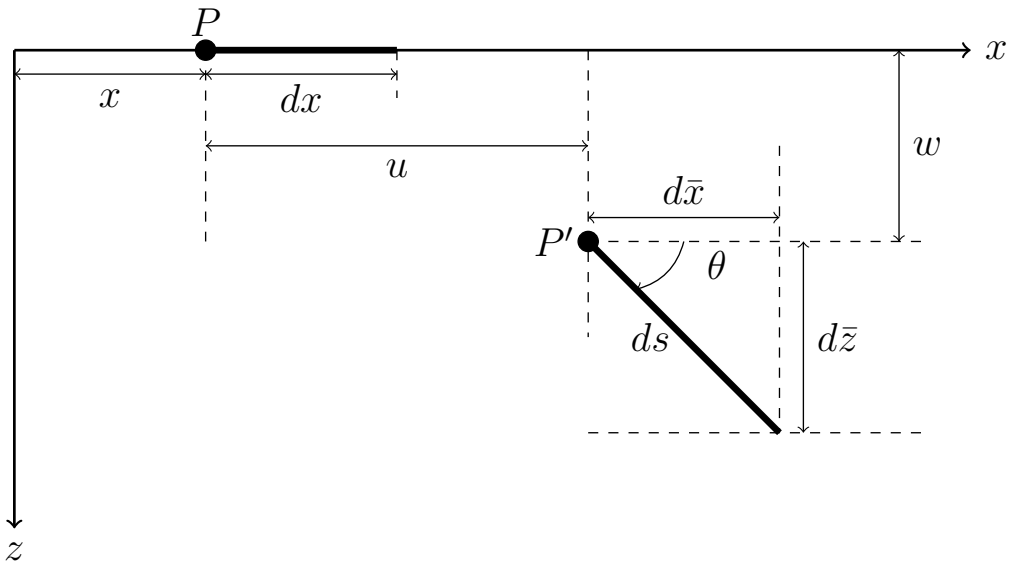

Figure 3.2 A segment on the beam before and after deformation

Consider a differential element of length dx with initial position defined by a point on that element, P. This point is located at a distance x along the x-axis as shown in Figure 3.2. The point P is displaced by a distance u along the x-axis and by a distance w along the z-axis. Also, the element length i.e. dx is deformed

to a length ds with an angle θ. The x and z components of ds are $d\bar{x}$ and $d\bar{z}$, respectively. Therefore, the new coordinates of the point P' after deformation are expressed as

$$\bar{x} = x + u \tag{3.3}$$

$$\bar{z} = w \tag{3.4}$$

The variation of the position of on the deformed element can be expressed by taking the derivative of eqs. (3.3) and (3.4) with respect to x. This yields

$$d\bar{x} = \left(1 + \frac{\partial u}{\partial x}\right)dx = (1 + u_x)dx \tag{3.5}$$

$$d\bar{z} = \left(\frac{\partial w}{\partial x}\right)dx = w_x dx \tag{3.6}$$

where the subscript x denotes derivative with respect to x. The length of the deformed element is then given as

$$ds = \sqrt{d\bar{x}^2 + d\bar{z}^2} = \sqrt{(1 + u_x)^2 + w_x^2}dx \tag{3.7}$$

Next, the axial strain is expanded in Taylor series and terms up to cubic order of w_x are retained [57]

$$\varepsilon = u_x + \frac{1}{2}w_x^2 + \dots \tag{3.8}$$

3.3 Kinetic Energy

Upon taking the time derivative of eqs. (3.3)–(3.4) we get

$$\frac{d\bar{x}}{dt} = \frac{\partial x}{\partial t} + \frac{\partial u}{\partial x}\frac{\partial x}{\partial t} + \frac{\partial u}{\partial t} = v + vu_x + u_t = v(1+u_x) + u_t \tag{3.9}$$

$$\frac{d\bar{z}}{dt} = \frac{\partial x}{\partial x}\frac{\partial x}{\partial t} = w_x v + w_t \tag{3.10}$$

where the subscript t denotes derivative with respect to the time and $\frac{\partial x}{\partial t} = v$ is the axial velocity of the micro-beam. Therefore, the velocity of a differential element in the micro-beam becomes

$$\bar{v} = v_l\hat{i} + v_t\hat{k} = [v(1+u_x) + u_t]\hat{i} + [vw_x + w_t]\hat{k} \tag{3.11}$$

The kinetic energy is then given as [58]

$$T = \frac{\rho A}{2}\int_0^L \left[(v(1+u_x) + u_t)^2 + (vw_x + w_t)^2\right] dx \tag{3.12}$$

where ρA is the constant mass per unit length of the beam material.

3.4 Strain Energy

The strain energy of the beam is due to the axial and flexural elastic deformation. And by considering the small size effect of the beam, based on the modified couple-

stress theory [14], the strain energy is given as

$$U = \int_0^L \left[P\varepsilon + \frac{1}{2}EA\varepsilon^2 + \frac{1}{2}(EI + GAl^2)w_{xx}^2 \right] dx \tag{3.13}$$

where G is shear modulus, l is the material length scale parameter and P is the axial tension

3.5 Hamilton Principle Application

The Hamilton principle states that for a particular period $[t_1 - t_2]$, for a conservative mechanical system, the integral of the Lagrangian, which is the difference between the kinetic and the potential energy, of the system is stationary [58], then

$$\int_{t_1}^{t_2} (\delta T - \delta U + \delta W) dt = 0 \tag{3.14}$$

where, T is the kinetic energy, U is the strain energy and W is the non-conservative work exerted on the system.

3.5.1 Variation of The Kinetic Energy

Let us expand the kinetic energy eq. (3.12) before applying Hamilton Principle to get

$$T = \frac{\rho A}{2}\int_0^L \Big[u_t^2 + 2vu_tu_x + 2u_tv + v^2u_x^2 + 2v^2u_x + v^2w_x^2 + v^2 + 2vw_tw_x + w_x^2\Big]dx \tag{3.15}$$

To find the variation of the kinetic energy δT, we let $u_t \to u_t + \delta u_t$ and $w_t \to w_t + \delta w_t$ after that we recover the original kinetic energy expression. Or we can use the following expression to find δT

$$\delta T = \sum\left(\frac{\partial T}{\partial u_t}\partial u_t + \frac{\partial T}{\partial w_t}\partial w_t + \frac{\partial T}{\partial u_x}\partial u_x + \frac{\partial T}{\partial w_x}\partial w_x\right) \tag{3.16}$$

Note that the terms inside the integral can be written as

$v\delta u_t = \frac{d}{dt}(v\delta u)$

$u_t\delta u_t = \frac{d}{dt}(u_t\delta u_t) - u_{tt}\delta u$

$vu_x\delta u_t = \frac{d}{dt}(vu_x\delta u) - vu_{xt}\delta u$

$w_t\delta w_t = \frac{d}{dt}(w_t\delta w) - w_{tt}\delta w$

$vw_x\delta w_x = \frac{d}{dt}(vw_x\delta w) - vw_{xt}\delta w$

$vu_t\delta u_x = \frac{d}{dx}(vu_t\delta u) - vu_{xt}\delta u$

$$v^2 u_x \delta u_x = \tfrac{d}{dx}(v^2 u_x \delta u) - v^2 u_{xx}\delta u$$

$$v^2 \delta u_x = \tfrac{d}{dx}(v^2 \delta u)$$

$$v w_t \delta w_x = \tfrac{d}{dx}(v w_t \delta w) - v w_{tx}\delta w$$

$$v^2 w_x \delta w_x = \tfrac{d}{dx}(v^2 w_x \delta w) - v^2 w_{xx}\delta w$$

Now let us substitute back the new expressions into eq. (3.16) to get

$$\begin{aligned}\delta T = \rho A \int_0^L \Big(&\frac{d}{dx}(v\delta u) + \frac{d}{dt}(u_t \delta u) - u_{tt}\delta u + \frac{d}{dt}(v u_x \delta u) - v u_{xt}\delta u \\ &+ \frac{d}{dt}(w_t \delta w) - w_t t \delta w + \frac{d}{dt} v w_x \delta w - v w_{xt}\delta w + \frac{d}{dt}(v u_t \delta u) - v u_{xt}\delta u \\ &+ \frac{d}{dx}(v^2 u_x \delta u) - v^2 u_{xx}\delta u + \frac{d}{dx}(v w_t \delta w) - v w_{xt}\delta w \\ &+ \frac{d}{dx}(v^2 w_x \delta w) - v^2 w_{xx}\delta w \Big) dx\end{aligned} \tag{3.17}$$

We integrate from t_1 to t_2 over time and from 0 to L over the length, x to get

$$\begin{aligned}\int_{t_1}^{t_2} \delta T dt = \rho A \Bigg\{ &\int_0^L \Big(\Big[v\delta u\Big]_{t_1}^{t_2} + \Big[u_t \delta u\Big]_{t_1}^{t_2} + \Big[v u_x \delta u\Big]_{t_1}^{t_2} + \Big[w_t \delta w\Big]_{t_1}^{t_2} + \Big[v\delta w\Big]_{t_1}^{t_2} \Big) dx \\ &+ \int_{t_1}^{t_2} \Big(\Big[v u_t \delta u\Big]_0^L + \Big[v^2 u_x \delta u\Big]_0^L + \Big[v^2 \delta u\Big]_0^L \\ &+ \Big[v w_t \delta w\Big]_0^L + \Big[v^2 w_x \delta w\Big]_0^L + \Big[v^2 w_x \delta u\Big]_0^L + \Big[v^2 w_x \delta u\Big]_0^L \Big) dt \\ &- \int_{t_1}^{t_2} \int_0^L \Big(\Big[u_{tt}\delta u\Big] + \Big[v u_{xt}\delta u\Big] + \Big[w_{tt}\delta w\Big] + \Big[v w_{xt}\delta w\Big] + \Big[v u_{xt}\delta u\Big] \\ &+ \Big[v^2 u_{xx}\delta u\Big] + \Big[v w_{tx}\delta w\Big] + \Big[v^2 w_{xx}\delta w\Big] \Big) dx dt \Bigg\}\end{aligned} \tag{3.18}$$

For the considered boundary conditions eq. (3.2), there is no displacement at $x = 0$ and $x = L$. Evaluating the integrals in eq. (3.18)

$$\int_{t_1}^{t_2} \delta T dt = -\rho A \int_{t_1}^{t_2} \int_0^L \left\{ \left(u_{tt} + 2v u_{xt} + v^2 u_{xx} \right) \delta u + \left(w_{tt} + 2v w_{xt} + v^2 w_{xx} \right) \delta w \right\} dx dt \tag{3.19}$$

3.5.2 Variation of the potential energy

Substituting the strain eq. (3.8) into the potential energy eq. (3.13) yields

$$\begin{aligned} U = \int_0^L \Big[& \frac{1}{2}(AGl^2 + EI) w_{xx}^2 + \frac{1}{2} AE u_x^2 + \frac{1}{2} AE u_x w_x^2 + P u_x \\ & + \frac{1}{8} AE w_x^4 + \frac{1}{2} P w_x^2 \Big] dx \end{aligned} \tag{3.20}$$

The variation of the potential energy, δU, is given as [58]

$$\delta U = \sum \left(\frac{\partial U}{\partial u_x} \delta u_x + \frac{\partial U}{\partial w_x} \delta w_x + \frac{\partial U}{\partial w_x x} \delta w_{xx} \right) \tag{3.21}$$

Evaluating the three terms of the variation of the potential energy eq. (3.21)

$$\frac{\partial U}{\partial u_x} \delta u_x = \left(\frac{1}{2} AE w_x^2 + P + AE u_x \right) \delta u_x \tag{3.22}$$

$$\frac{\partial U}{\partial w_x} \delta w_x = \left(P w_x + \frac{1}{2} AE w_x^3 + AE u_x w_x \right) \delta w_x \tag{3.23}$$

$$\frac{\partial U}{\partial w_{xx}} \delta w_{xx} = \left(AGl^2 + EI \right) w_{xx} \delta w_{xx} \tag{3.24}$$

Substituting eqs. (3.22)–(3.24) into the variation of the potential energy eq. (3.21) to get

$$\begin{aligned}\delta U = &\frac{1}{2}AEw_x^2\delta u_x + P\delta u_x + AEu_x\delta u_x + Pw_x\delta w_x\frac{1}{2}AEw_x^3\delta w_x \\ &+ AEu_xw_x\delta w_x + (AGl^2 + EI)w_{xx}\delta w_{xx}\end{aligned} \tag{3.25}$$

Let us rewrite each term in eq. (3.25) as

$$\frac{1}{2}AEw_x^2\delta u_x = \frac{d}{dx}(\frac{1}{2}AEw_x^2\delta u) - AEw_xw_{xx}\delta u$$

$$P\delta u_x = \frac{d}{dx}(P\delta u)$$

$$AEu_x\delta u_x = \frac{d}{dx}(AEu_x\delta u) - AEu_{xx}\delta u$$

$$Pw_x\delta w_x = \frac{d}{dx}(Pw_x\delta w) - P(w_{xx}\delta w)$$

$$\frac{1}{2}AEw_x^3\delta w_x = \frac{d}{dx}\left(\frac{1}{2}AEw_x^3\delta w\right) - \frac{3}{2}AEw_x^2w_{xx}\delta w$$

$$AEu_xw_x\delta w_x = \frac{d}{dx}\left(AEu_xw_x\delta w\right) - AE(u_{xx}w_x + u_xw_{xx})\delta w$$

$$(AGl^2 + EI)w_{xx}\delta w_{xx} = \frac{d}{dx}[(AGl^2 + EI)w_{xx}\delta w_x] - \frac{d}{dx}[(AGl^2 + EI)w_{xxx}\delta w] + (AGl^2 + EI)w_{xxxx}\delta w$$

Substituting the above expanded terms into eq. (3.21) and integrate it over time from t_1 to t_2. This yields

$$\begin{aligned}\int_{t_1}^{t_2} \delta U dt = \int_{t_1}^{t_2} \Bigg\{ & \left[\frac{1}{2} AE w_x^2 \delta u\right]_0^L + [P\delta u]_0^L + [AE u_x \delta u]_0^L + \left[\frac{1}{2} AE w_x^3 \delta w\right]_0^L \\ & + [AE u_x w_x \delta w]_0^L + \left[(AGl^2 + EI) w_{xxx} \delta w\right]_0^L \\ & + \left[(AGl^2 + EI) w_{xx} \delta w_x\right]_0^L - \int_0^L \Big(AE w_x w_{xx} \delta + AE u_{xx} \delta u + P w_{xx} \delta w \\ & + \frac{3}{2} AE w_x^2 w_{xx} \delta w + AE(u_{xx} w_x + u_x + w_{xx}) \delta w \\ & + (AGl^2 + EI) w_{xxxx} \delta w \Big) dx \Bigg\} dt \end{aligned} \tag{3.26}$$

And by evaluating the integrals reduces eq. (3.26) to

$$\begin{aligned}\int_{t_1}^{t_2} \delta U dt = - \int_{t_1}^{t_2} \int_0^L \Bigg\{ & (AE w_x w_{xx} + AE u_{xx}) \delta u + \Big(P w_{xx} + \frac{3}{2} AE w_x^2 w_{xx} \\ & + AE(u_{xx} w_x + w_x w_{xx}) + (AGl^2 + EI) w_{xxxx} \Big) \delta w \Bigg\} dx dt \end{aligned} \tag{3.27}$$

The integral of the variation of the external forces is expressed as

$$\delta W = \int_0^L (F_{damp} + F_{elec})\ dx \tag{3.28}$$

where F_{damp} is the viscous damping force, which is given as

$$F_{damp} = -c\ w_t \tag{3.29}$$

with c being the damping coefficient per unit length. The electrostatic force with fringing field is calculated by Palmer's formula [59] as

$$F_{elec} = \frac{\varepsilon b \left[V_{DC} + V_{AC}\cos\omega t\right]^2}{2(g-w)}\left(1+\beta\frac{g-w}{b}\right) \tag{3.30}$$

Finally, substituting eqs. (3.19), (3.27) and (3.28) into eq. (3.14) yields

$$\begin{aligned}\int_{t_1}^{t_2}(\delta T - \delta U + \delta W) = \int_{t_1}^{t_2}\int_0^L \Bigg(& -\rho A(u_{tt}+2vu_{xt}+v^2u_{xx})\delta u \\ & -\rho A(w_{tt}+2vw_{xt}+v^2w_{xx})\delta w \\ & +AE(w_xw_{xx}+u_{xx})\delta u \\ & +\Big[Pw_{xx}+\frac{3}{2}AEw_x^2w_{xx} \\ & +AE(u_{xx}w_x+u_xw_{xx})-(AGl^2+EI)w_{xxxx} \\ & +\frac{\epsilon b[V_{DC}+V_{AC}\cos\omega t]^2}{2(g-w)}(1+\beta\frac{g-w}{b}) \\ & -cw_t\Big]\delta w\Bigg)dxdt\end{aligned} \tag{3.31}$$

Since the above equation must hold for any arbitrary δu and δw, the integrand part must be zero, which gives the governing equations of motion for transverse and longitudinal vibrations of the beam. By collecting the terms with the coefficients δu one can get

$$\Big[-\rho A(u_{tt}+2vu_{xt}+v^2u_{xx})+AE(w_xw_{xx}+u_xx)\Big]\delta u = 0 \tag{3.32}$$

And the longitudinal vibration equation is

$$\left\{\rho A(u_{tt}+2vu_{xt}+v^2u_{xx})-AE\frac{\partial}{\partial x}(wu_x+\frac{1}{2}w_x^2)\right\}=0 \tag{3.33}$$

Similarly, after collecting the terms with the coefficients δw, one can get

$$\begin{aligned}&\Big[-\rho A(w_{tt}+2vw_{xt}+v^2w_{xx})+Pw_{xx}+\frac{3}{2}AEw_x^2w_{xx}\\&+AE(u_{xx}w_x+u_xw_{xx})-(AGl^2+EI)w_{xxxx}\\&+\frac{\epsilon b[V_{DC}+V_{AC}\cos\omega t]^2}{2(g-w)}(1+\beta\frac{g-w}{b})-cw_t\Big]\delta w=0\end{aligned} \tag{3.34}$$

Dropping δw and moving the forcing term to the right hand side results in

$$\begin{aligned}-\rho A(w_{tt}+2vw_{xt}+v^2w_{xx})+Pw_{xx}+\frac{3}{2}AEw_x^2w_{xx}+AE(u_{xx}w_x+u_xw_{xx})\\-(AGl^2+EI)w_{xxxx}-cw_t=\frac{\epsilon b[V_{DC}+V_{AC}\cos(\omega t)]^2}{2(g-w)}(1+\beta\frac{g-w}{b})\end{aligned} \tag{3.35}$$

And by rearranging the terms we get the transverse vibration equation as

$$\begin{aligned}\Big(AGl^2+EI\Big)w_{xxxx}+\rho Aw_{tt}+cw_t+2\rho Avw_{xt}+\rho Av^2w_{xx}-Pw_{xx}\\-AE\frac{\partial}{\partial x}\Big((u_x+\frac{1}{2}w_x^2)w_x\Big)=\frac{\epsilon b[V_{DC}+V_{AC}\cos(\omega t)]^2}{2(g-w)^2}\Big(1+\beta\frac{g-w}{b}\Big)\end{aligned} \tag{3.36}$$

The longitudinal displcament u could be eliminated in the transverse vibration eq. (3.36) by using the approximation given by [40]. It is assumed that the effect of the longitudinal inertia is small, then eq. (3.33) becomes

$$\frac{\partial}{\partial x}\left(u_x+\frac{1}{2}w_x^2\right)=0 \tag{3.37}$$

And the axial strain is approximated to

$$\frac{\partial u_x}{\partial x} = \varepsilon_x = \int_0^L \frac{1}{2} w_x^2 dx \tag{3.38}$$

Substituting eqs. (3.37) and (3.38) into eq. (3.36) yields

$$\begin{aligned} &(AGl^2 + EI)w_{xxxx} + \rho A w_{tt} + c w_t + 2\rho A v w_{xt} + (\rho A v^2 - P) w_{xx} \\ &-AE w_{xx}\Big(\int_0^L \frac{1}{2} w_x^2 dx\Big) = \frac{\epsilon b[V_{DC} + V_{AC}\cos(\omega t)]^2}{2(g-w)^2}\Big(1 + \beta\frac{g-w}{b}\Big) \end{aligned} \tag{3.39}$$

Equations (3.33) and (3.39) describe the longitudinal and transverse vibrations of the micro-beam, respectively. To solve these equations, we introduce the following non-dimensional variables for normalization:

$$\hat{w} = \frac{w}{g} \qquad \hat{x} = \frac{x}{L} \qquad \hat{t} = \frac{t}{T} \tag{3.40}$$

Substitute the non-dimensional variables into eq. (3.39) we get

$$\begin{aligned} &(AGl^2 + EI)\frac{\partial^4 (g\hat{w})}{\partial (L\hat{x})^4} + \rho A \frac{\partial^2 (g\hat{w})}{\partial (T\hat{t})^2} + c\frac{\partial (g\hat{w})}{\partial (\hat{t}T)} + 2\rho A v \frac{\partial^2 (g\hat{w})}{\partial (L\hat{x}T\hat{t})} + \\ &\left(\rho A v^2 - P\right)\frac{\partial^2 (g\hat{w})}{\partial (L\hat{x})^2} - AE\frac{\partial^2 (g\hat{w})}{\partial (L\hat{x})^2}\left(\int_0^1 \frac{1}{2}\left(\frac{\partial (g\hat{w})}{\partial (L\hat{x})}\right)^2 dx\right) \\ &= \frac{\epsilon b\left[V_{DC} + V_{AC} cos\left(\omega \hat{t} T\right)\right]^2}{2\left(g - g\hat{w}\right)^2}\left(1 + \beta\frac{g - g\hat{w}}{b}\right) \end{aligned} \tag{3.41}$$

By further simplification

$$\left(\frac{AGl^2g}{L^4}+\frac{EIg}{L^4}\right)\hat{w}_{\hat{x}\hat{x}\hat{x}\hat{x}}+\frac{\rho Ag}{T^2}\hat{w}_{\hat{t}\hat{t}}+\frac{cg}{T}\hat{w}_{\hat{t}}+\frac{2\rho Avg}{LT}\hat{w}_{\hat{x}\hat{t}}+\left(\frac{\rho Av^2g}{L^2}-\frac{Pg}{L^2}\right)\hat{w}_{\hat{x}\hat{x}}-$$
$$\frac{1}{2}\frac{AEg^3}{L^4}\hat{w}_{\hat{x}\hat{x}}\left(\int_0^1\hat{w}_{\hat{x}}^2dx\right)=\frac{\epsilon b\left[V_{DC}+V_{AC}cos\left(\omega\hat{t}T\right)\right]^2}{2g^2\left(1-\hat{w}\right)^2}\left(1+\frac{\beta g}{b}\left(1-\hat{w}\right)\right) \tag{3.42}$$

Multiply the above equation by $\frac{L^4}{EIg}$

$$\left(\frac{AGl^2}{EI}+1\right)\hat{w}_{\hat{x}\hat{x}\hat{x}\hat{x}}+\frac{\rho AL^4}{EIT^2}\hat{w}_{\hat{t}\hat{t}}+\frac{cL^4}{TEI}\hat{w}_{\hat{t}}+\frac{2\rho AvL^3}{EIT}\hat{w}_{\hat{x}\hat{t}}+$$
$$\left(\frac{\rho Av^2L^2}{EI}-\frac{PL^2}{EI}\right)\hat{w}_{\hat{x}\hat{x}}-\frac{1}{2}\frac{Ag^2}{I}\hat{w}_{\hat{x}\hat{x}}\left(\int_0^1\hat{w}_{\hat{x}}^2dx\right)= \tag{3.43}$$
$$\frac{\epsilon bL^4\left[V_{DC}+V_{AC}cos\left(\omega\hat{t}T\right)\right]^2}{2EIg^3\ \left(1-\hat{w}\right)^2}\left(1+\frac{\beta g}{b}\left(1-\hat{w}\right)\right)$$

By writing the explicit expressions of $A=bh$ and $I=(\frac{1}{12})bh^3$ to cancel out b from all terms, except from the fringing field term, eq. (3.43) becomes

$$\left(\frac{AGl^2}{EI}+1\right)\hat{w}_{\hat{x}\hat{x}\hat{x}\hat{x}}+\frac{\rho AL^4}{EIT^2}\hat{w}_{\hat{t}\hat{t}}+\frac{cL^4}{TEI}\hat{w}_{\hat{t}}+\frac{2\rho AvL^3}{EIT}\hat{w}_{\hat{x}\hat{t}}+$$
$$\left(\frac{\rho Av^2L^2}{EI}-\frac{PL^2}{EI}\right)\hat{w}_{\hat{x}\hat{x}}-\frac{6g^2}{h^2}\hat{w}_{\hat{x}\hat{x}}\left(\int_0^1\hat{x}_{\hat{x}}^2dx\right)= \tag{3.44}$$
$$\frac{6\epsilon L^4\left[V_{DC}+V_{AC}cos\left(\omega\hat{t}T\right)\right]^2}{Eh^3g^3\ \left(1-\hat{w}\right)^2}\left(1+\frac{\beta g}{b}\left(1-\hat{w}\right)\right)$$

Introducing the dimensionless quantities in Table 3.1, we get the following dimensionless governing equation:

$$\begin{aligned}(\zeta+1)\,\hat{w}_{\hat{x}\hat{x}\hat{x}\hat{x}}+\hat{w}_{\hat{t}\hat{t}}+\hat{c}\hat{w}_{\hat{t}}+2\hat{v}\hat{w}_{\hat{x}\hat{t}}+\left(\hat{v}^2-\hat{P}\right)\hat{w}_{\hat{x}\hat{x}}-\alpha\hat{w}_{\hat{x}\hat{x}}\left(\int_0^1\hat{w}_{\hat{x}}^2dx\right)=\\ \frac{\left[\hat{V}_{DC}+\hat{V}_{AC}cos\left(\Omega\hat{t}\right)\right]^2}{\left(1-\hat{w}\right)^2}\left(1+\hat{\beta}\left(1-\hat{w}\right)\right)\end{aligned} \tag{3.45}$$

Let us further simplify eq. (3.45) by dropping the hat notation to get

$$\begin{aligned}(\zeta+1)\,w_{xxxx}+w_{tt}+cw_t+2vw_{xt}+\left(v^2-P\right)w_{xx}-\alpha w_{xx}\left(\int_0^1 w_x^2dx\right)=\\ \frac{\left[V_{DC}+V_{AC}cos\left(\Omega t\right)\right]^2}{\left(1-w\right)^2}\Big(1+\beta(1-w)\Big)\end{aligned} \tag{3.46}$$

Table 3.1 Dimensionless quantities

Parameter	**Definition**
$\zeta = \frac{GAl^2}{EI}$	Dimensionless size effect
$\alpha = 6\left(\frac{g}{h}\right)^2$	Stretching parameter
$\hat{v} = vL\sqrt{\frac{\rho A}{EI}}$	Dimensionless axial velocity
$\hat{P} = \frac{PL^2}{EI}$	Dimensionless residual axial force
$T = L^2\sqrt{\frac{\rho A}{EI}}$	Dimensionless time parameter
$\hat{\beta} = \frac{0.65g}{b}$	Fringing field parameter
$\hat{c} = \frac{cL^2}{\sqrt{\rho AEI}}$	Dimensionless damping coefficient
$\hat{V}_{DC} = V_{DC}\sqrt{\frac{6\epsilon L^4}{Eh^3g^3}}$	Dimensionless DC voltage
$\hat{V}_{AC} = V_{AC}\sqrt{\frac{6\epsilon L^4}{Eh^3g^3}}$	Dimensionless AC voltage amplitude
$\Omega = \omega T$	Dimensionless angular frequency

Chapter 4

Free Vibration

4.1 Galerkin Methods

We solve Equation (3.46) by applying the Galerkin method to discretize it into a set of non-linear ordinary differential equations. We select the eigenfunctions of a simply-simply supported beam as the basis functions for the following:

$$w(x,t) = \sum_{i=1}^{n} \phi_i(x)\, q_i(t) \tag{4.1}$$

where $\phi_i(x)$ is the mode shape of the transverse motion of a simply supported beam given as

$$\phi_i(x) = \sin(i\pi x) \tag{4.2}$$

where i is the number of vibration mode, and $q\,(t)$ represents the time function for transverse displacement. By removing the electrostatic force terms from eq. (3.46) we get

$$(\zeta+1)\,w_{xxxx}+w_{tt}+cw_t+2vw_{xt}+\left(v^2-P\right)w_{xx}-\alpha w_{xx}\left(\int_0^1 w_x^2 dx\right)=0 \quad (4.3)$$

Equation (4.3) describes the free transverse vibration of a simply supported axially moving micro-beam. Considering the first mode shape (i.e., $i=1$) and substituting eqs. (4.1) and (4.2) and their derivatives into eq. (4.3) we get

$$\begin{aligned}(\zeta+1)\,\phi_{xxxx}q_1+\phi\ddot{q}_1+c\phi\dot{q}_1+2v\phi_x q_1+\left(v^2-P\right)\phi_{xx}q_1\\ -\alpha\phi_{xx}q_1\int_0^1\phi_x^2q_1^2dx=0\end{aligned} \quad (4.4)$$

Substiting the explicit expression of the mode shape eq. (4.2) with its derivatives yields

$$\begin{aligned}\pi^4(\zeta+1)\sin(\pi x)q_1+\sin(\pi x)\ddot{q}_1+c\sin(\pi x)\dot{q}_1+2\pi v\cos(\pi x)q_1\\ -\pi^2(v^2-P)\sin(\pi x)q_1+\pi^4\alpha\sin(\pi x)q_1^3\int_0^1\cos(\pi x)^2dx=0\end{aligned} \quad (4.5)$$

Multiplying eq. (4.5) by the first mode shape then integrating with respect to x over the domain from 0 to 1 we get

$$\begin{aligned}\pi^4(\zeta+1)q_1\int_0^1\sin(\pi x)^2dx+\ddot{q}_1\int_0^1\sin(\pi x)^2dx+c\dot{q}_1\int_0^1\sin(\pi x)^2dx\\ +2\pi v q_1\int_0^1\sin(\pi x)\cos(\pi x)dx-\pi^2(v^2-P)q_1\int_0^1\sin(\pi x)^2dx\\ +\frac{1}{2}\pi^4\alpha q_1^3\int_0^1\sin(\pi x)^2=0\end{aligned}\tag{4.6}$$

And by evaluating the integrals

$$\frac{\pi^4}{2}(\zeta+1)q_1+\frac{1}{2}\ddot{q}_1+\frac{1}{2}c\dot{q}_1-\frac{\pi^2}{2}(v^2-P)q_1+\frac{1}{4}\pi^4\alpha q_1^3=0\tag{4.7}$$

Multiplying eq. (4.7) by 2 and rearranging the terms to get

$$\ddot{q}_1+c\,\dot{q}_1+\Big[\pi^4(\zeta+1)+\pi^2(P-v^2)\Big]q_1+\frac{1}{2}\pi^4\alpha q_1^3=0\tag{4.8}$$

The natural frequency of the beam is given as

$$\omega_1^2=\pi^4(\zeta+1)+\pi^2(P-v^2)\tag{4.9}$$

Finally

$$\ddot{q}_1+c\,\dot{q}_1+\omega_1^2q_1+\frac{\pi^4}{2}\alpha q_1^3=0\tag{4.10}$$

Equation (4.10) describes the free transverse vibration of the micro-beam. A quality factor is frequently used to study the damping effect. Therefore, the

damping coefficient in eq. (4.10) can be replaced by

$$c = \frac{\omega}{Q} \tag{4.11}$$

For the second mode shape (i.e., $i = 2$) the equation of motion becomes

$$\ddot{q}_2 + c\dot{q}_2 + 8\Big[\pi^4(\zeta + 1) + 2\pi^2(P - v^2)\Big]q_2 + \frac{1}{2}\pi^4\alpha q_2^3 = 0 \tag{4.12}$$

And the second natural frequency of the beam is

$$\omega_2^2 = 8\pi^4(\zeta + 1) + 2\pi^2(P - v^2) \tag{4.13}$$

For the third mode shape (i.e., $i = 3$) the equation of motion becomes

$$\ddot{q}_3 + c\dot{q}_3 + 81\Big[\pi^4(\zeta + 1) + 9\pi^2(P - v^2)\Big]q_3 + \frac{81}{2}\pi^4\alpha q_3^3 = 0 \tag{4.14}$$

And the third natural frequency of the beam is

$$\omega_3^2 = 81\pi^4(\zeta + 1) + 9\pi^2(P - v^2) \tag{4.15}$$

An axially moving micro-beam made of silicon material is used with the following properties (Table 4.1) to understand the dynamic behavior of the micro-beam.

Table 4.1 Micro-beam properties and dimensions

Definition	**Value**	**Unit**
Youngs Modulus	$E = 160$	GPa
Poisson's ratio	$\nu = 0.26$	—
Density	$\rho = 2332$	$\mathrm{kg\,m^{-3}}$
Beam thickness	$h = 10$	µm
Length scale parameter	$l = [0 - 1]h$	µm
Beam width	$b = 50$	µm
Dimensionless tension	$P = [0 - 5]$	—
Beam length	$L = 500$	µm
Gap width	$g = 2$	µm
V_{DC}	$[2 - 70]$	V
Permittivity of free space	$\epsilon = 8.85 \times 10^{-12}$	$\mathrm{F\,m^{-1}}$
V_{AC}	$[0 - 2]$	V

4.2 Natural Frequencies

The normalized natural frequencies of the beam using properties and dimensions given in Table 4.1 are

$$\begin{aligned} \omega_1 &= 9.87 \\ \omega_2 &= 39.48 \\ \omega_3 &= 88.83 \end{aligned} \tag{4.16}$$

4.2.1 Length scale parameter

Figure 4.1 shows the effect of the length scale parameter on the natural frequencies. As the length scale parameter increases the dimensionless frequencies increase. We can see that the third natural frequency increases faster. Therefore, the variation of the third natural frequency with respect to the length scale parameter is significant.

4.2.2 Dimensionless axial velocity

Figure 4.2 shows the effect of the dimensionless axial velocity on the dimensionless natural frequencies of the micro-beam. Also, a contour plot Figure (4.3) shows the effect of sweeping both l and v on the first dimensionless frequency. As we can see from the plot, as the axial velocity increased the dimensionless frequencies

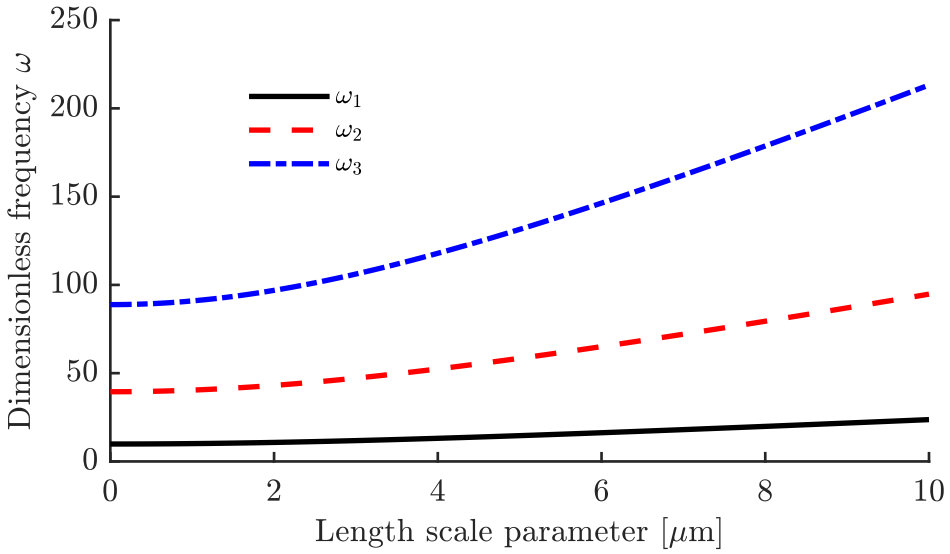

Figure 4.1 Variation of the dimensionless frequencies with respect to l

decreased. The axial velocity at which the natural frequency becomes zero is called the critical axial velocity. Therefore, the critical velocities for the three modes were 3.2, 6.4 and 9.5, respectively.

4.2.3 Dimensionless tension

Figure 4.4 shows that as the applied dimensionless tension increasesd, the dimensionless natural frequencies increased as well. Figure 4.5 shows a contour plot showing the efft of changing both P and v on the first dimensionless frequency.

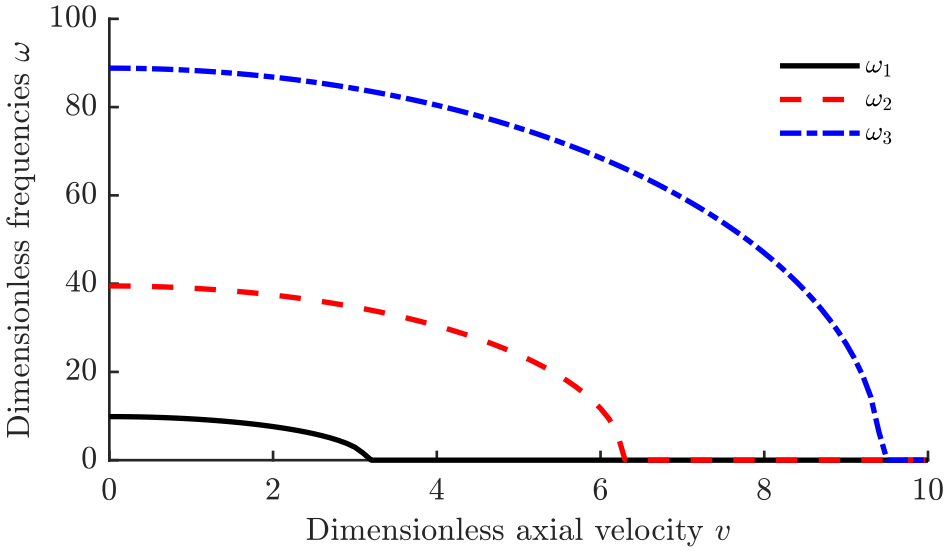

Figure 4.2 Variation of dimensionless frequencies with respect to v

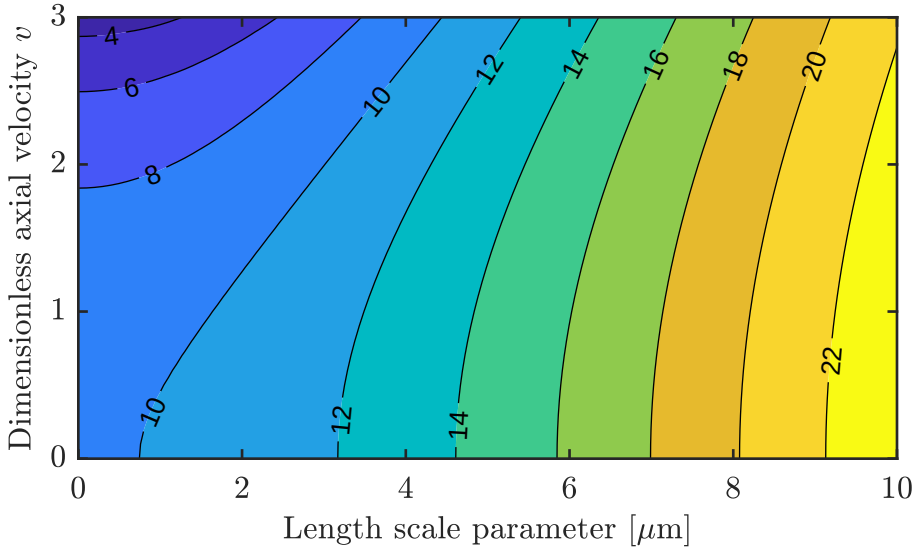

Figure 4.3 Variation of the first dimensionless frequency with respect to v and l

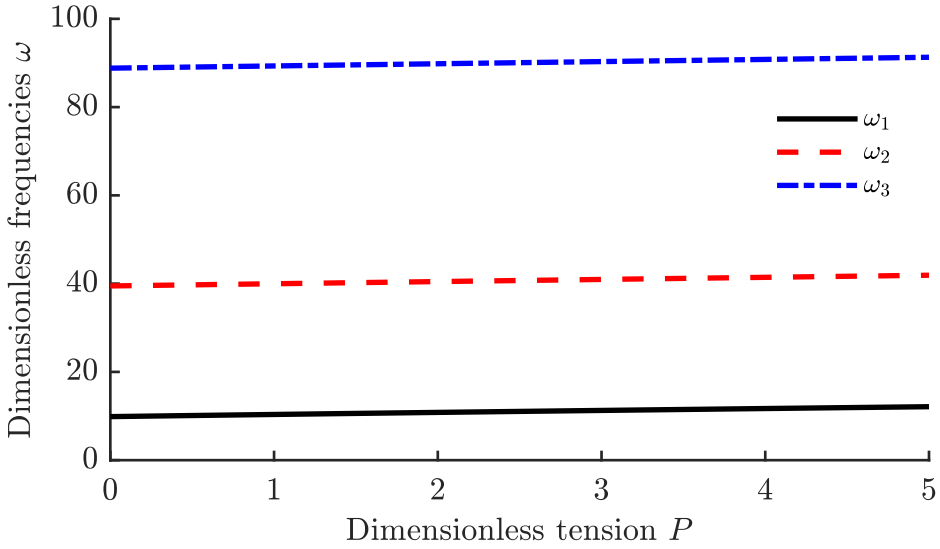

Figure 4.4 Variation of the dimensionless frequencies with respect to P

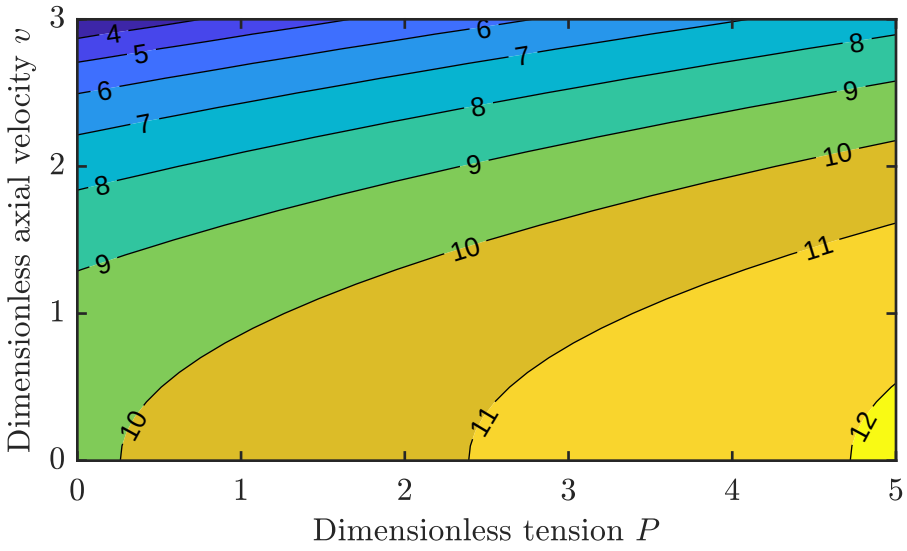

Figure 4.5 Variation of the first dimensionless frequency with respect to v and P

4.3 Critical Axial Velocity

The critical axial velocity of a moving micro-beam is the value that makes the fundamental frequency vanish [60]. If we set eqs. (4.9), (4.13) and (4.15) to zero and solve for the dimensionless axial velocity, we get

$$v_{\mathrm{cr1}} = \sqrt{P + \pi^2(\zeta + 1)} \tag{4.17}$$

$$v_{\mathrm{cr2}} = \sqrt{P + 4\pi^2(\zeta + 1)} \tag{4.18}$$

$$v_{\mathrm{cr3}} = \sqrt{P + 9\pi^2(\zeta + 1)} \tag{4.19}$$

Figure 4.6 shows the effect of the length scale parameter on the dimensionless

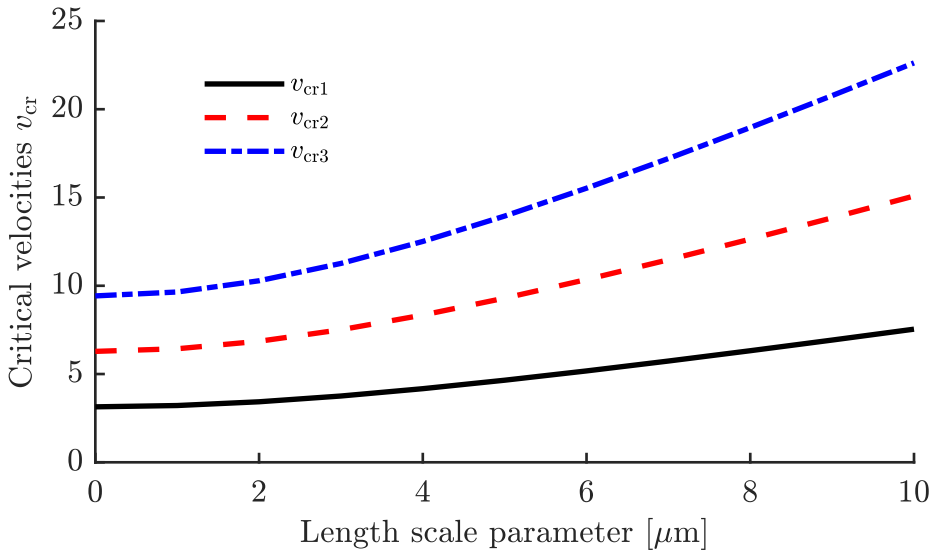

Figure 4.6 Variation of dimensionless critical axial velocity with respect to l

critical velocities for the three modes. As the length scale parameter increased the

critical velocities increased. Figure 4.7 shows that as the dimensionless tension increased the critical axial velocity increased. Figure 4.8 shows the combined effect of both the dimensionless tension and the length scale parameter on the critical axial velocity of the first mode.

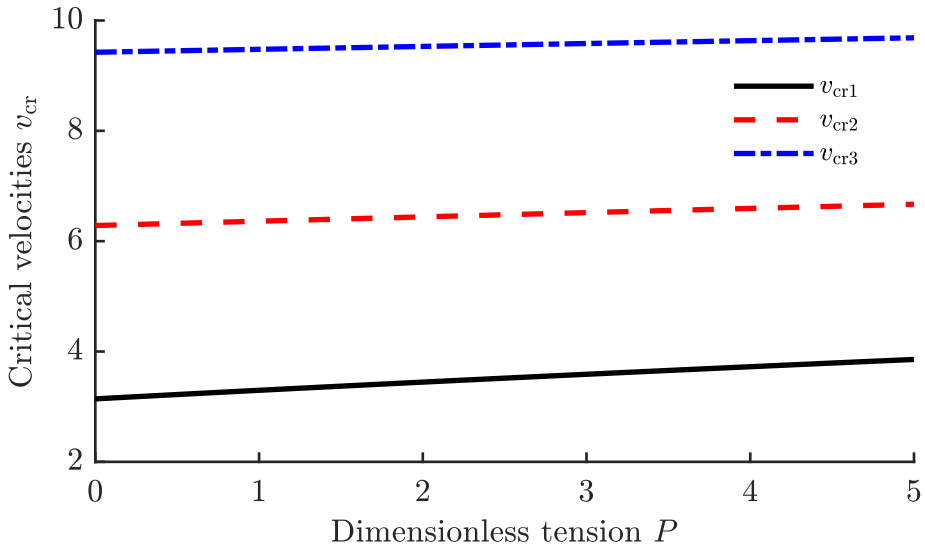

Figure 4.7 Variation of dimensionless critical axial velocity with respect to P

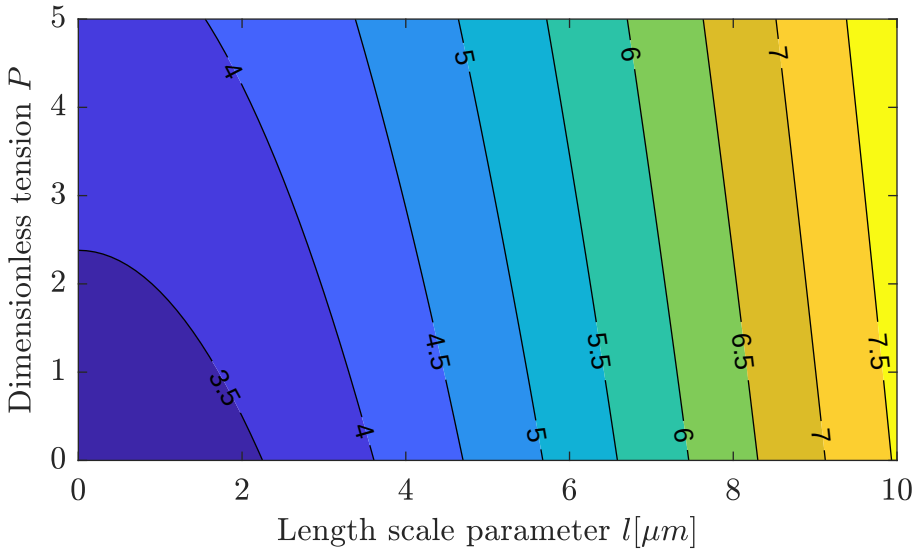

Figure 4.8 Variation of dimensionless critical axial velocity with respect to P and l

4.4 Time History

In this section, we invistigate the time history due to initial conditions. The propagation of the waveform is studied with respect to different parameters including: dimensionless axial velocity, length scale parameter and dimensionless tension.

4.4.1 Effect of dimensionless axial velocity

Figure 4.9 shows the wave form when the dimensionless axial velocity is in the range of [0–2.5] when $q_1 = 0.01$ and $\dot{q}_1 = 0$. We can see that as the axial velocity increases the natural frequency decreases.

4.4.2 Effect of length scale parameter

Figure 4.10 shows the effect of the material length scale parameter on the wave form. Although the effect is not clear, we note that the maximum displacement shifted for different values of l. This indicates that the natural frequency changed and this change is quadratic, by tracing the peak values in the waveform.

4.4.3 Effect of dimensionless tension

Figure 4.11 shows the waveform at various tensions P. We can see the linear effect of changing P by examining the maximum displacement that occured at

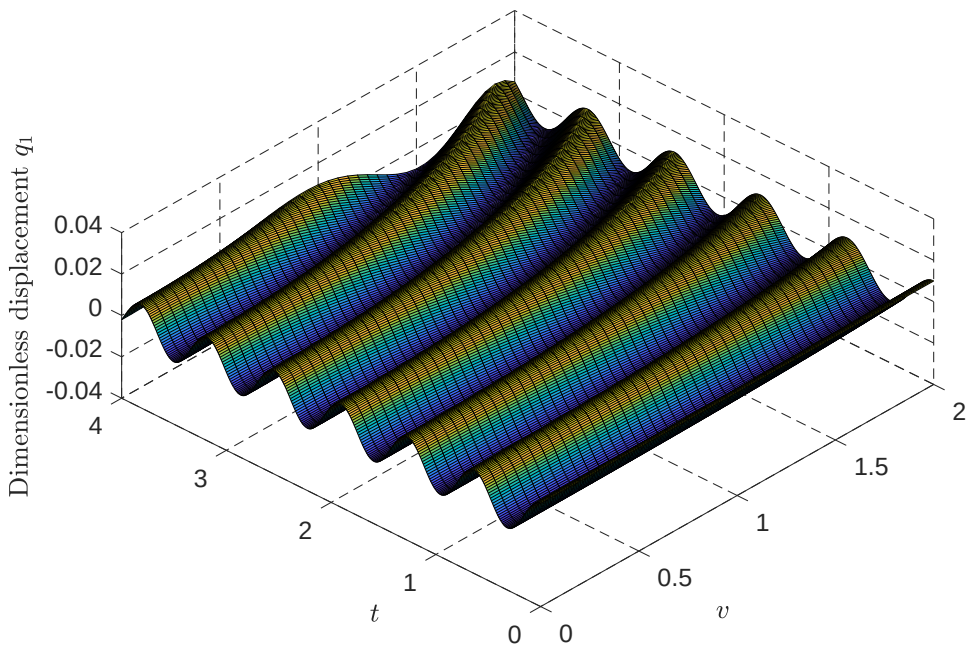

Figure 4.9 Waveform at various v

each value of P. The effect of P was clear by stretching the waveform outward therefore increasing the natural frequency of the micro-beam.

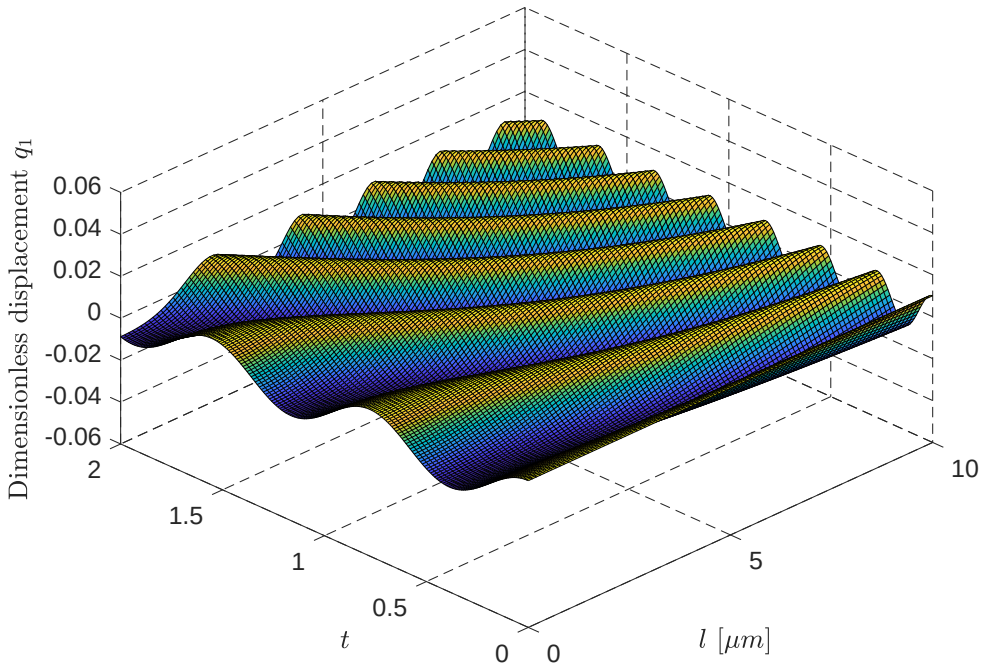

Figure 4.10 Waveform at various l

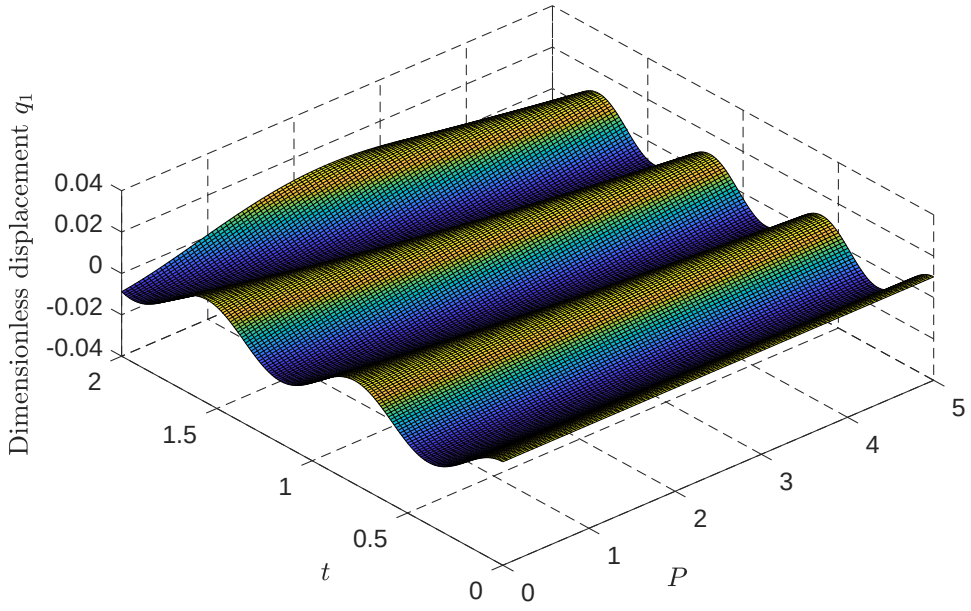

Figure 4.11 Waveform at various P

Chapter 5

Forced Vibration

Equation (3.46) can be simplified if we multiply it by $(1-w)^2$ to remove the transverse displacement from the denominator. This yields

$$\begin{aligned}(1-w)^2(\zeta+1)w_{xxxx}+(1-w)^2 w_{tt}+(1-w)^2 cw_t+(1-w)^2 2vw_{xt}\\ +(1-w)^2\left(v^2-P\right)w_{xx}-\alpha(1-w)^2 w_{xx}\left(\int_0^1 w_x^2 dx\right)\\ =\left[V_{\mathrm{DC}}+V_{\mathrm{AC}}\cos(\Omega t)\right]^2(1+\beta(1-w))\end{aligned} \tag{5.1}$$

To solve eq. (6.9), we apply Galerkin method to descritize it into a set of ordinary differential equations. The transverse displacement is expressed as

$$w(x,t)=\sum_{i=1}^{n} q_i(t)\,\phi_i(x) \tag{5.2}$$

Substituting eq. (6.10) into eq. (6.9), and multiply it by the mode shape $\phi_i(x)$ and integrate over x from 0 to 1 lead to

$$\begin{aligned}
&\int_0^1 \phi_i \left(1-\sum_{i=1}^{n} q_i\phi_i\right)^2 (\zeta+1)\sum_{i=1}^{n} q_i\phi_i''''dx + \int_0^1 \phi_i \left(1-\sum_{i=1}^{n} q_i\phi_i\right)^2 \sum_{i=1}^{n} \ddot{q}_i\phi_i dx \\
&+c\int_0^1 \phi_i \left(1-\sum_{i=1}^{n} q_i\phi_i\right)^2 \sum_{i=1}^{n} \dot{q}_i\phi_i dx + 2v\int_0^1 \phi_i \left(1-\sum_{i=1}^{n} q_i\phi_i\right)^2 \sum_{i=1}^{n} q_i\phi_i' dx \\
&+\left(v^2-P\right)\int_0^1 \phi_i \left(1-\sum_{i=1}^{n} q_i\phi_i\right)^2 \sum_{i=1}^{n} q_i\phi_i'' dx \\
&-\alpha\int_0^1 \phi_i \left[\left(1-\sum_{i=1}^{n} q_i\phi_i\right)^2 \sum_{i=1}^{n} q_i\phi_i'' \int_0^1 \left\{\left(\sum_{i=1}^{n} q_i\phi_i'\right)^2\right\} dx\right] dx \\
&=\int_0^1 \phi_i \left[V_{\mathrm{DC}}+V_{\mathrm{AC}}\cos(\Omega t)\right]^2 \left(1+\beta\left(1-\sum_{i=1}^{n} q_i\phi_i\right)\right) dx
\end{aligned} \tag{5.3}$$

Using four terms ($n=4$) in the Galerkin expansion reduces eq. (6.12) to

$$\begin{aligned}
&\ddot{q}_1\left(1-\frac{16}{3\pi}q_1+\frac{3}{4}q_1^2\right)+c\,\dot{q}_1\left(1-\frac{16}{3\pi}q_1+\frac{3}{4}q_1^2\right)+A_1\,q_1+B_1\,q_1^2 \\
&+C_1\,q_1^3+D_1\,q_1^4+E_1\,q_1^5+F_1=0
\end{aligned} \tag{5.4}$$

$$\begin{aligned}
&\ddot{q}_2\left(1+\frac{3}{4}q_2^2\right)+c\,\dot{q}_2\left(1+\frac{3}{4}q_2^2\right)+A_2\,q_2+B_2\,q_2^2+C_2\,q_2^3+D_2\,q_2^4 \\
&+E_2\,q_2^5+F_2=0
\end{aligned} \tag{5.5}$$

$$\begin{aligned}
&\ddot{q}_3\left(1-\frac{16}{3\pi}q_3+\frac{3}{4}q_3^2\right)+c\,\dot{q}_3\left(1-\frac{16}{3\pi}q_3+\frac{3}{4}q_3^2\right)+A_3\,q_3+B_3\,q_3^2 \\
&+C_3\,q_1^3+D_3\,q_3^4+E_3\,q_3^5+F_3=0
\end{aligned} \tag{5.6}$$

$$\ddot{q}_4\left(1+\frac{3}{4}q_4^2\right)+c\ \dot{q}_4\left(1+\frac{3}{4}q_4^2\right)+A_4\ q_4+B_4\ q_4^2+C_4\ q_4^3+D_4\ q_2^4 \\ +E_4\ q_4^5+F_4=0 \tag{5.7}$$

Equations (5.4)–(5.7) can be written in matrix form as

$$M\ddot{q}+cM\dot{q}+Aq+Bq^2+Cq^3+Dq^4+Eq^5+F=0 \tag{5.8}$$

where

$$q=\begin{bmatrix}q_1 & q_2 & q_3 & q_4\end{bmatrix}^T \tag{5.9}$$

$$M=\begin{bmatrix}\left(1-\frac{16}{3\pi}q_1+\frac{3}{4}q_1^2\right) & \left(1+\frac{3}{4}q_2^2\right) & \left(1-\frac{16}{3\pi}q_3+\frac{3}{4}q_3^2\right) & \left(1+\frac{3}{4}q_4^2\right)\end{bmatrix}^T \tag{5.10}$$

$$A=\begin{bmatrix}A_1 & A_2 & A_3 & A_4\end{bmatrix}^T \tag{5.11}$$

$$B=\begin{bmatrix}B_1 & B_2 & B_3 & B_4\end{bmatrix}^T \tag{5.12}$$

$$C=\begin{bmatrix}C_1 & C_2 & C_3 & C_4\end{bmatrix}^T \tag{5.13}$$

$$D=\begin{bmatrix}D_1 & D_2 & D_3 & D_4\end{bmatrix}^T \tag{5.14}$$

$$E=\begin{bmatrix}E_1 & E_2 & E_3 & E_4\end{bmatrix}^T \tag{5.15}$$

$$F=\begin{bmatrix}F_1 & F_2 & F_3 & F_4\end{bmatrix}^T \tag{5.16}$$

The Coefficients of eqs. (6.18)–(6.23) are as follows:

$$
\begin{aligned}
A_1 &= \beta[V_{\mathrm{DC}} + V_{\mathrm{AC}}\cos(\Omega t)]^2 + \pi^2(P - v^2) + \pi^4(\zeta + 1) \\
B_1 &= \frac{16}{3}[(\pi(v^2 - P) - \pi^3(\zeta + 1)] \\
C_1 &= \frac{1}{4}[3\pi^2(P - v^2) + 3\pi^4(\zeta + 1) + 2\pi^4\alpha] \\
D_1 &= -\frac{8}{3}\pi^3\alpha \\
E_1 &= \frac{3}{8}\pi^4\alpha \\
F_1 &= -\frac{4}{\pi}(\beta + 1)[V_{\mathrm{DC}} + V_{\mathrm{AC}}\cos(\Omega t)]^2
\end{aligned}
\tag{5.17}
$$

$$
\begin{aligned}
A_2 &= \beta[V_{\mathrm{DC}} + V_{\mathrm{AC}}\cos\Omega t]^2 + 4\pi^2(P - v^2) + 16\pi^4(\zeta + 1) \\
B_2 &= 0 \\
C_2 &= 3\pi^2(P - v^2) + 12\pi^4(\zeta + 1) + 8\alpha\pi^4 \\
D_2 &= 0 \\
E_2 &= 6\pi^4\alpha \\
F_2 &= 0
\end{aligned}
\tag{5.18}
$$

$$
\begin{aligned}
A_3 &= \beta[V_{\mathrm{DC}} + V_{\mathrm{AC}} \cos \Omega t]^2 + 9\pi^2(P - v^2) + 81\pi^4(\zeta + 1) \\
B_3 &= \pi 16(v^2 - P) - \pi^3 144(\zeta + 1) \\
C_3 &= \frac{1}{4}[27\pi^2(P - v^2) + 243\pi^4(\zeta + 1) + 162\alpha\pi^4] \\
D_3 &= -72\alpha\pi^3 \\
E_3 &= \frac{243}{8}\pi^4\alpha \\
F_3 &= -\frac{4}{3\pi}(\beta + 1)[V_{\mathrm{DC}} + V_{\mathrm{AC}} \cos \Omega t]^2
\end{aligned}
\tag{5.19}
$$

$$
\begin{aligned}
A_4 &= \beta[V_{\mathrm{DC}} + V_{\mathrm{AC}} \cos \Omega t]^2 + 16\pi^2(P - v^2) + 256\pi^4(\zeta + 1) \\
B_4 &= 0 \\
C_4 &= 12\pi^2(P - v^2) + 192\pi^4(\zeta + 1) + 128\alpha\pi^4 \\
D_4 &= 0 \\
E_4 &= 96\pi^4\alpha \\
F_4 &= 0
\end{aligned}
\tag{5.20}
$$

The natural frequencies are

$$\omega_1 = \sqrt{\beta[V_{\mathrm{DC}} + V_{\mathrm{AC}}\cos(\Omega t)]^2 + \pi^2(P - v^2) + \pi^4(\zeta + 1)} \tag{5.21}$$

$$\omega_2 = \sqrt{\beta[V_{\mathrm{DC}} + V_{\mathrm{AC}}\cos\Omega t]^2 + 4\pi^2(P - v^2) + 16\pi^4(\zeta + 1)} \tag{5.22}$$

$$\omega_3 = \sqrt{\beta[V_{\mathrm{DC}} + V_{\mathrm{AC}}\cos\Omega t]^2 + 9\pi^2(P - v^2) + 81\pi^4(\zeta + 1)} \tag{5.23}$$

$$\omega_4 = \sqrt{\beta[V_{\mathrm{DC}} + V_{\mathrm{AC}}\cos\Omega t]^2 + 16\pi^2(P - v^2) + 256\pi^4(\zeta + 1)} \tag{5.24}$$

To study the "static" behavior (pull-in voltage of the axially moving micro-beam under DC voltage) the time-varying model coordinates are set to zero and the resulted nonlinear algebraic equations are solved numerically using the Newton–Raphson method. To find the frequency response curves, the second-order differential eq. (5.8) are solved numerically by the commercial software MATLAB. The function ode45, based on an explicit Runge-Kutta method, is adopted. The initial conditions, deflection and velocity, are taken to be zero ($q_1 = \dot{q}_1 = 0$). The equation is solved over a long period of dimensionless time $t = [0 - 2000]$ to obtain the steady-state solution, the so-called long-time integration.

5.1 Effect of Applied Voltages on The First Natural Frequency

The fundamental frequency eq. (5.21) of the beam is a function of the applied DC and AC voltages. Figure 5.1 shows the variation of the first dimensionless frequency with respect to the applied DC voltage. The AC voltage amplitude equals 0. We can see that the effect of the DC voltage is due to the presence of the fringing field parameter β and as this parameter increases the effect of the DC voltage on the dimensionless frequency becomes relatively significant.

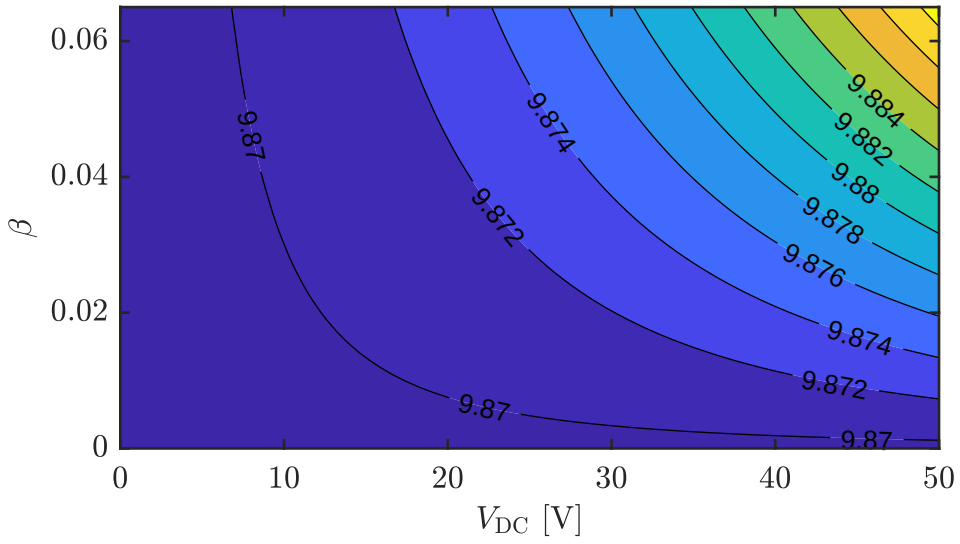

Figure 5.1 Variation of ω_1 with respect to V_{DC} and β

5.2 Response Under DC Load

The static behavior and voltage pull-in for simply supported micro-beams are presented in this section. For static response, all terms with time varying are set to zero. The time-varying model coordinates are replaced with unknown constant coefficients. The result is a system of nonlinear algebraic equations, which can be solved numerically using the Newton–Raphson method [9] . Equation (5.4) becomes

$$A\ q_1 + B\ q_1^2 + C\ q_1^3 + D\ q_1^4 + E\ q_1^5 + F = 0 \tag{5.25}$$

where

$$\begin{aligned}
A &= \beta V_{\mathrm{DC}}^2 + \pi^2(P - v^2) + \pi^4(\zeta + 1) \\
B &= \frac{16}{3}\Big[\pi(v^2 - P) - \pi^3(\zeta + 1)\Big] \\
C &= \frac{1}{4}\Big[3\pi^2(P - v^2) + 3\pi^4(\zeta + 1) + 2\pi^4\alpha\Big] \\
D &= -\frac{8}{3}\pi^3\alpha \\
E &= \frac{3}{8}\pi^4\alpha \\
F &= -\frac{4}{\pi}(\beta + 1)V_{\mathrm{DC}}^2
\end{aligned} \tag{5.26}$$

5.2.1 Effect of governing parameters

Throughout the analysis of the static response, we will take the length scale parameter as $l = 0$ µm and the gap width is $g = 2$ µm unless otherwise mentioned. The following subsections show the effect of dimensionless axial velocity, applied DC voltage on the deflection of the beam.

Effect of dimensionless axial velocity

Figure 5.2 shows that as the axial velocity increases the beam's deflection increases. This might be critical when the applied DC voltage is near the pull-in voltage

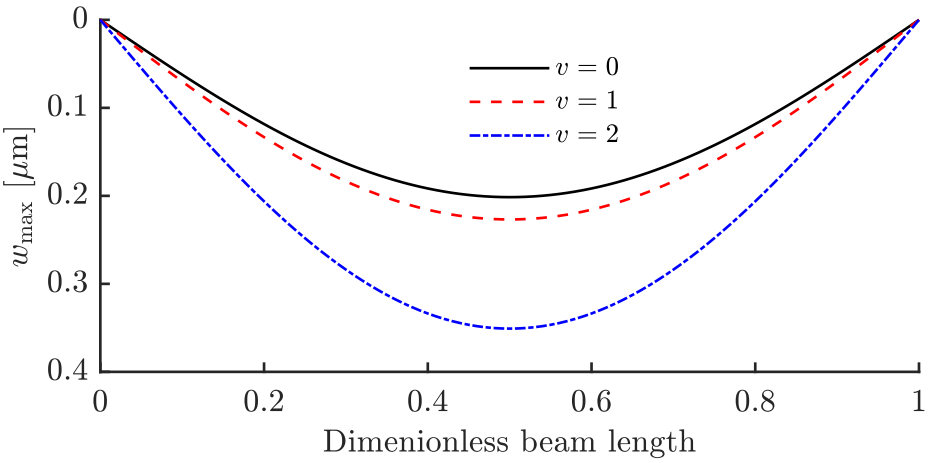

Figure 5.2 Beam deflection versus beam length at $V_{\mathrm{DC}} = 50$ V

Effect of applied DC voltage

Figure 5.3 shows the effect of changing the DC voltage on the deflection of the beam. It is clear that as the DC voltage increases the beam deflects more and more.

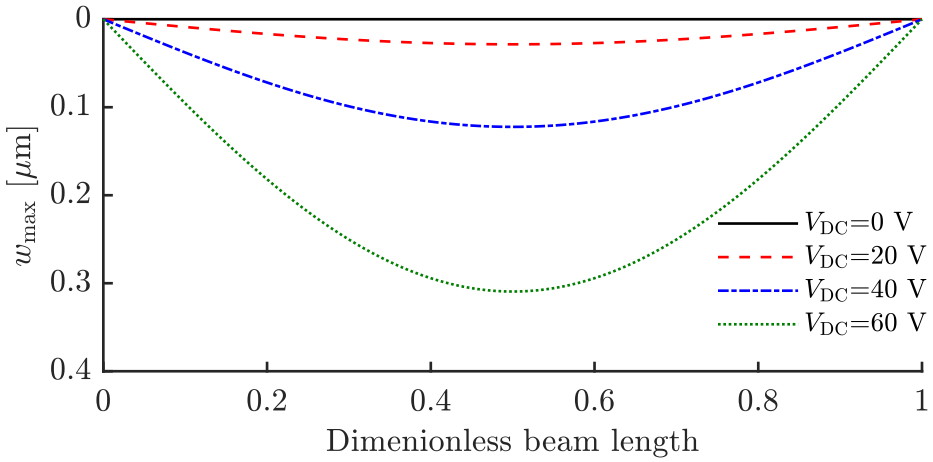

Figure 5.3 Beam deflection versus beam length at $v = 0$

5.2.2 Pull-in Voltage

The applied DC voltage has an upper limit after which the electrostatic force does not balance the elastic restoring force in the deformable micro-beam. When the applied DC voltage exceeds this limit, the micro-beam collapses. This phenomenon is called pull-in instability which has been observed experimentally by early studies [61,62]. In designing MEMS devices, the determination of the pull-in

voltage is crucial. For some applications like micro-mirrors, e.g., [63] and micro-resonators, e.g., [64] the designer needs to avoid this critical voltage to achieve a stable motion. While in switching applications, e.g., [65], the designer takes advantage of this phenomenon to enhance the performance of their devices. Several factors affect the accuracy of determining the pull-in voltage including the electromechanical coupling and the nonlinear nature of the electrostatic force. Fringing field effect, mid-plane stretching, axial tension, small-size effect add further complexity to the model. Therefore, numerical investigations of the parameters mentioned above are considered in this section.

Figure 5.4 shows the maximum deflection of the beam which occurs at $x = \frac{L}{2}$ at different DC voltages. The pull-in voltage was found to be 72 V.

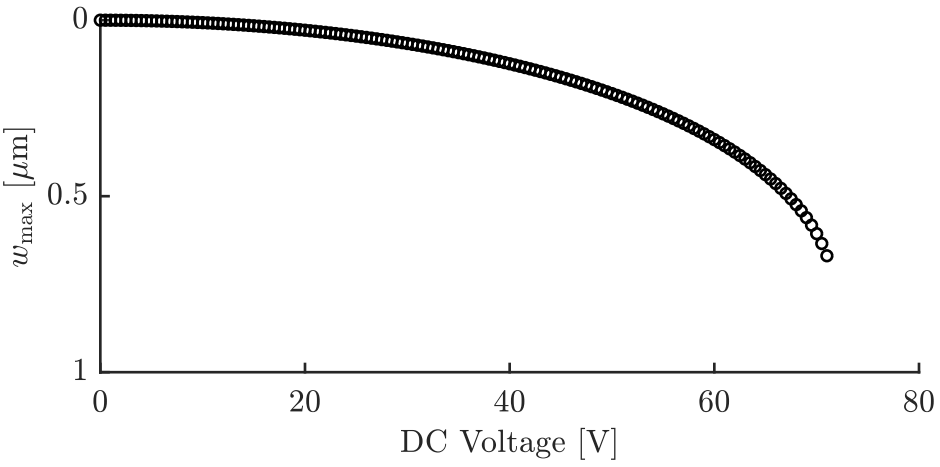

Figure 5.4 Maximum deflection versus DC voltage

Dimensionless axial velocity

Figure 5.5 shows the effect of increasing the dimensionless axial velocity on the pull-in voltage. As shown in the figure, the increase in the dimensionless axial velocity caused the pull-in voltage to drop significantly. That is, the increase in the axial velocity weakened the stiffness of the micro-beam. The percent drop of pull-in voltage at different velocities are presented in Table 5.1.

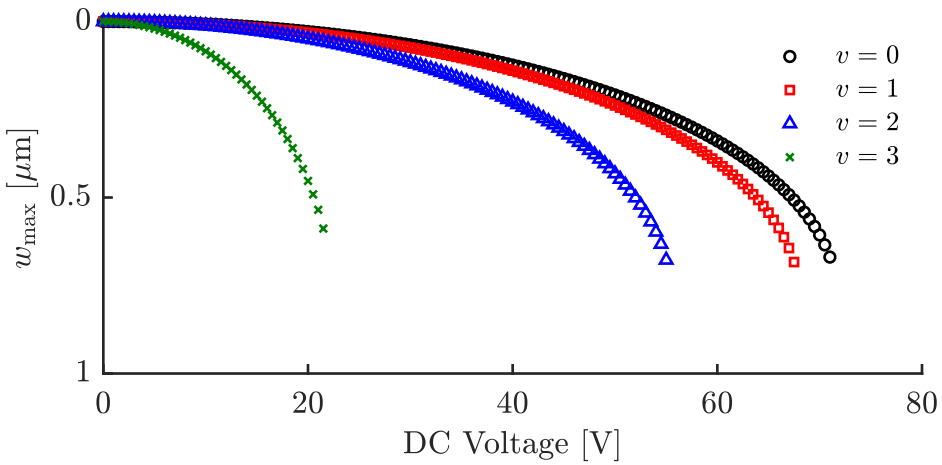

Figure 5.5 Maximum deflection versus DC voltage at different v

Table 5.1 Percent drop in pull-in voltage for different velocities

v	$V_{\text{pull-in}}$	Percent drop in $V_{\text{pull-in}}$
0	71	0
1	67.5	4.93
2	55	22.53
3	21.5	69.72

Length scale parameter

The effect of the material length scale parameter is shown in Figure 5.6. As the material scale parameter increased, the pull-in voltage increased. In other word, the appearance of the material length scale parameter increased the stiffness of the micro-beam. The percent increase in the pull-in voltage is presented in Table 5.2.

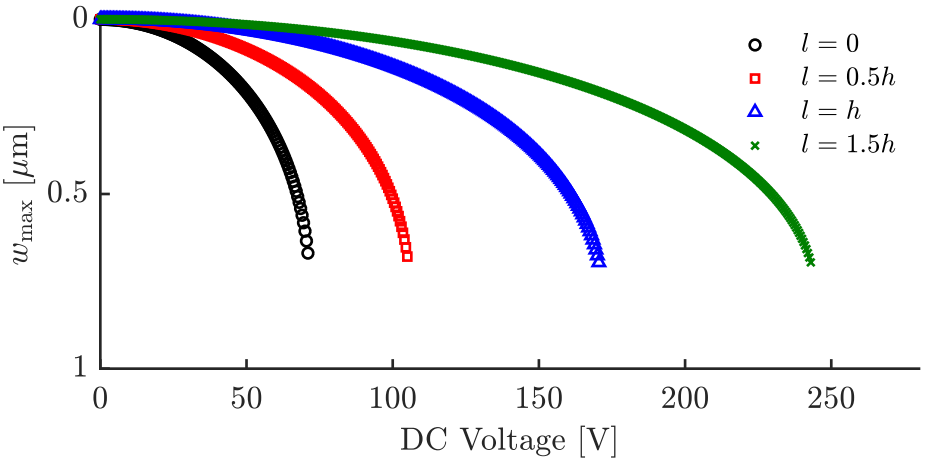

Figure 5.6 Maximum deflection versus DC voltage at different l

Table 5.2 Percent increase in pull-in voltage for different length scale parameters

l	$V_{\text{pull-in}}$	Percent increase in $V_{\text{pull-in}}$
0	71	0
$0.5h$	105	47.98
h	170.5	140.14
$1.5h$	243	242.25

Fringing field parameter

Figure 5.7 shows a zoom-in view of the effect of the fringing field parameter on the pull-in voltage. It was observed that when the fringing field was considered, the pull-in phenomenon occured at lower voltages.

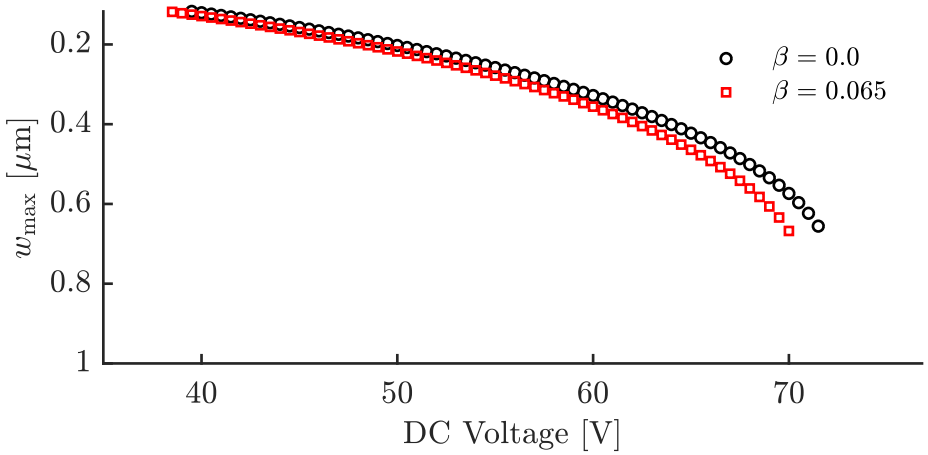

Figure 5.7 Pull-in voltages at different β

Dimensionless tension

The effect of the dimensionless tension, in the studied levels, was insignificant. Figure 5.8 shows that the effect of P takes place in increasing the maximum deflection of the micro-beam before pull-in voltage occured. However, the pull-in voltage was found to be the same 72 V.

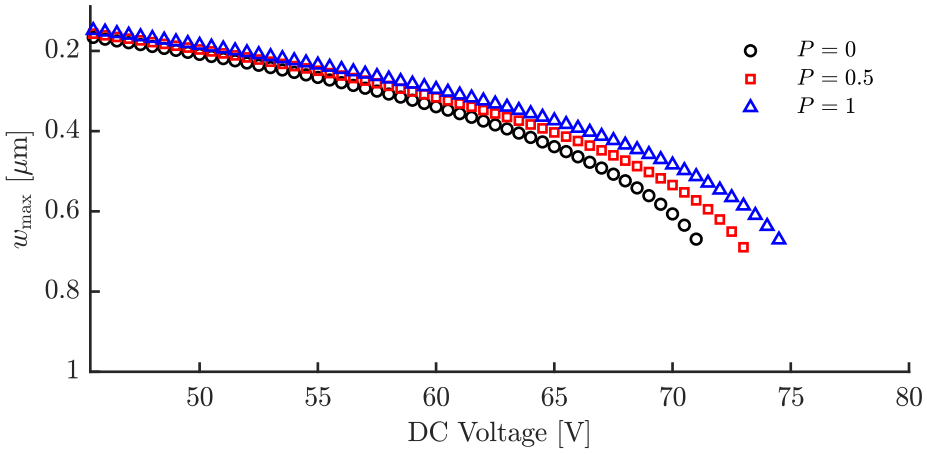

Figure 5.8 Pull-in voltages at different P

Mid-plane stretching parameter

Figure 5.9 indicates that as the stretching parameter increased the the pull-in voltage increased as well.

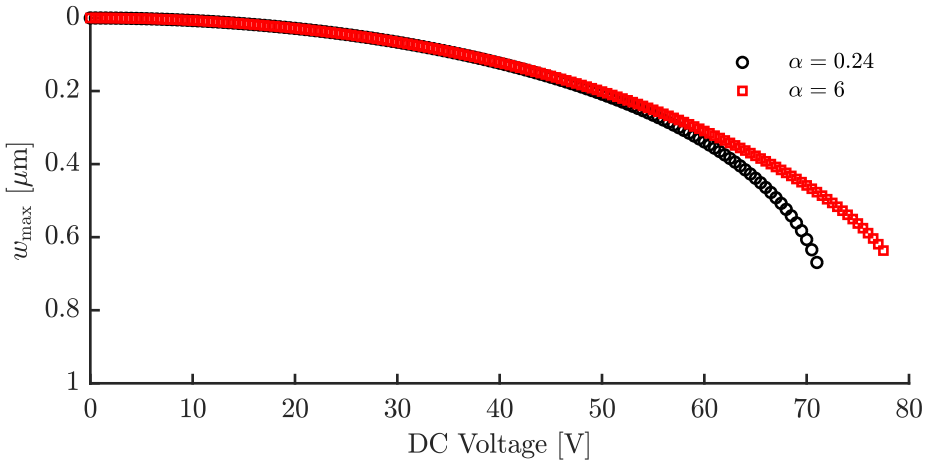

Figure 5.9 Pull-in voltages at different α

5.3 Response Under DC and AC Loads

The dynamic response of the system was analyzed through phase portrait, time history and frequency response curves for primary resonance excitation.

5.3.1 Phase portrait for stationary micro-beams

Waveforms and phase portraits can be used to differentiate chaotic behaviors from regular behaviors of dynamical systems. In this section, we plot the waveform and phase portrait for the forced vibration of an axially moving micro-beam in transverse vibration.

Generally, visualization of time waveforms is a straightforward method for dynamic system analysis because periodic waveforms represent a patter. On the other hand, chaotic waveforms appear to be shaking. Waveforms of equilibrium or periodic behaviors are regular while waveforms of chaotic behaviors are irregular.

The phase portrait is the geometric representation of the system trajectories in the phase plane and includes coordinate frames defined by the independent variables that describe the system dynamics where all possible states (position and veloc-

ity) can be represented. Phase portraits are essential for the study of dynamical systems. They unveil information such as whether an attractor or a limit cycle is presented for a chosen parameter values. In the phase plane, a fixed point represents a stationary system, while a closed orbit (limit cycle) represents a periodic system. Chaotic behavior is characterized by irregular trajectories confined to a well-defined region in the phase plane, known as stranger attractor, where orbits never repeat the same trajectory.

The phase portrait and time history for a stationary micro-beam are shown in Figure 5.10. We consider two sets of applied DC and AC voltages. The first set is when $V_{\text{AC}} = 2$ V and $V_{\text{DC}} = 50$ V. And the second one is when $V_{\text{AC}} = 2$ V and $V_{\text{DC}} = 50$ V. The AC frequency Ω is 8 which is near the fundamental frequency of the micro-beam ($\omega_1 = 9.87$). For a higher applied DC voltage Figure 5.10(a), the deflection was larger than the one in Figure 5.10(b) which was anticipated since higher DC voltages resulted in a higher deflection of the micro-beam. The selection of these two sets of applied voltages will be justified when we discuss the frequency response amplitude.

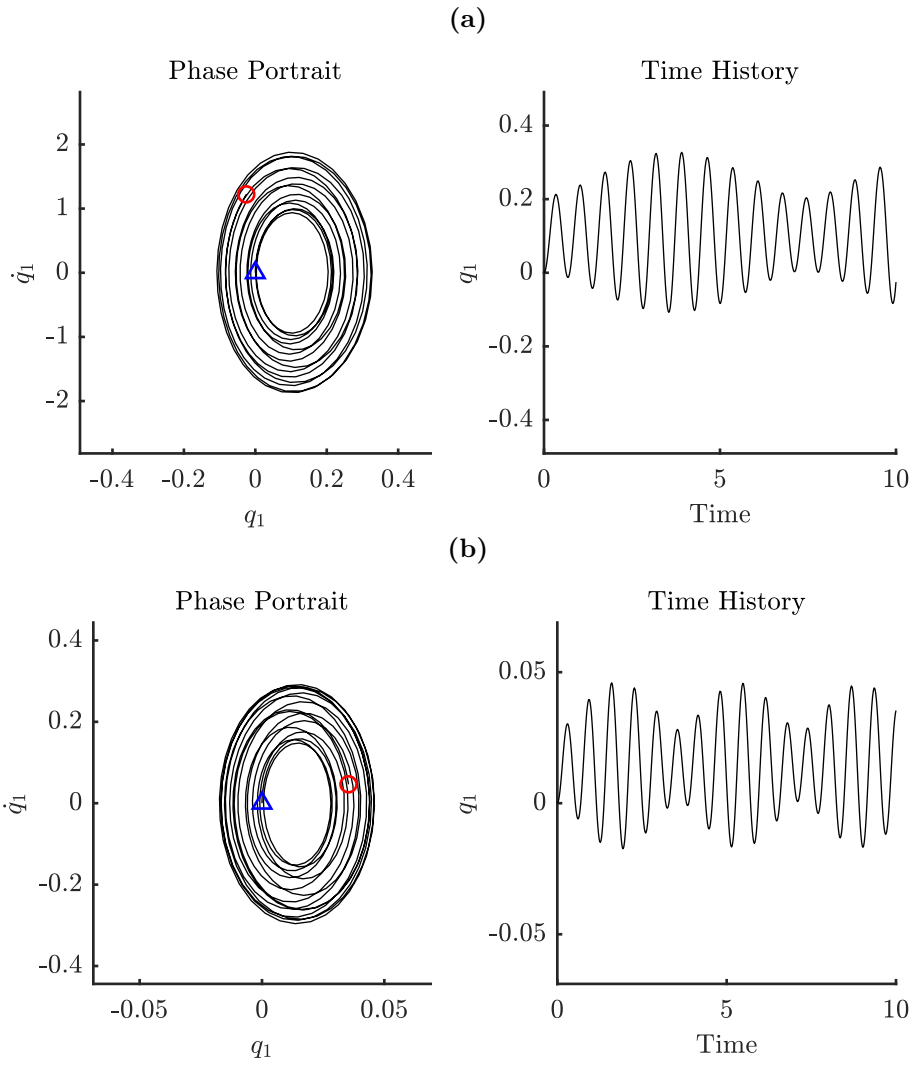

Figure 5.10 Phase portraits when $V_{\mathrm{AC}} = 2$ V and (a) $V_{\mathrm{DC}} = 50$ V (b) $V_{\mathrm{DC}} = 20$ V

5.3.2 Phase portrait for axially moving micro-beams

In this subsection, we study the effect of the axial speed on the phase portrait and the time history of the micro-beam. We apply two different sets of DC and AC defined in the previous Section 5.3.1.

Figure 5.11 shows the phase portrait and time history when $V_{\mathrm{DC}} = 50$ V and $V_{\mathrm{AC}} = 2$ V for different axial speeds. Figures 5.11(a)–5.11(e) indicate that the micro-beam was stable over this range of velocities. The maximum deflection of the micro-beam that could occur without losing stability was shown in the case of Figure 5.11(b). However, once the axial speeds exceeded 2.1 the micro-beam collapsed as shown in Figures 5.11(f) and 5.11(g). The corresponding natural frequency and maximum deflection at each level of the axial velocity are presented in Table 5.3(a).

Figure 5.12 shows the phase portrait and time history when $V_{\mathrm{DC}} = 20$ V and $V_{\mathrm{AC}} = 2$ V. All figures show stable response. However, when the axial velocity v was1.8 the fundamental frequency of the micro-beam ω_1 became 8.1 which is very close to the excitation frequency Ω; hence, the amplitude increased at

this particular axial velocity as shown in Figure 5.12(d). Once the axial velocity further increased, the fundamental frequency decreased and shifted away from the excitation frequency. The fundamental frequencies and maximum deflections are presented in Table 5.3(b).

(a)

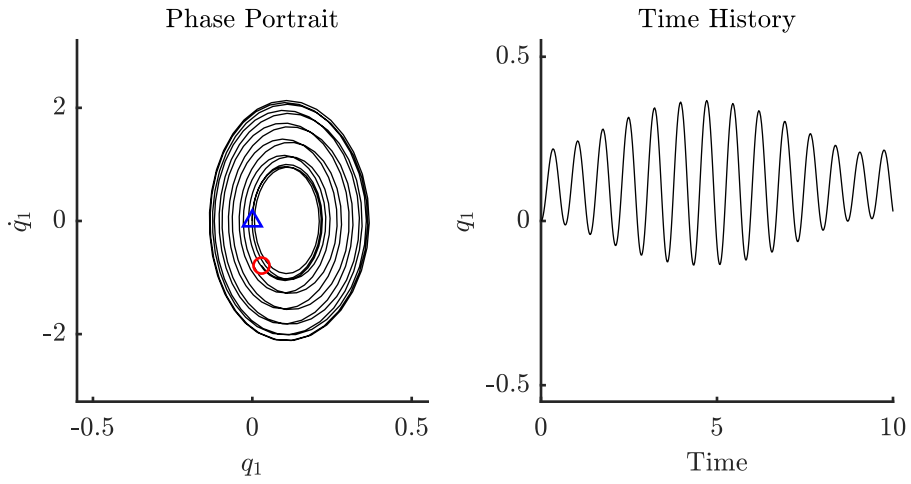
Phase Portrait
Time History
2
0
-2
$\dot{q}_1$
-0.5
0
0.5
q_1
0.5
0
-0.5
q_1
0
5
10
Time

(b)

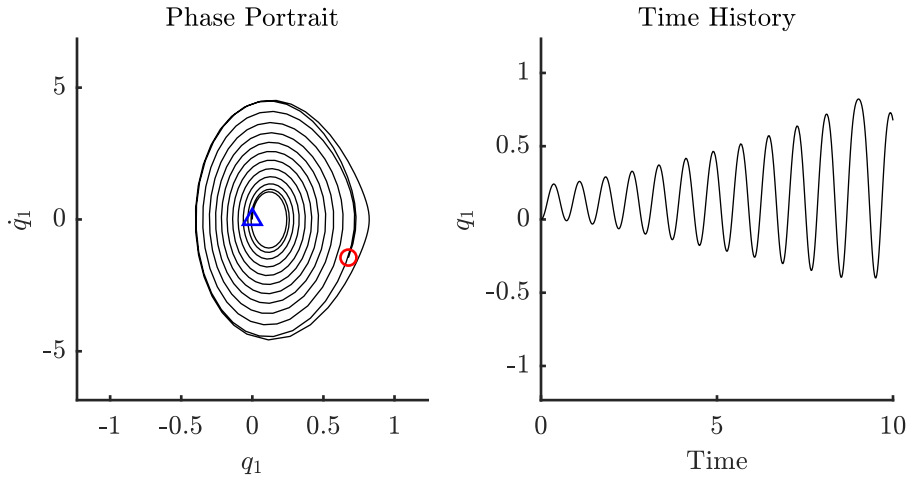
Phase Portrait
Time History
5
0
-5
$\dot{q}_1$
-1
-0.5
0
0.5
1
q_1
1
0.5
0
-0.5
-1
q_1
0
5
10
Time

(c)

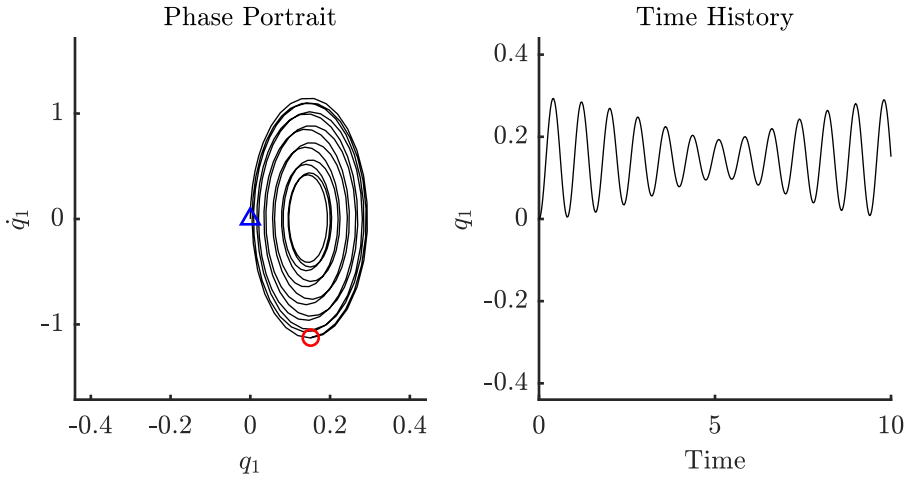
Phase Portrait
Time History
$\dot{q}_1$
q_1
Time
1
0
-1
-0.4
-0.2
0.2
0.4
5
10

(d)

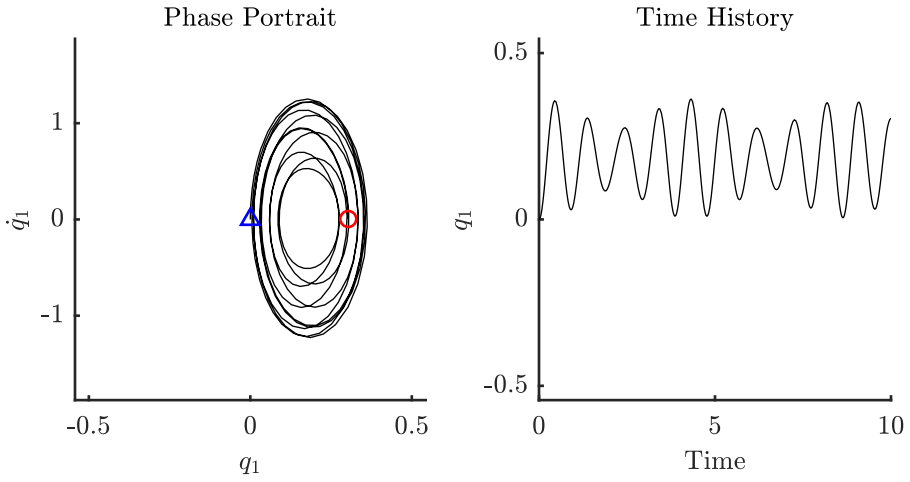
Phase Portrait
Time History
$\dot{q}_1$
q_1
Time
1
0
-1
-0.5
0.5
5
10

(e)

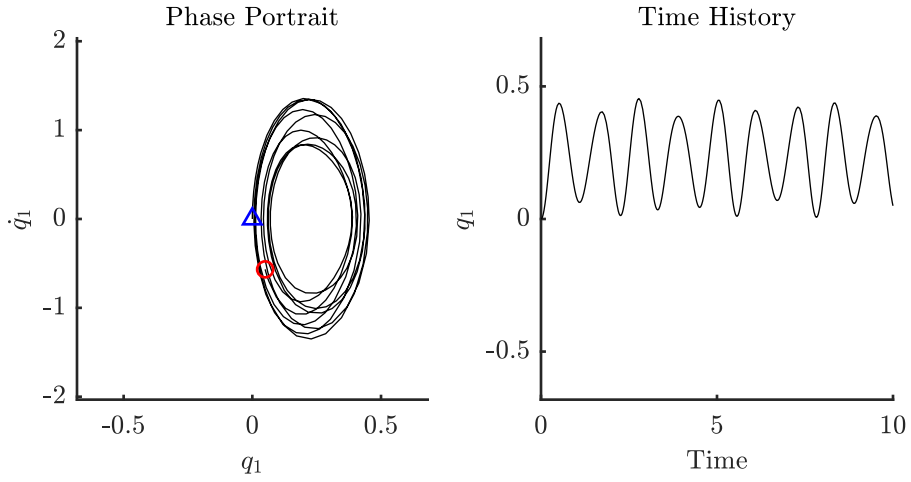
Phase Portrait
Time History
$\dot{q}_1$
q_1
Time
2
1
0
-1
-2
-0.5
0
0.5
0.5
0
-0.5
0
5
10

(f)

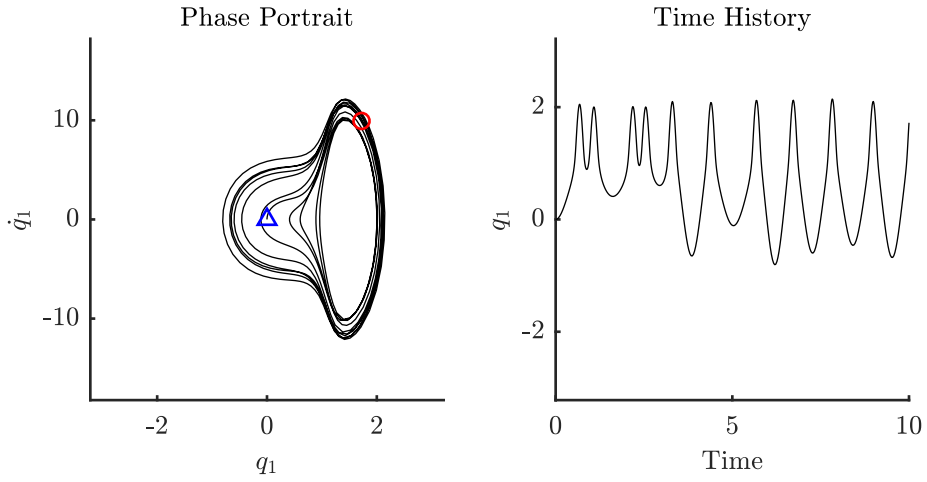
Phase Portrait
Time History
$\dot{q}_1$
q_1
Time
10
0
-10
-2
0
2
2
0
-2
0
5
10

(g)

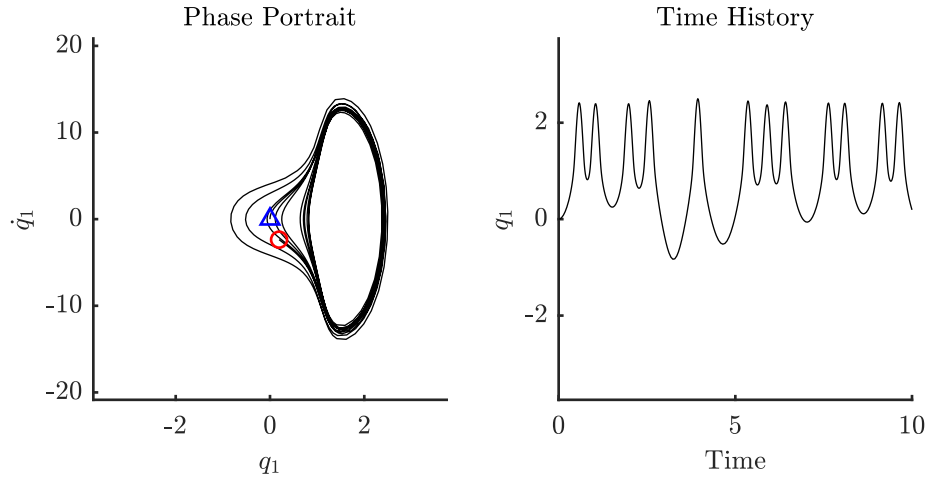

Figure 5.11 Phase portrait and time history at $V_{\mathrm{DC}} = 50$ V and $V_{\mathrm{AC}} = 2$ V for (a) $v = 0.5$ (b)) $v = 1$ (c) $v = 1.5$ (d) $v = 1.8$ (e) $v = 2$ ((f) $v = 2.5$ (g) $v = 3$. The trajectories start from (△) and end at (○)

Table 5.3 Maximum deflections and natural frequencies at different v

(a) Figure 5.11

v	ω_1	q_1
0	9.88	0.327
0.5	9.75	0.367
1	9.37	0.821
1.5	8.68	0.293
1.8	8.1	0.362
2	7.62	0.454
2.5	5.99	2.145
3	2.96	2.485

(b) Figure 5.12

v	ω_1	q_1
0	9.88	0.046
0.5	9.75	0.048
1	9.37	0.058
1.5	8.68	0.098
1.8	8.1	0.181
2	7.62	0.067
2.5	5.99	0.081
3	2.96	0.448

(a)

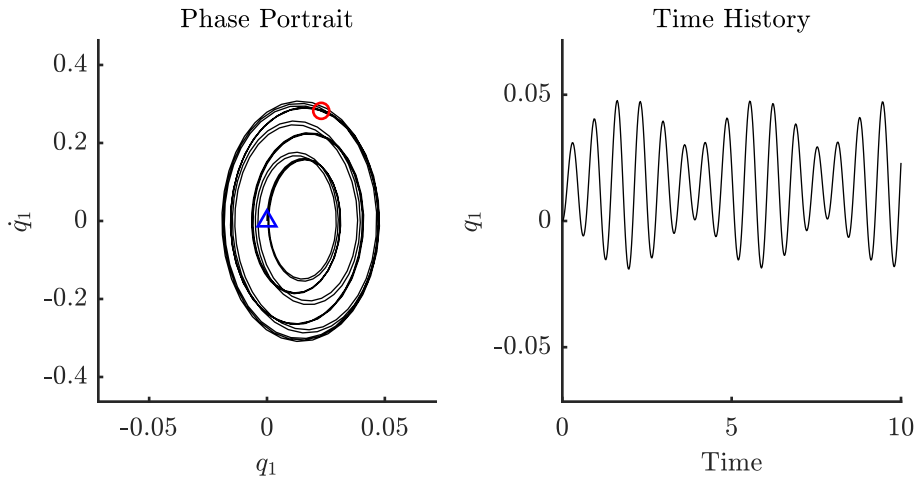
Phase Portrait
Time History
0.4
0.2
0
-0.2
-0.4
$\dot{q}_1$
-0.05
0
0.05
q_1
0.05
0
-0.05
q_1
0
5
10
Time

(b)

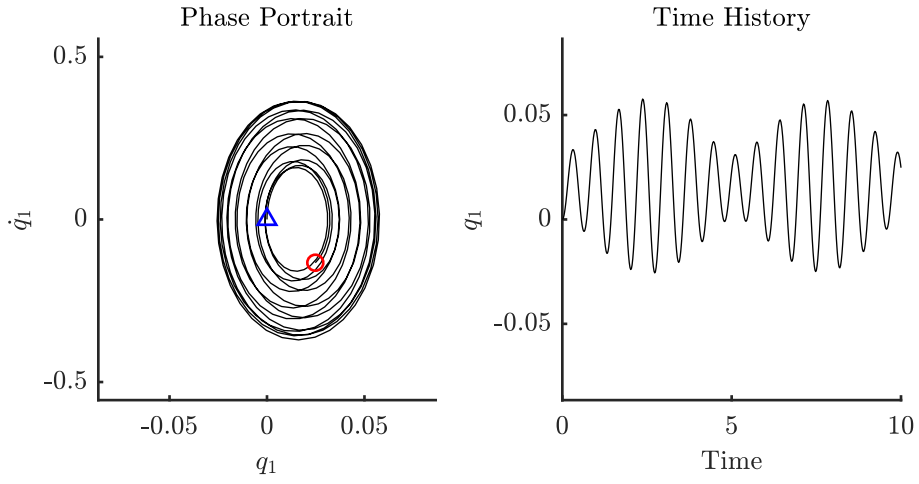
Phase Portrait
Time History
0.5
0
-0.5
$\dot{q}_1$
-0.05
0
0.05
q_1
0.05
0
-0.05
q_1
0
5
10
Time

(c)

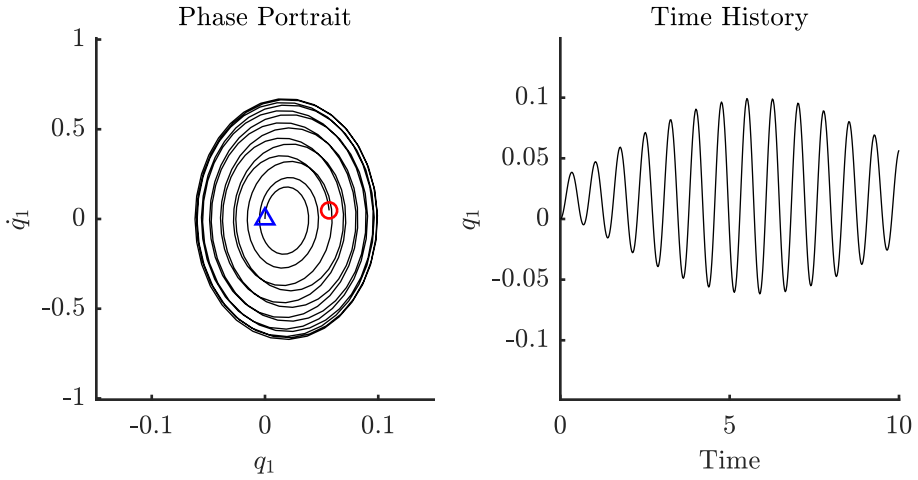
Phase Portrait
Time History
1
0.5
0
-0.5
-1
$\dot{q}_1$
-0.1
0
0.1
q_1
0.1
0.05
0
-0.05
-0.1
q_1
0
5
10
Time

(d)

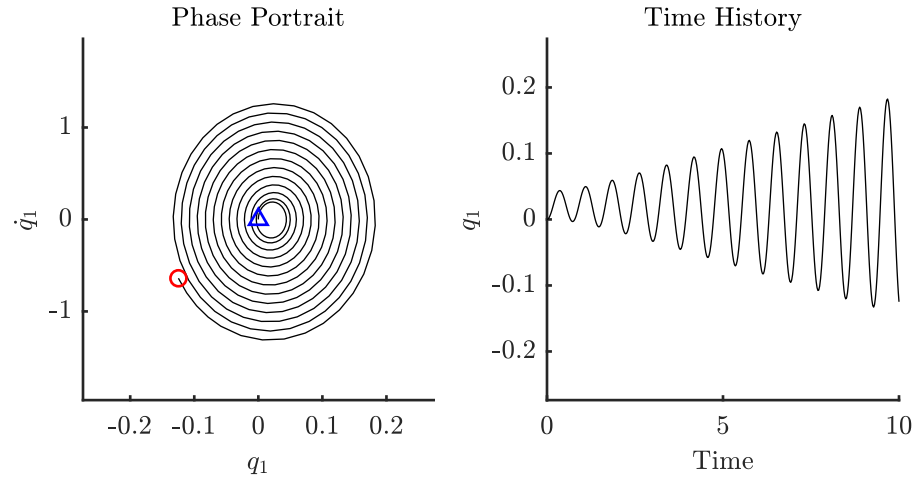
Phase Portrait
Time History
1
0
-1
$\dot{q}_1$
-0.2
-0.1
0
0.1
0.2
q_1
0.2
0.1
0
-0.1
-0.2
q_1
0
5
10
Time

(e)

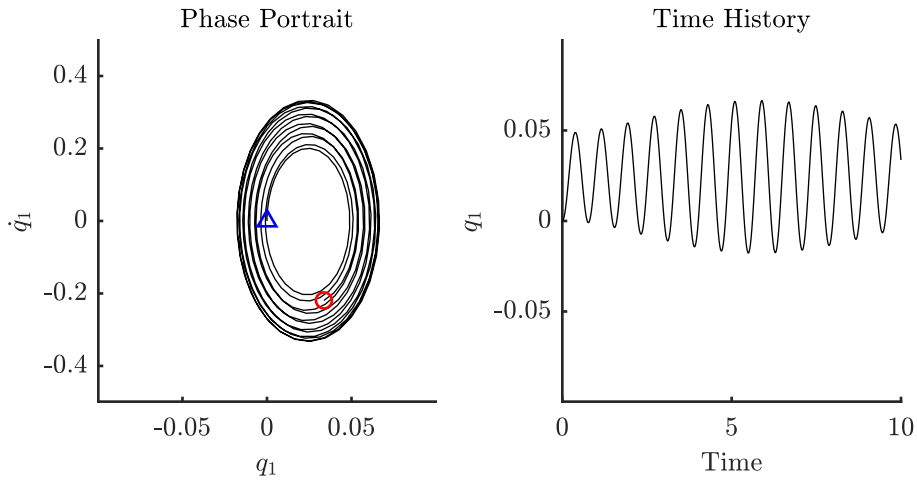
Phase Portrait
Time History
0.4
0.2
0
-0.2
-0.4
$\dot{q}_1$
-0.05
0
0.05
q_1
0.05
0
-0.05
q_1
0
5
10
Time

(f)

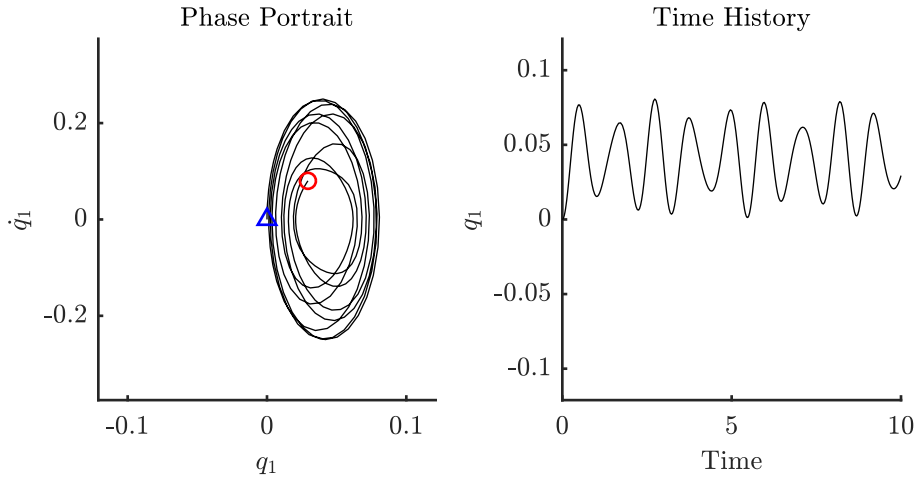
Phase Portrait
Time History
0.2
0
-0.2
$\dot{q}_1$
-0.1
0
0.1
q_1
0.1
0.05
0
-0.05
-0.1
q_1
0
5
10
Time

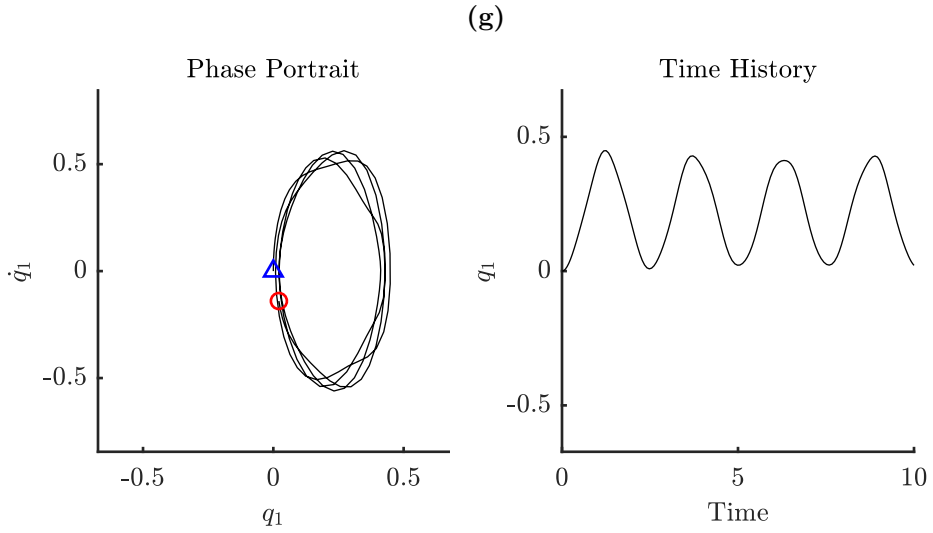

Figure 5.12 Phase portrait and time history at $V_{\mathrm{DC}} = 20$ V and $V_{\mathrm{AC}} = 2$ V for (a) $v = 0.5$ (b)) $v = 1$ (c) $v = 1.5$ (d) $v = 1.8$ (e) $v = 2$ ((f) $v = 2.5$ (g) $v = 3$. The trajectories start from (△) and end at (○)

5.3.3 Frequency response curves

Effect of applied voltages

Consider the the micro-beam properties given in Table 4.1. Figure 5.13 indicates a linear frequency response when the applied AC and DC voltages are low, i.e., $V_{\mathrm{DC}} = 5$ V and $V_{\mathrm{AC}} = 0.1$ V, The maximum deflection changed gradually with the increase of the dimensionless angular frequency. At a given angular frequency Ω, slight increase in Ω resulted in a gradual decrease of the maximum deflection. We did not observe any jump phenomenon.

Figure 5.14 shows a hardening frequency response behavior when we increased the applied DC and AC voltages to 20 V and 2 V, respectively. The maximum deflection increased gradually with the increase of the dimensionless angular frequency. Then the maximum deflection suddenly decreased, this point is called the first saddle-node bifurcation point. When the dimensionless angular frequency decreases from a high value, the maximum deflection increases gradually to a point where the maximum deflection jumps to the highest point, this point is called second-saddle bifurcation point.

Figure 5.15 indicates a softening frequency response when both DC and AC

voltages are at high values, $V_{\mathrm{DC}} = 50$ V and $V_{\mathrm{AC}} = 2$ V. The maximum deflection increased with the increase of the dimensionless angular frequency to a point where it suddenly jumped to a maximum value, first saddle-node bifurcation point. Then, the maximum deflection gradually decreased.

Figures 5.14 and 5.15 show that in order to have nonlinear frequency response, the AC voltage should be high enough, $V_{\mathrm{AC}} = 2$ V. The value of the applied DC voltage determines whether it is softening or hardening.

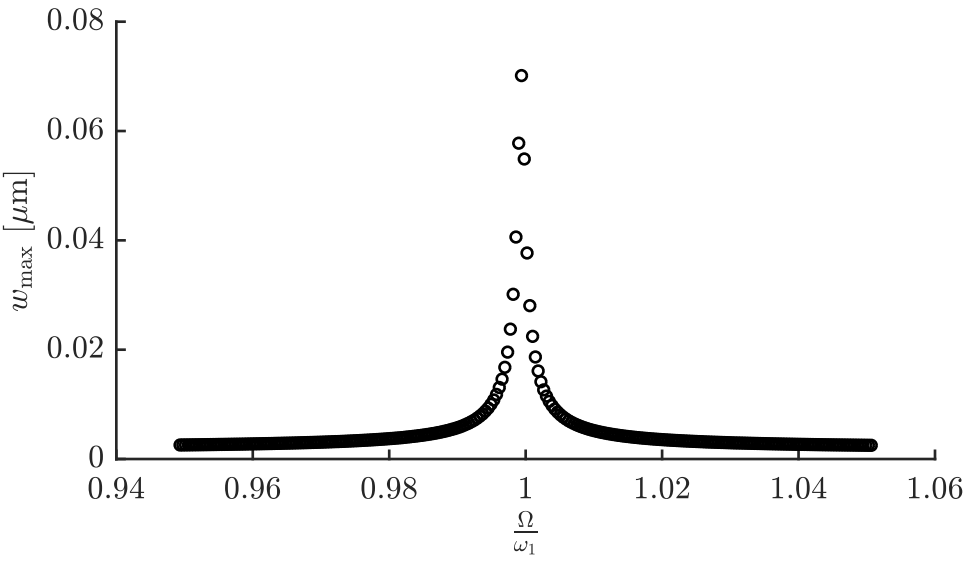

Figure 5.13 Linear frequency-response curve $V_{\mathrm{DC}} = 5$ V and $V_{\mathrm{AC}} = 0.1$ V

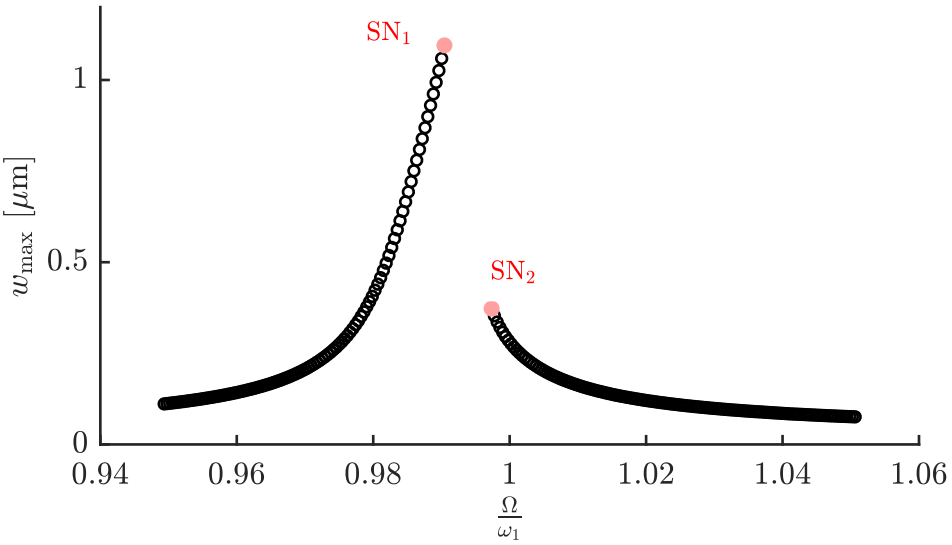

Figure 5.14 Hardening frequency response curve when $V_{\mathrm{DC}} = 20$ V and $V_{\mathrm{AC}} = 2$ V. SN_1 and SN_2 are saddle-point bifurcation

Effect of stretching parameter

Figure 5.16 shows the effect of increasing the stretching parameter α when we have hardening frequency response (i.e., $V_{DC} = 20$ V and $V_{AC} = 2$ V. It is shown that when the stretching parameter increaded, the hardening effect strenghtened due to increasing the mid-plane stretching which has a hardening effect.

Figure 5.17 shows the effect of increasing α when we have softening frequency response. When the stretching parameter was low ($\alpha = 0.24$) the electrostatic force dominated and hence we had softening effect. As the stretching parameter increased to 6, we observed that the effect of mid-plane stretching dominated the electrostatic force, and hence the frequency response exhibited hardening behav-

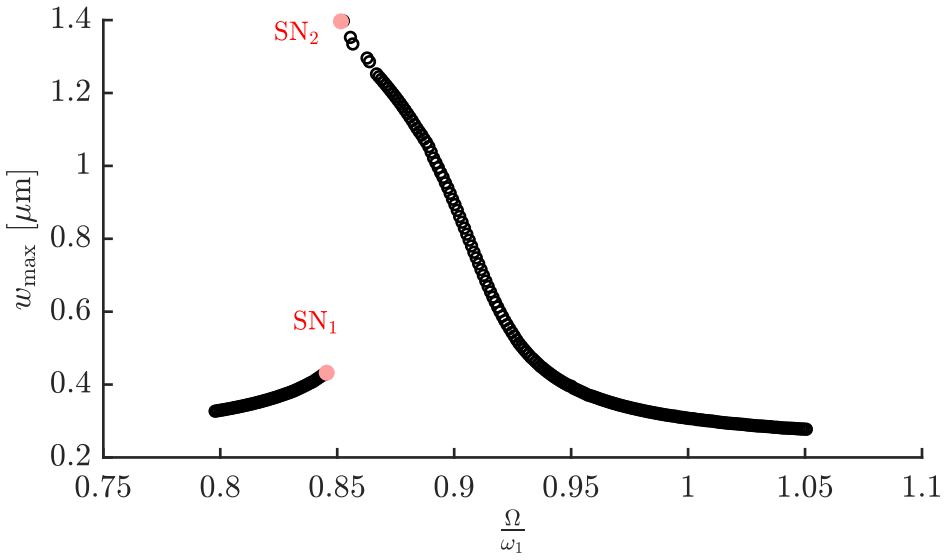

Figure 5.15 Softening frequency response curve when $V_{\mathrm{DC}} = 50$ V and $V_{\mathrm{AC}} = 2$ V. SN_1 and SN_2 are saddle-point bifurcation

ior.

The stretching parameter α quantifies the effect of mid-plane stretching, by increasing α the mid-plane stretching becomes more significant.

Effect of quality factor

Figures 5.18 and 5.19 shows the frequency response of the micro-beam at different levels of the quality factor. Both figures indicate that increasing the quality factor increased the hardening and softening effects. Therefore, the minimum AC voltage required to induce a softening / hardening nonlinearities decreased with the

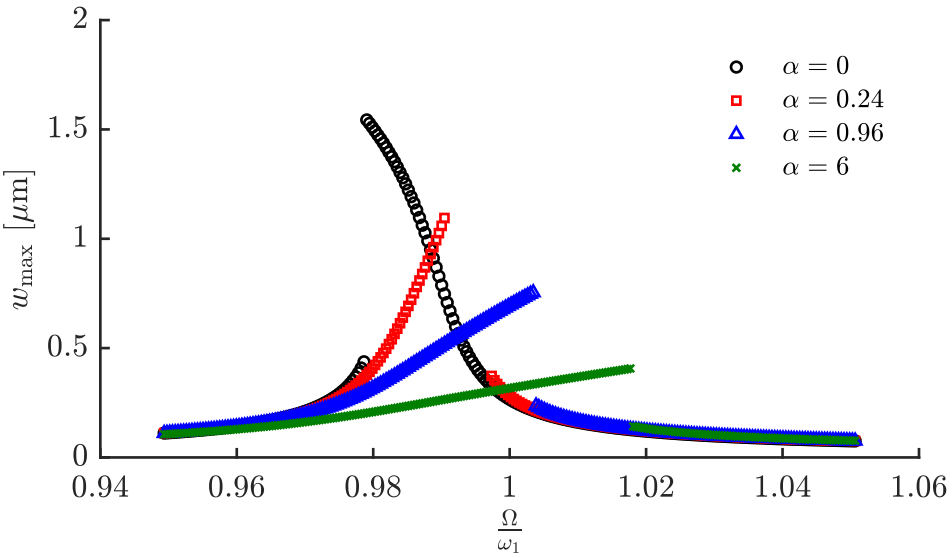

Figure 5.16 Hardening frequency response curves at different stretching parameters

increase of the quality factor. By referring to Equation (4.11), it indicates that the quality factor is inversely proportional to the dimensionless damping coefficient c. Therefore, the increase of Q reduced the damping effect, which eventually increased the beam's deflection. In this case, the nonlinear effects due to mid-plane stretching and electrostatic force became more significant, and a smaller AC voltage was needed to induce nonlinear frequency responses.

Effect of dimensionless axial velocity

Figures 5.20 and 5.21 show the frequency-response curves for different dimensionless velocities, v. It was observed that as the axial velocity increased the first saddle-node bifurcation points occured at lower dimensionless angular frequency.

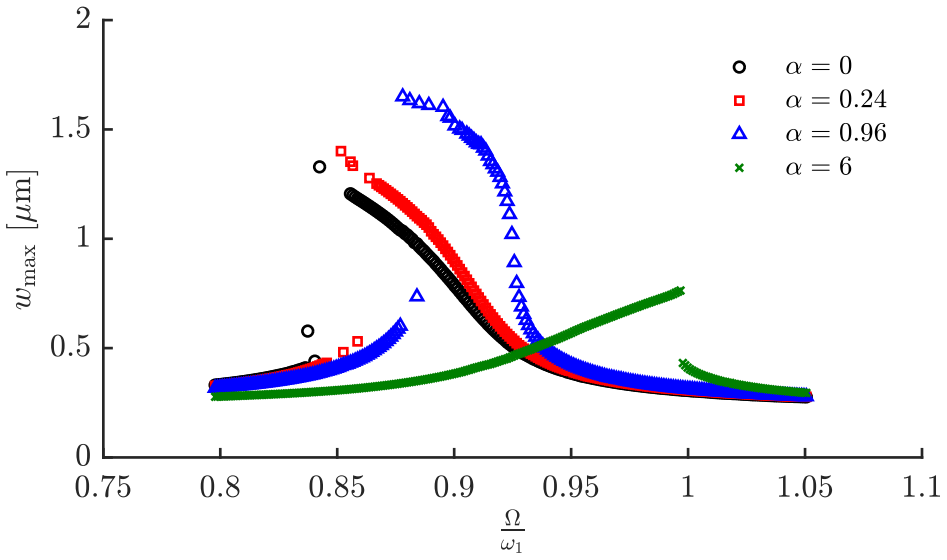

Figure 5.17 Softening frequency-response at different stretching parameters

This is explained by referring to the free vibration(Chapter 4) and see the effect of the axial velocity on the natural frequency which as the axial velocity increased the natural frequency of the micro-beam decreased Figure 4.4. Moreover, the shape of the frequency response curves were remained unchanged for both combinations of AC and DC voltages.

Effect of length scale parameter

Figure 5.22 depicts the effect of the length scale parameter on the softening frequency response ($V_{DC} = 50$ V and $V_{AC} = 2$ V) when the micro-beam is stationary. The increase in the length scale parameter decreased the maximum amplitude in the frequency response. Furthermore, the nonlinearity of the system decreased,

Table 5.4 Maximum deflection at different quality factors for (a) hardening frequency and (b) softening frequency.

(a) Figure 5.19

Q	c	$w_{\max}$	Percent Increase
100	0.0987	0.179	0
700	0.0141	0.764	3.08
1000	0.0055	0.782	3.17
1800	0.0099	0.867	3.62

(b) Figure 5.18

Q	c	$w_{\max}$	Percent Increase
100	0.0987	0.714	0
700	0.0141	0.993	0.34
1000	0.0055	1.010	0.36
1800	0.0099	1.061	0.43

by observing the shift of the nonlinear resonance frequency toward the linear natural frequency ω_1 (See Table 5.5). The same observation isshown for a hardening frequency response ($V_{DC} = 20$ V and $V_{AC} = 2$ V) in Figure 5.23.

Table 5.5 Occurrence of jump phenomenon for softening and hardening frequency response curves at different l

(a) Softening

l	$\frac{\Omega}{\omega_1}$
0	0.858
$0.5h$	0.949
h	0.983
$1.5h$	0.992

(b) Hardening

l	$\frac{\Omega}{\omega_1}$
0	0.997
$0.5h$	0.998
h	0.999
$1.5h$	0.999

Fringing field effect

The fringing field effect due to the finite size of the beam width is described by a fringing field parameter β which is defined in Table 3.1. The frequency response curves at different levels of the fringing field parameter are depicted in Figure 5.24. It was observed that the effect of β at the studied level wasinsignificant.

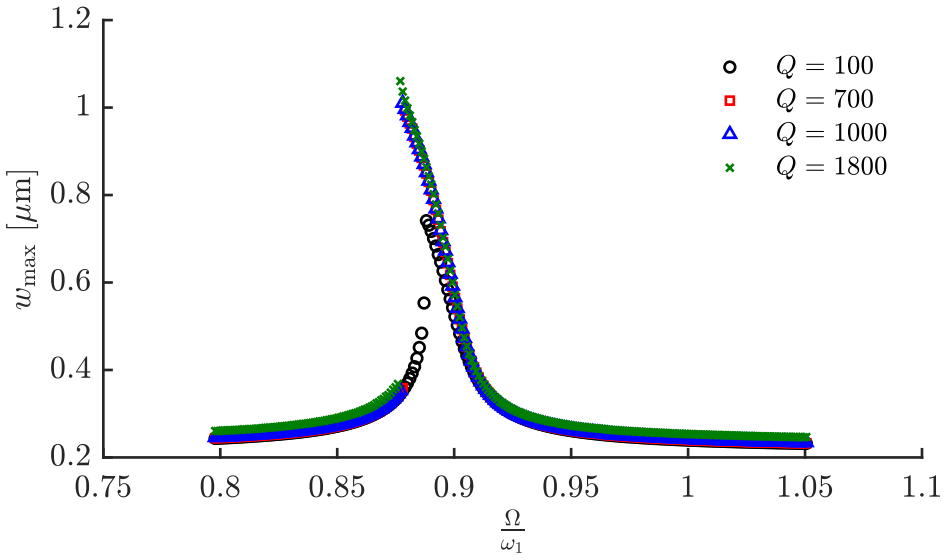

Figure 5.18 Frequency response curves at different quality factors when $V_{\mathrm{DC}} = 50$ V and $V_{\mathrm{AC}} = 0.5$ V

Effect of dimensionless tension

Figure 5.25 shows the effect of the dimensionless tension on the frequency response curves when the applied DC and AC voltages are 50 V and 20 V, respectively. As shown in the figure, the frequency response curves kept their shapes unchanged, but each curve shifted to the left. This is due to the increase of the dimensionless tension. From the free vibration chapter in Figure 4.4, we showed that the dimensionless natural frequency increased as the dimensionless tension increased.

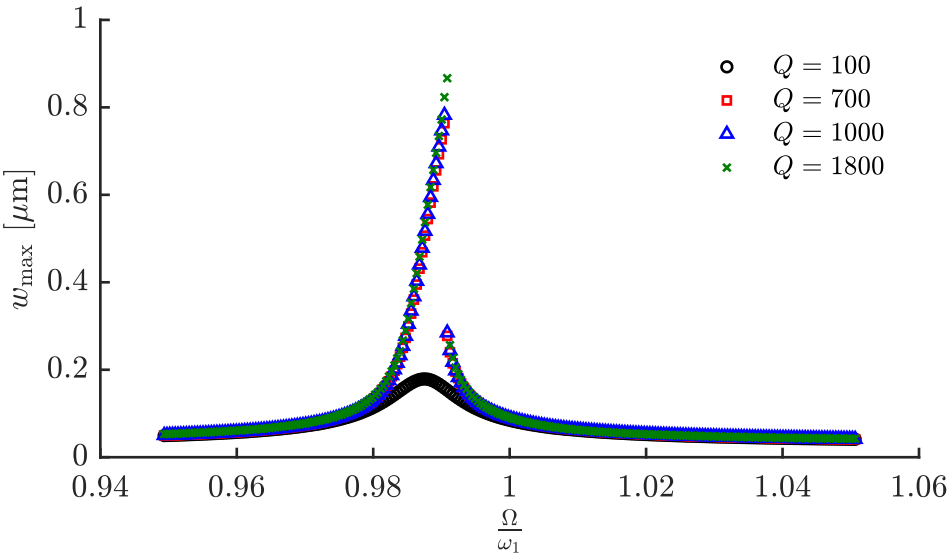

Figure 5.19 Frequency response curves at different quality factors, when $V_{\mathrm{DC}} = 50\mathrm{V}$ and $V_{\mathrm{AC}} = 0.5\mathrm{V}$

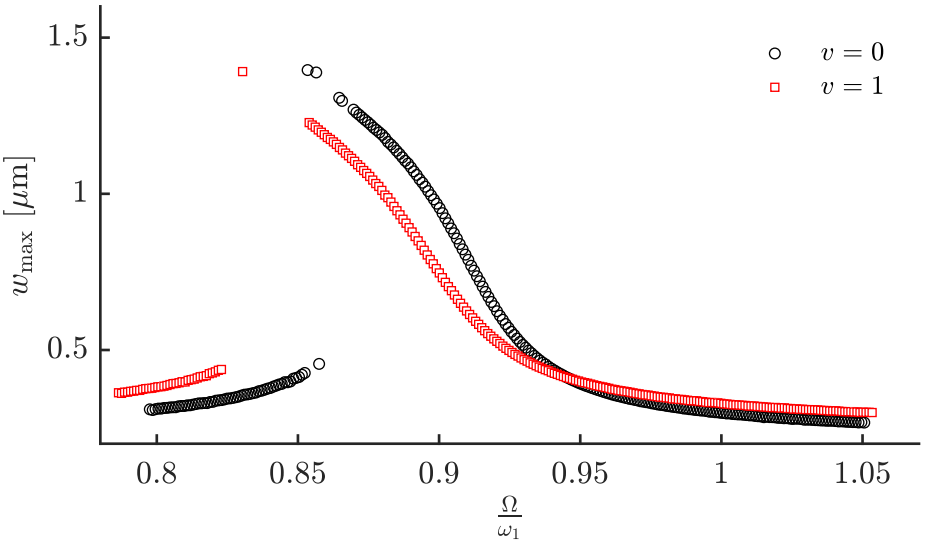

Figure 5.20 Softening frequency-response curves at at different v, when $V_{\mathrm{DC}} = 50$ V and $V_{\mathrm{AC}} = 2$ V

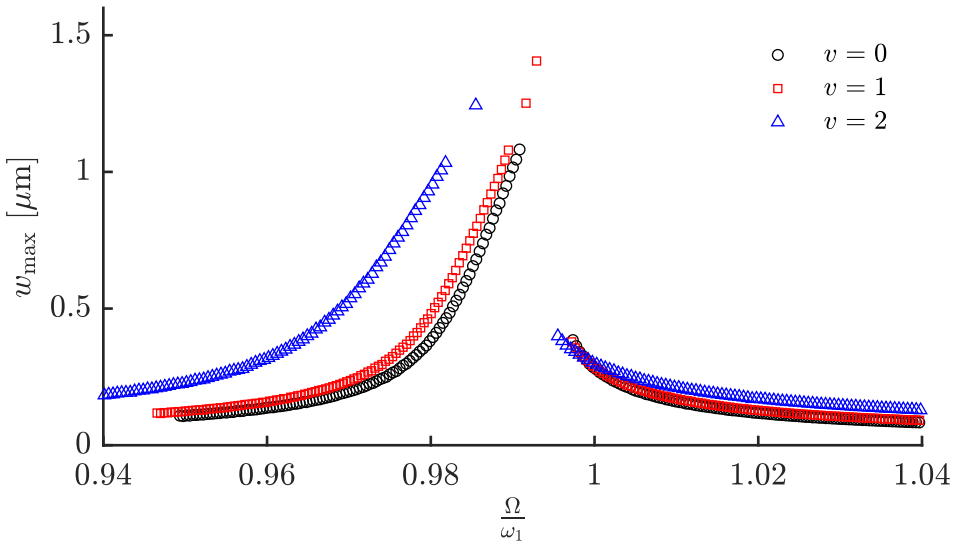

Figure 5.21 Hardening frequency-response curves at at different v, when $V_{\mathrm{DC}} = 50$ V and $V_{\mathrm{AC}} = 2$ V

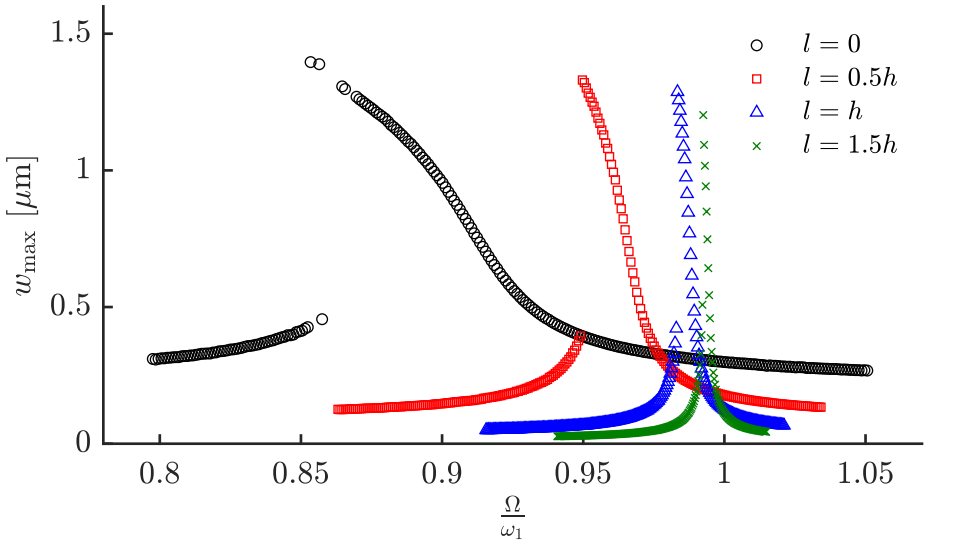

Figure 5.22 Softening frequency response curves at different l, when $\mathrm{V_{DC}} = 50$ V and $\mathrm{V_{AC}} = 2$ V

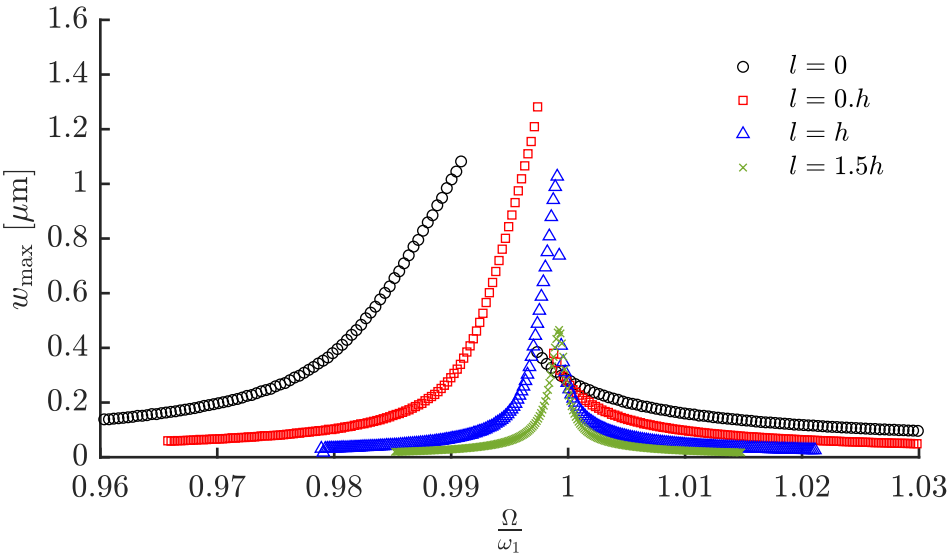

Figure 5.23 Hardening frequency response curves at different l, when $V_{DC} = 20$ V and $V_{AC} = 2$ V

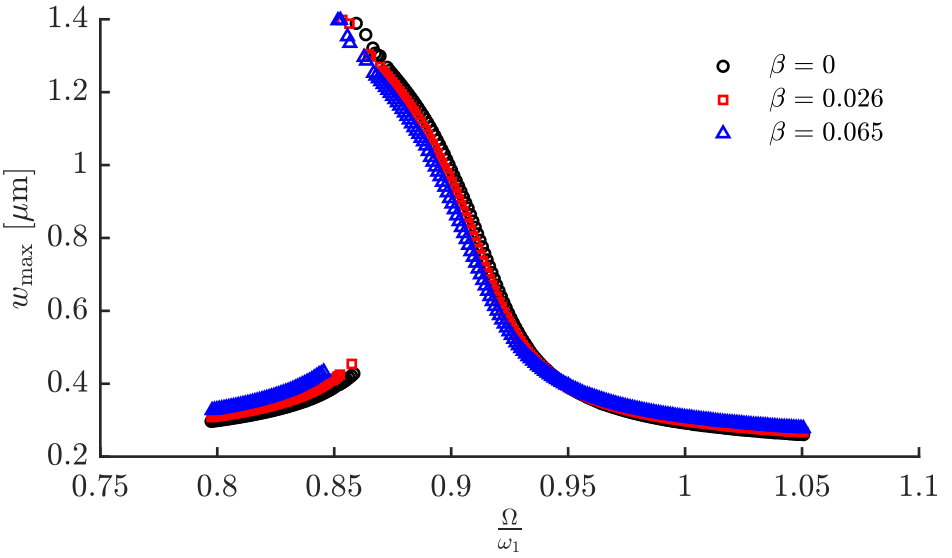

Figure 5.24 Softening frequency-response curves at different β

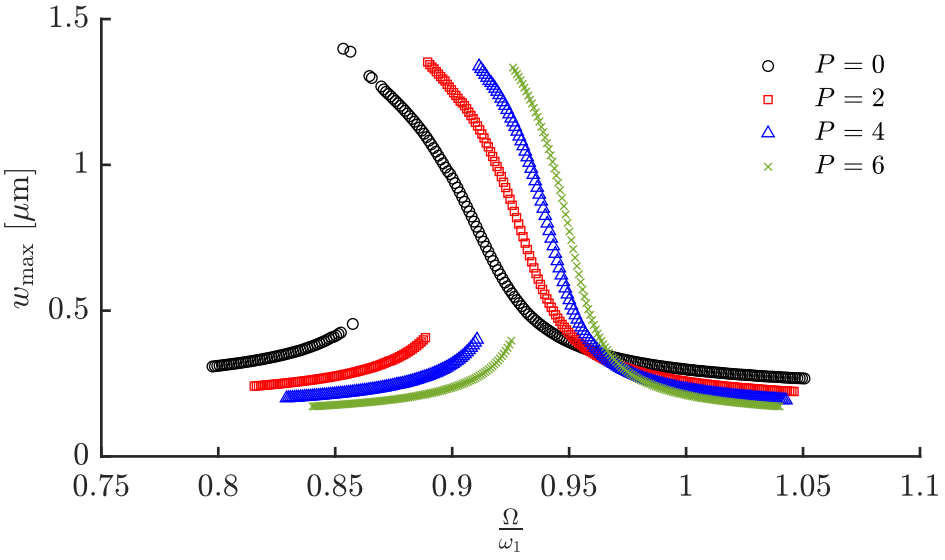

Figure 5.25 Softening frequency-response curves at at different P

Chapter 6

Micro-Beams Over Linearly Varying Electrostatic Gap

In this Chapter, we will consider two non-uniform electrostatic gap width models. The first model is when the micro-beam axially moves over a linearly increasing electrostatic gap width. The second model is when the micro-beam moves over a linearly decreasing electrostatic gap width.

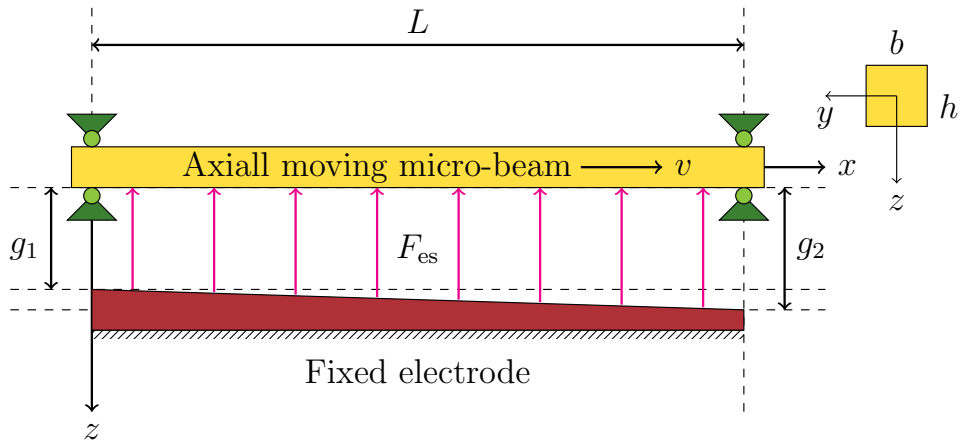

Figure 6.1 Axially moving micro-beam over linearly varying electrostatic gap

Figure 6.1 depicts an axially moving micro-beam over linearly varying electrostatic gap. This gap between the electrode and the bottom of the axially moving micro-beam has value of g_1 at $x = 0$ and a value of g_2 at $x = L$. The slope of the electrode, m, is given as

$$m = \frac{g_2 - g_1}{L} \tag{6.1}$$

Note that if g_2 is greater than g_1, m is positive and the gap is linearly increasing, and if g_2 less than g_1, m is negative, the gap is linearly decreasing. If $m = 0$, the gap is constant. Therefore, the explicit expression of the electrostatic gap size is

$$g(x) = g_1 + mx \tag{6.2}$$

Following the normalization given in eq. (3.40), the coordinate x should be normalized with respect to the beam length. Therefore, eqs. (3.40) and (6.1) are

substituted in eq. (6.2) to get the explicit expression of the gap size as

$$g(\hat{x}) = g_1 + (g_2 - g_1)\,\hat{x} \tag{6.3}$$

Hence, the electrostatic force becomes

$$F_{es} = \frac{\epsilon b\Big[V_{\mathrm{DC}} + V_{\mathrm{AC}}\cos(\omega t)\Big]^2}{2(g(\hat{x}) - w)^2}\left(1 + \beta\frac{g(\hat{x}) - w}{b}\right) \tag{6.4}$$

The electrostatic force eq. (6.4) is a function of two variables the transverse displacement w and the coordinate x. The dependence on x through the gap width in eq. (6.4) makes the electrostatic force to be variable over the beam's length. In other words, a point on the beam located near $x = 0$ experiences less attraction force than a point on the beam located near $x = L$. The transverse displacement is normalized with respect to the average gap size as follows:

$$\hat{w} = \frac{w}{\bar{g}} \quad \text{, where} \quad \bar{g} = \frac{g_1 + g_1}{2} \tag{6.5}$$

Substituting eq. (6.5) in eq. (6.4) and simplifying gives

$$F_{es} = \frac{\epsilon b\Big[V_{\mathrm{DC}} + V_{\mathrm{AC}}\cos(\omega t)\Big]^2}{2\bar{g}\,(\gamma g\,(\hat{x}) - \hat{w})^2}\left(1 + \frac{\beta\bar{g}}{b}\,(\gamma g\,(\hat{x}) - \hat{w})\right) \tag{6.6}$$

where $\gamma = \frac{1}{\bar{g}}$. Then, the equation of motion for the transverse vibration becomes

$$\begin{aligned}(\zeta+1)\,\hat{w}_{\hat{x}\hat{x}\hat{x}\hat{x}} + \hat{w}_{\hat{t}\hat{t}} + \hat{c}\hat{w}_{\hat{t}} + 2\hat{v}\hat{w}_{\hat{x}\hat{t}} + \left(\hat{v}^2 - \hat{P}\right)\hat{w}_{\hat{x}\hat{x}} - \alpha\hat{w}_{\hat{x}\hat{x}}\left(\int_0^1 \hat{w}_{\hat{x}}^2 dx\right) \\ = \frac{\left[\hat{V}_{\mathrm{DC}} + \hat{V}_{\mathrm{AC}}\cos\left(\Omega\hat{t}\right)\right]^2}{\left(\gamma g(\hat{x}) - \hat{w}\right)^2}\left(1 + \hat{\beta}\left(\gamma g\left(\hat{x}\right) - \hat{w}\right)\right)\end{aligned} \tag{6.7}$$

For convenience, let us drop the hat notation in eq. (6.7). This yields

$$\begin{aligned}(\zeta+1)\,w_{xxxx} + w_{tt} + cw_t + 2vw_{xt} + \left(v^2 - P\right)w_{xx} - \alpha w_{xx}\left(\int_0^1 w_x^2 dx\right) \\ = \frac{\left[V_{\mathrm{DC}} + V_{\mathrm{AC}}\cos\left(\Omega t\right)\right]^2}{\left(\gamma g(x) - w\right)^2}\left(1 + \beta\left(\gamma g(x) - w\right)\right)\end{aligned} \tag{6.8}$$

6.1 Galerkin Method

Equation (6.8) is simplified if it is multiplied by $(\gamma g(x) - w)^2$ to remove the transverse displacement from the denominator. In order to reduce the computational cost in the numerical integration, this yields

$$\begin{aligned}&(\gamma g(x) - w)^2\,(\zeta+1)\,w_{xxxx} + (\gamma g(x) - w)^2 w_{tt} + (\gamma g(x) - w)^2 c w_t \\ &+ (\gamma g(x) - w)^2 2vw_{xt} + (\gamma g(x) - w)^2(v^2 - P)w_{xx} - \alpha(\gamma g(x) - w)^2 w_{xx}\left(\int_0^1 w_x^2 dx\right) \\ &= \left[V_{\mathrm{DC}} + V_{\mathrm{AC}}\cos(\Omega t)\right]^2\left(1 + \beta(\gamma g(x) - w)\right)\end{aligned} \tag{6.9}$$

To solve eq. (6.9), we apply the Galerkin method to get the reduced-order model (ROM) [66]. The transverse deflection is approximated as

$$w\left(x,t\right)=\sum_{i=1}^{n}q_i\left(t\right)\phi_i\left(x\right) \tag{6.10}$$

where $\phi_i(x)$ is the mode shape of the transverse motion of a simply supported stationary beam, which is given as

$$\phi_i(x)=\sin(i\pi x) \tag{6.11}$$

Substituting eq. (6.10) into eq. (6.9), multiplying by the mode shape $\phi_i\left(x\right)$, then integrating the resulting equation over x from 0 to 1 lead to

$$\begin{aligned}
&\int_0^1\phi_i\left(g(x)-\sum_{i=1}^{n}q_i\phi_i\right)^2(\zeta+1)\sum_{i=1}^{n}q_i\phi_i''''dx+\int_0^1\phi_i\left(g(x)-\sum_{i=1}^{n}q_i\phi_i\right)^2\sum_{i=1}^{n}\ddot{q}_i\phi_i dx\\
&+c\int_0^1\phi_i\left(g(x)-\sum_{i=1}^{n}q_i\phi_i\right)^2\sum_{i=1}^{n}\dot{q}_i\phi_i dx+2v\int_0^1\phi_i\left(g(x)-\sum_{i=1}^{n}q_i\phi_i\right)^2\sum_{i=1}^{n}q_i\phi_i' dx\\
&+\left(v^2-P\right)\int_0^1\phi_i\left(g(x)-\sum_{i=1}^{n}q_i\phi_i\right)^2\sum_{i=1}^{n}q_i\phi_i'' dx\\
&-\alpha\int_0^1\phi_i\left[\left(g(x)-\sum_{i=1}^{n}q_i\phi_i\right)^2\sum_{i=1}^{n}q_i\phi_i''\int_0^1\left\{\left(\sum_{i=1}^{n}q_i\phi_i'\right)^2\right\}dx\right]dx\\
&=\int_0^1\phi_i\left[V_{\mathrm{DC}}+V_{\mathrm{AC}}\cos\left(\Omega t\right)\right]^2\left(1+\beta\left(g(x)-\sum_{i=1}^{n}q_i\phi_i\right)\right)dx
\end{aligned} \tag{6.12}$$

Using four terms ($n = 4$) in the Galerkin expansion converts eq. (6.12) into

$$A_1\ \ddot{q}_1 + B_1\ \dot{q}_1 + C_1\ q_1 + D_1\ q_1^2 + E_1\ q_1^3 + F_1\ q_1^4 + G_1\ q_1^5 + H_1 = 0 \tag{6.13}$$

$$A_2\ \ddot{q}_2 + B_2\ \dot{q}_2 + C_2\ q_2 + D_2\ q_2^2 + E_2\ q_2^3 + F_2\ q_2^4 + G_2\ q_2^5 + H_2 = 0 \tag{6.14}$$

$$A_3\ \ddot{q}_3 + B_3\ \dot{q}_3 + C_3\ q_3 + D_3\ q_3^2 + E_3\ q_3^3 + F_3\ q_3^4 + G_3\ q_3^5 + H_3 = 0 \tag{6.15}$$

$$A_4\ \ddot{q}_4 + B_4\ \dot{q}_4 + C_4\ q_4 + D_4\ q_4^2 + E_4\ q_4^3 + F_4\ q_4^4 + G_4\ q_4^5 + H_4 = 0 \tag{6.16}$$

Equations (6.13)–(6.16) are written in matrix form as

$$A\ \ddot{q} + B\ \dot{q} + C\ q + D\ q^2 + E\ q^3 + F\ q^4 + G\ q^5 + H = 0 \tag{6.17}$$

where

$$A = \begin{bmatrix} A_1 & A_2 & A_3 & A_4 \end{bmatrix}^T \tag{6.18}$$

$$B = \begin{bmatrix} B_1 & B_2 & B_3 & B_4 \end{bmatrix}^T \tag{6.19}$$

$$C = \begin{bmatrix} C_1 & C_2 & C_3 & C_4 \end{bmatrix}^T \tag{6.20}$$

$$D = \begin{bmatrix} D_1 & D_2 & D_3 & D_4 \end{bmatrix}^T \tag{6.21}$$

$$E = \begin{bmatrix} E_1 & E_2 & E_3 & E_4 \end{bmatrix}^T \tag{6.22}$$

$$F = \begin{bmatrix} F_1 & F_2 & F_3 & F_4 \end{bmatrix}^T \tag{6.23}$$

$$G = \begin{bmatrix} G_1 & G_2 & G_3 & G_4 \end{bmatrix}^T \tag{6.24}$$

$$H = \begin{bmatrix} H_1 & H_2 & H_3 & H_4 \end{bmatrix}^T \tag{6.25}$$

The coefficients A_i, B_i, C_i, D_i, E_i, F_i, G_i and H_i are given in Section A.1.

To study the "static" behavior (pull-in voltage of the axially moving microbeam under DC voltage) the time-varying model coordinates are set to zero and the resulted nonlinear algebraic equations are solved numerically using a Newton–Raphson scheme. To find the frequency response curves, the second-order differential eqs. (6.13)–(6.16) are solved numerically using MATLAB. The function ode45, based on an explicit Runge-Kutta method, is utilized. The initial conditions, of deflection and velocity, are set to zero (i.e., $q_1 = \dot{q}_1 = 0$). In order

to obtain the steady-state solution, the equation is solved over a long period of dimensionless time $t = [0 - 2000]$, the so-called long-time integration.

6.2 Numerical Illustrations and Discussion

An axially moving micro-beam made of silicon, with the properties listed in Table 4.1 is investigated to understand its dynamic behavior.

6.2.1 Stationary Micro-beams

As a first step, the pull-in and frequency response curves are investigated in this section. When the micro-beam is stationary (i.e., $v = 0$).

Pull-in Voltage

Figure 6.2 shows to configurations of the fixed electrode. In Figure 6.2(a), positive values of the angle θ ($g_2 > g_1$) represent a linearly increasing electrostatic gap. On the other, negative values of the angle θ ($g_2 < g_1$) represent a linearly decreasing electrostatic gap as shown in Figure 6.2(b).

Figure 6.3 shows the effect of changing the slope m (or the angle θ between the electrode and a horizontal line) on the pull-in voltage. Different values of the

angle are considered while keeping the average gap width unchanged of $\bar{g} = 2$ µm. The same pull-in voltage of $V_{pull-in} = 70$ V is observed for all angles.

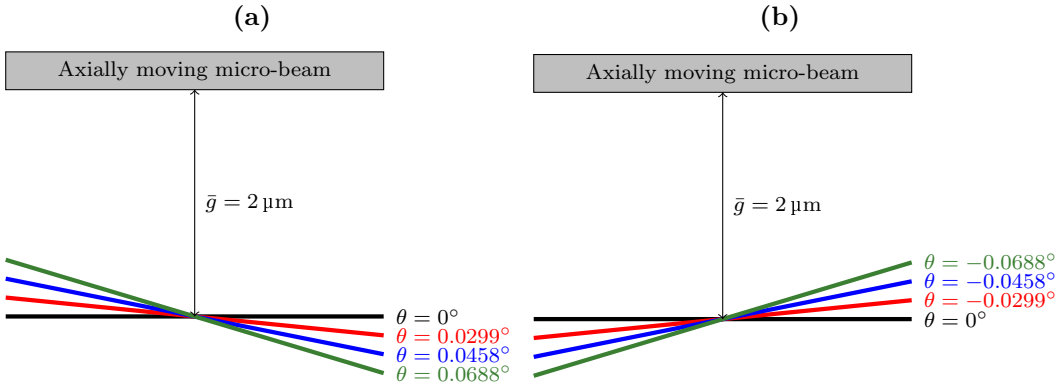

Figure 6.2 Illustration of how the electrode's angle is calculated (a) positive angle θ and (b) negative angle θ

Frequency Response Curves

Numerical results in this paper are obtained for two sets of AC and DC voltages. The first set is when the applied DC and AC voltages are 20 V and 2 V, respectively. The second set is when DC and AC voltages are 50 V and 2 V, respectively. This selection of different voltages because the first set of DC and AC voltages produces hardening frequency response curves while the other one produces softening frequency response [27]. Since we are going to change parameters such as the angle θ and the velocity v, we need to examine the effect of the parameters mentioned above on the two selected sets of AC and DC voltages (hardening / softening behaviors).

Figure 6.4 shows the frequency response curves for positive and negative electrode's angles when the applied DC and AC voltages are 20 V and 2 V, respectively. As shown in the figure, the change of the angle θ did not affect the response. Figure 6.5 shows that same conclusion is observed when the applied DC and AC voltages are 50 V and 2 V, respectively.

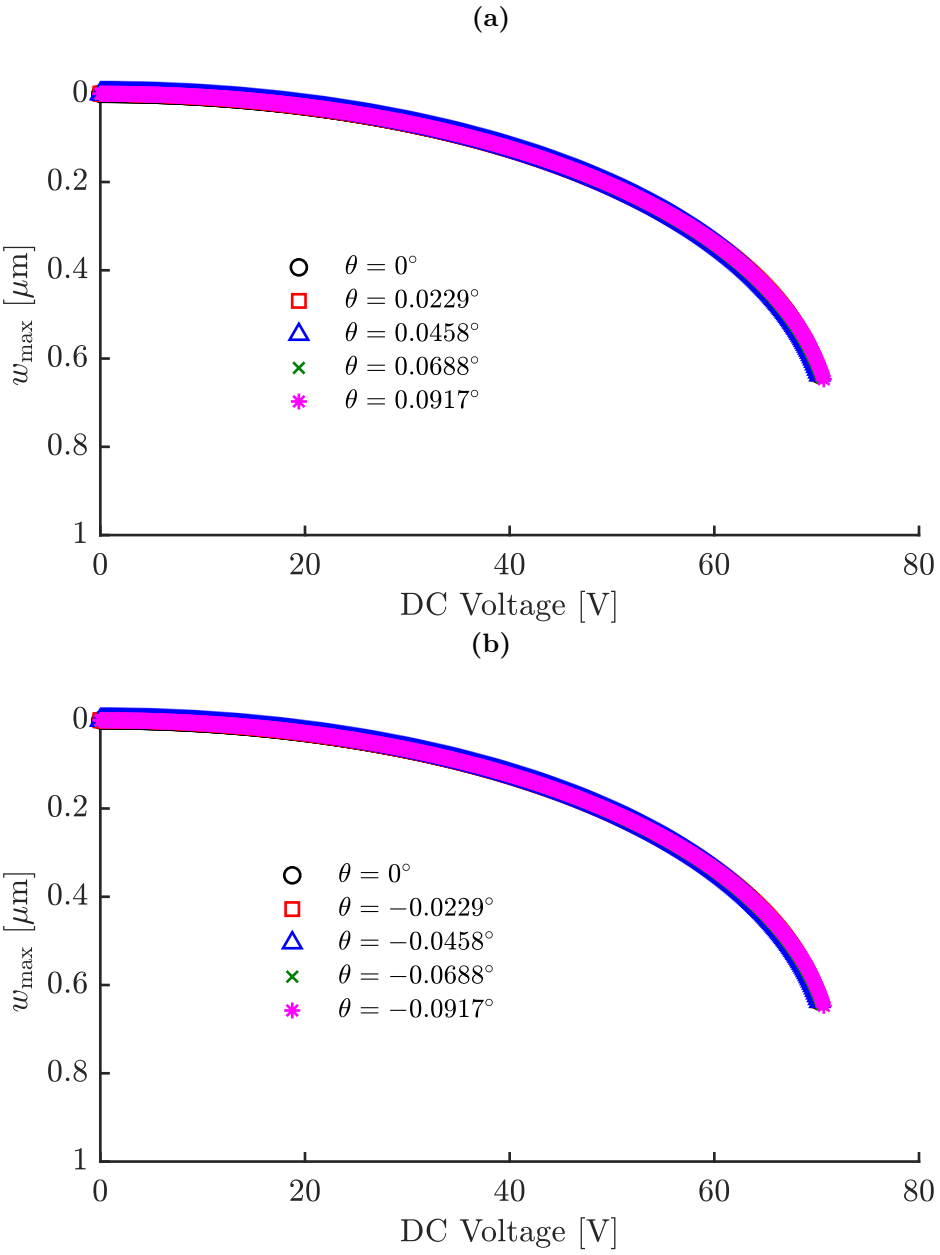

Figure 6.3 Pull-in voltages when $v = 0$ for different angles (a) positive θ and (b) negative θ

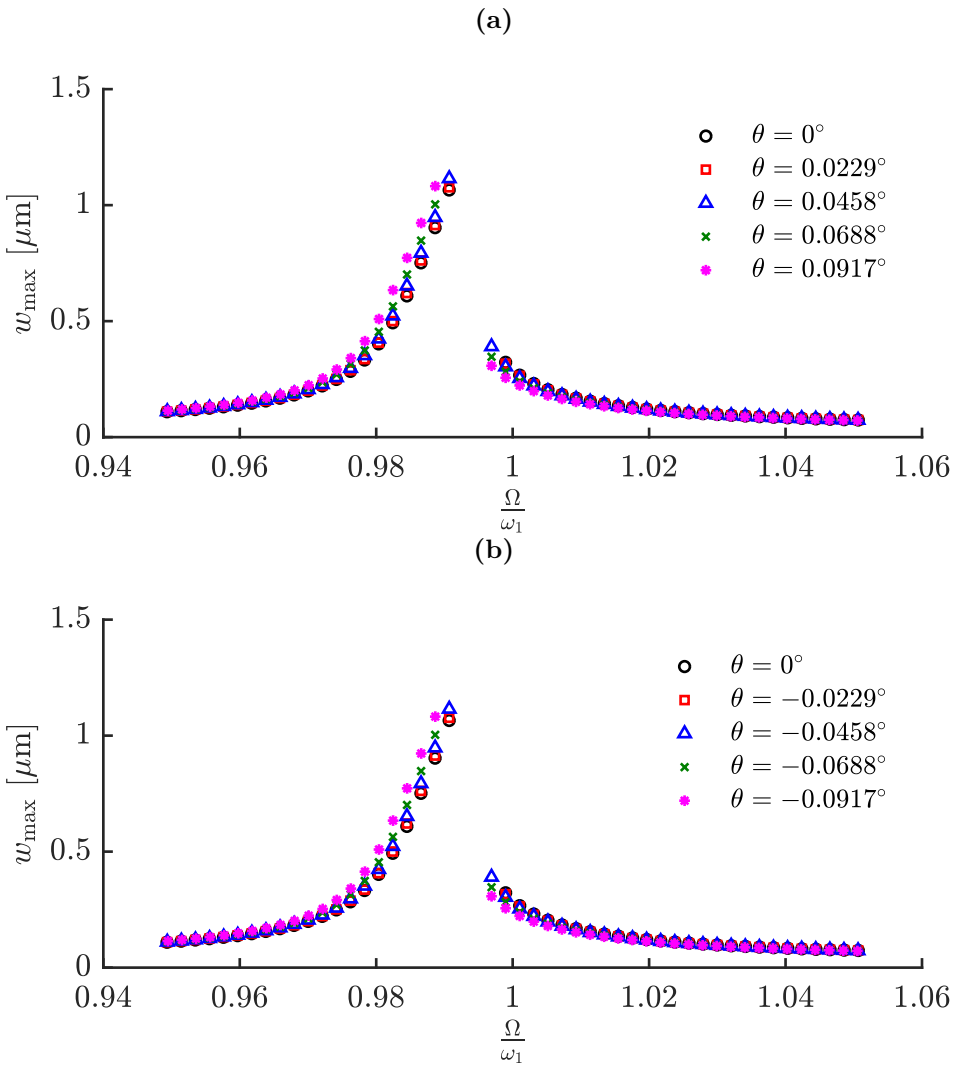

Figure 6.4 Frequency response curves for (a) positive θ and (b) negative θ. The applied DC and AC voltages are 20 V and 2 V, respectively

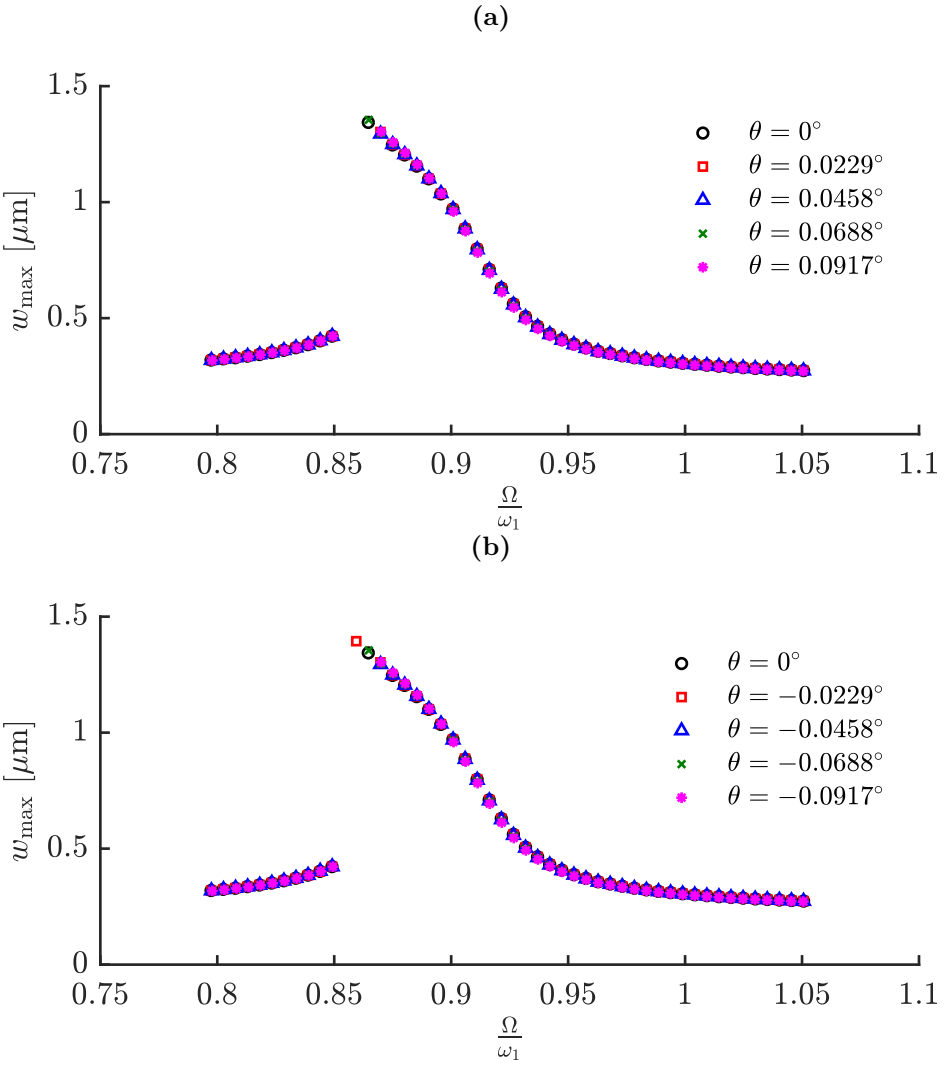

Figure 6.5 Frequency response curves for (a) positive θ and (b) negative θ. The applied DC and AC voltages are 50 V and 2 V, respectively

6.2.2 Axially Moving Micro-Beams

Pull-in voltage

The effect of the axial speed on the pull-in voltage is shown in Figure 6.6. As the axial speed increased, the pull-in voltage decreased. For all selected angles θ, the reduction in the pull-in voltage is the same for the selected angles.

(a)

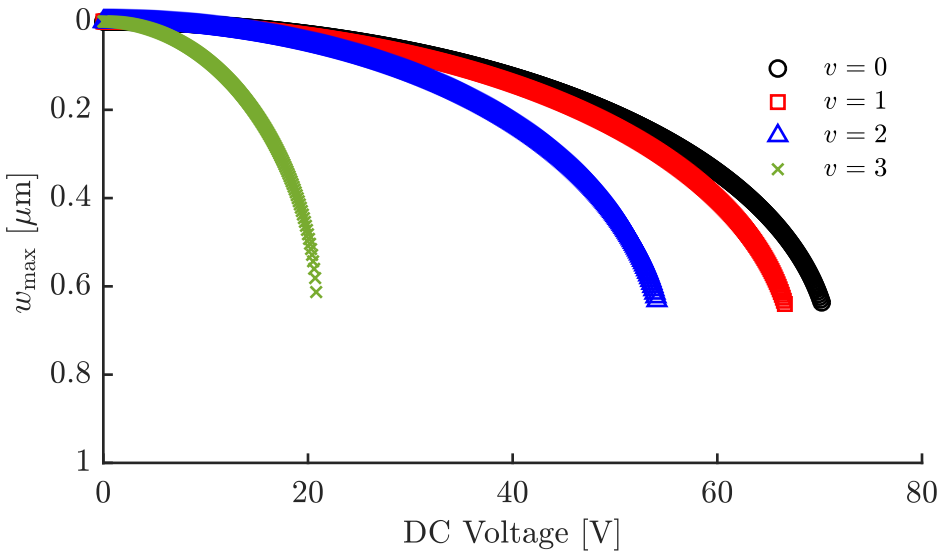

Frequency Response Curves

In this section, we examine the frequency response curves for different electrode angles θ along with different applied voltages. Figure 6.7 shows the effect of increasing the axial speed on the frequency response curves when the angle θ is

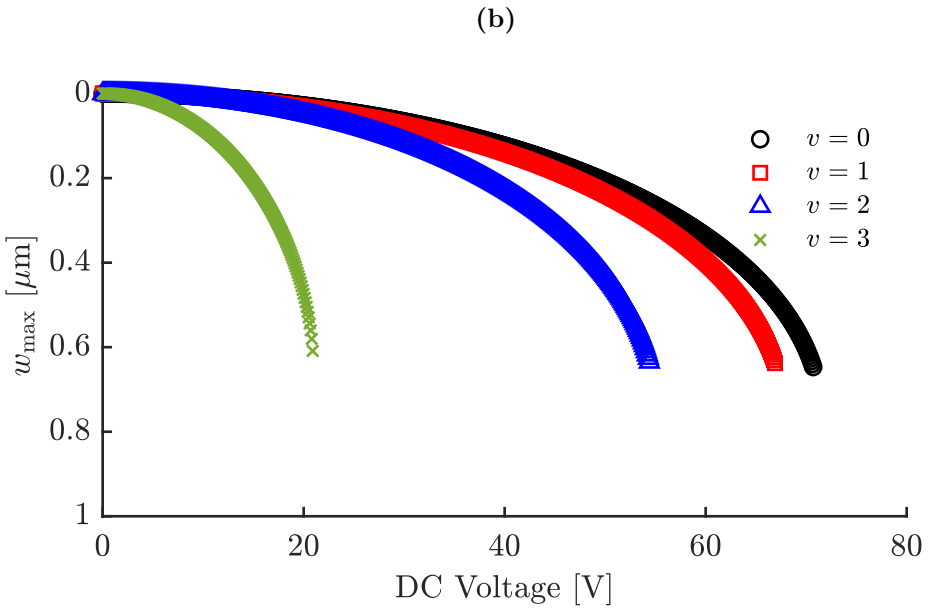

Figure 6.6 Pull-in voltage at different axial speeds when (a) $\theta = -0.0917°$ and (b) $\theta = 0.0917°$

$0.0917°$. As the the axial speed increases, the maximum amplitude increases. In other words, the effect of increasing the axial speed contributes to decrease the damping of the system.

Figure 6.8 shows the effect of increasing the axial speed when angle θ is $-0.0917°$. In contrast, as the axial speed increases, the maximum deflection decreases. This is because the negative slope (or angle) contributes to increase the damping of the system which in turns decreases the maximum deflection. Furthermore, the effect of the high damping, when v is 0.1 , results in a linear frequency response.

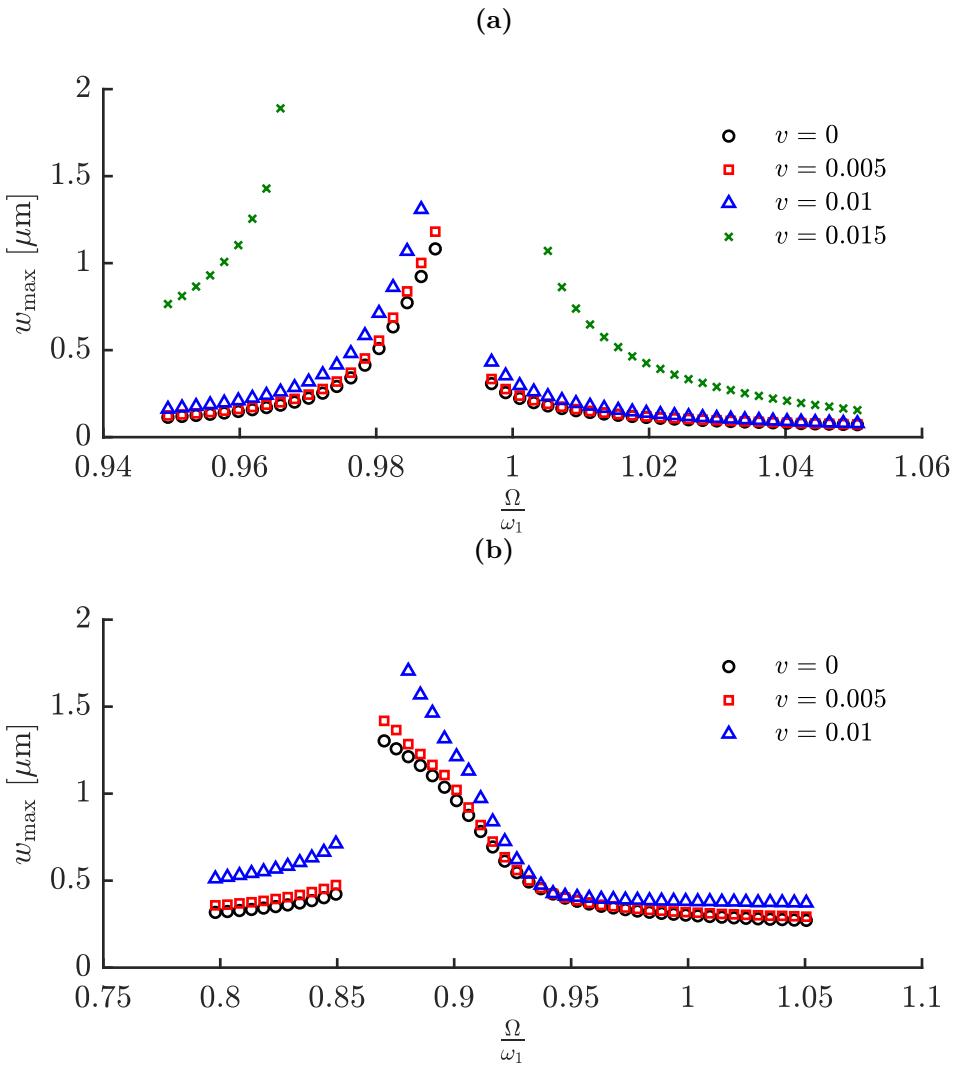

Figure 6.7 Frequency response curves for different axial speed when $\theta = 0.0917°$ (a) $V_{\mathrm{DC}} = 20$ V and $V_{\mathrm{AC}} = 2$. (b) $V_{\mathrm{DC}} = 50$ V and $V_{\mathrm{AC}} = 2$

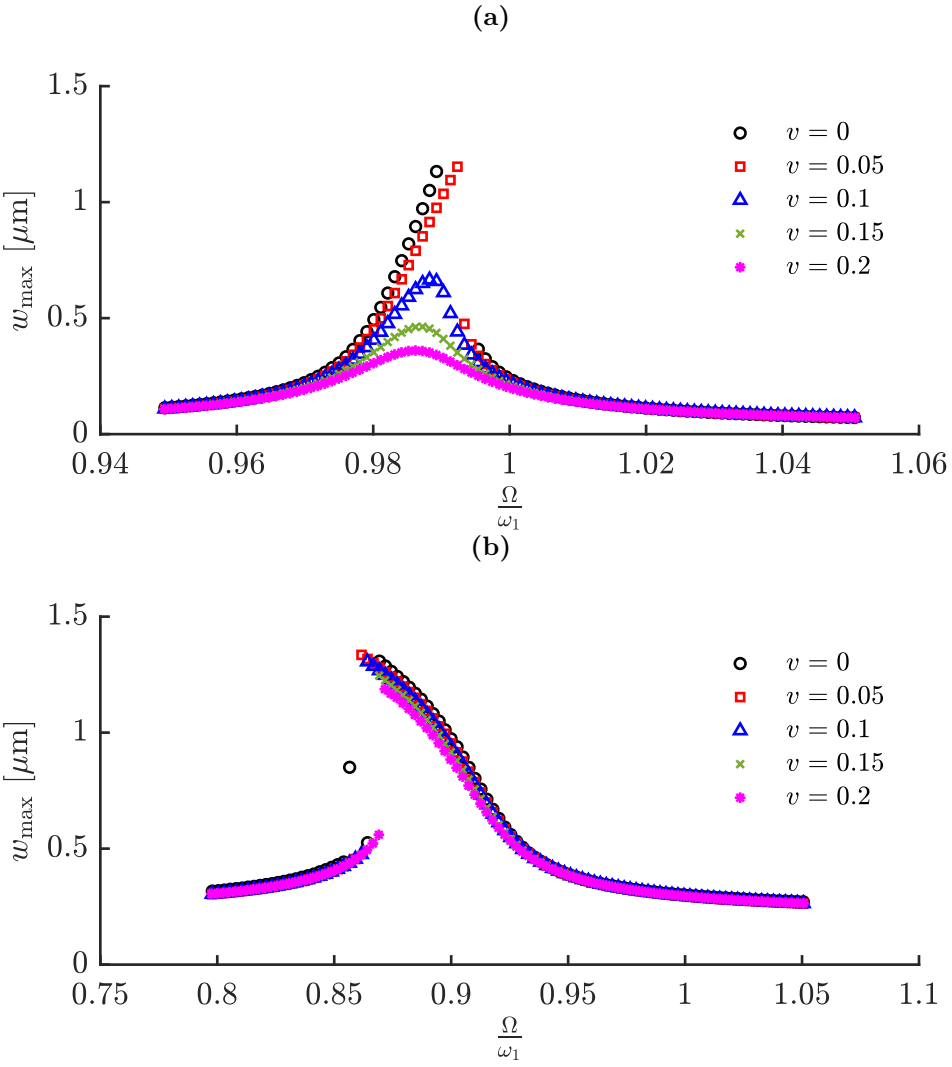

Figure 6.8 Frequency response curves for different axial speed when $\theta = -0.0917°$ (a) $V_{\mathrm{DC}} = 20$ V and $V_{\mathrm{AC}} = 2$.(b) $V_{\mathrm{DC}} = 50$ V and $V_{\mathrm{AC}} = 2$

Waveform and phase portrait

Figure 6.9 shows the waveforms and phase portraits when the angle of the electrode is 0.0917° and the applied DC and AC voltages are 20 V and 2 V, respectively. Figure 6.9(a) depicts the phase portrait and time history when the micro-beam is stationary. In this case, the micro-beam is stationary and the maximum deflection is 0.05. However, when the system starts to move axially, the maximum deflection starts to increase with time. And as the axial speed increases, the system loses its stability faster. This is shown in Figure 6.9(b), the axial speed is 0.5 and the maximum deflection reached when $t = 10$ is 0.2. For higher axial speed, $v = 1$, Figure 6.9(c) shows the maximum deflection reached when $t = 10$ to be 2. The same conclusion is observed, as the axial speed increases, the amplitude increases.

Figure 6.10 depicts the case when the electrode has an angle of $-0.0917°$ under the same applied DC and AC voltages of 20 V and 2 V, respectively. As shown in Figure 6.10(a), the system behavior is similar to that shown in Figure 6.9(a) when it is stationary. The differences become significant when the micro-beam moves axially. In contrast to Figures 6.9(b) and 6.9(c), as the axial speed increases the maximum deflection decreases. This decrease in maximum deflection becomes

faster for higher axial speeds as shown in Figures 6.10(b) and 6.10(c).

Figures 6.11 and 6.12 show the cases when θ is $0.0917°$ and $-0.0917°$, respectively. The applied DC and AC voltages are 50 V and 2 V, respectively. The same conclusion is observed, for positive angles, the increase of the axial speed is found to increase the maximum deflection, and for negative angle electrodes, the increase in the axial speed results in a decrease of the maximum deflection. However, in these cases, the increase in the axial speed resulted in a significant increase in the maximum deflection. The percent increase and decrease of the maximum deflection with respect to the axial speed for the cases mentioned above are summarized in Table 6.1

Table 6.1 Maximum deflection at different axial speeds with the percent increase/decrease for each case.

(a) Figure 6.9

v	$w_{\max}$	% increase in $w_{\max}$
0	0.046	0%
0.5	0.181	293%
1	2.281	1154%

(b) Figure 6.10

v	$w_{\max}$	% decrease in $w_{\max}$
0	0.046	0%
0.5	0.041	10.7%
1	0.039	4.9%

(c) Figure 6.11

v	$w_{\max}$	% increase in $w_{\max}$
0	0.314	0%
0.5	4	1174%
1	8.61	115%

(d) Figure 6.12

v	$w_{\max}$	% decrease in $w_{\max}$
0	0.314	0%
0.5	0.245	28%
1	0.219	12.4%

(a)

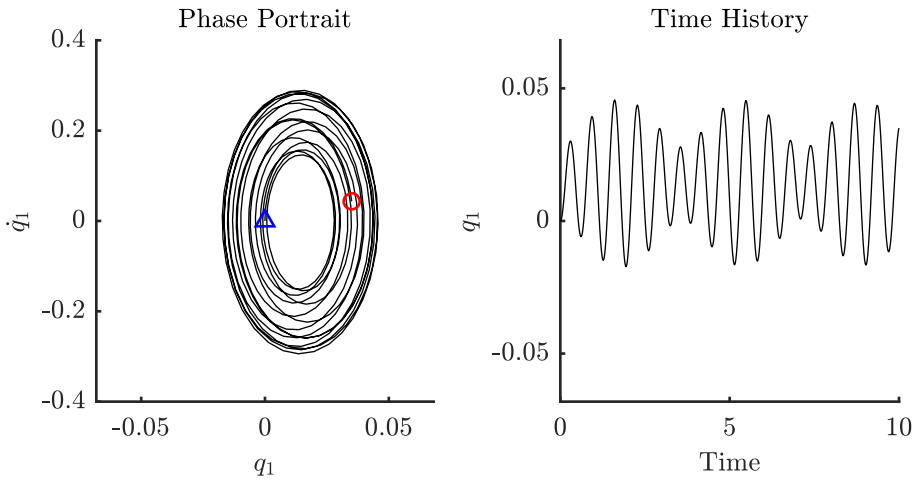
Phase Portrait
Time History
0.4
0.2
0
-0.2
-0.4
$\dot{q}_1$
-0.05
0
0.05
q_1
0.05
0
-0.05
q_1
0
5
10
Time

(b)

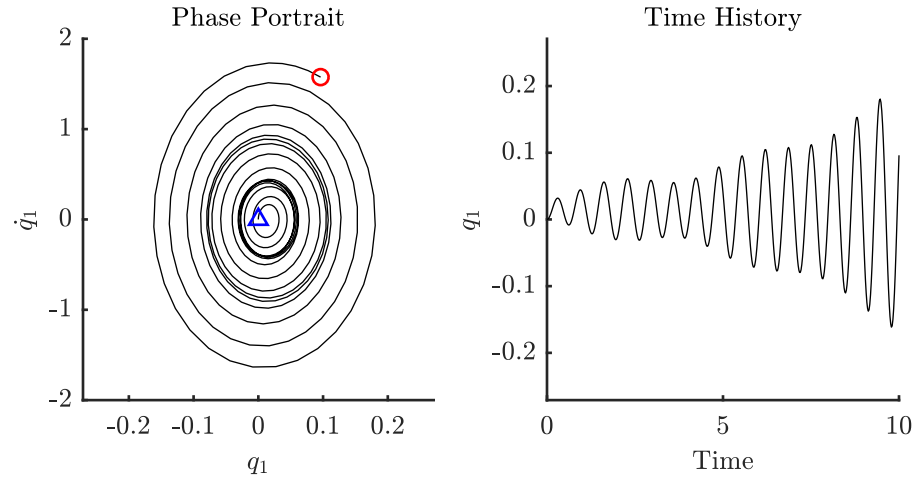
Phase Portrait
Time History
2
1
0
-1
-2
$\dot{q}_1$
-0.2
-0.1
0
0.1
0.2
q_1
0.2
0.1
0
-0.1
-0.2
q_1
0
5
10
Time

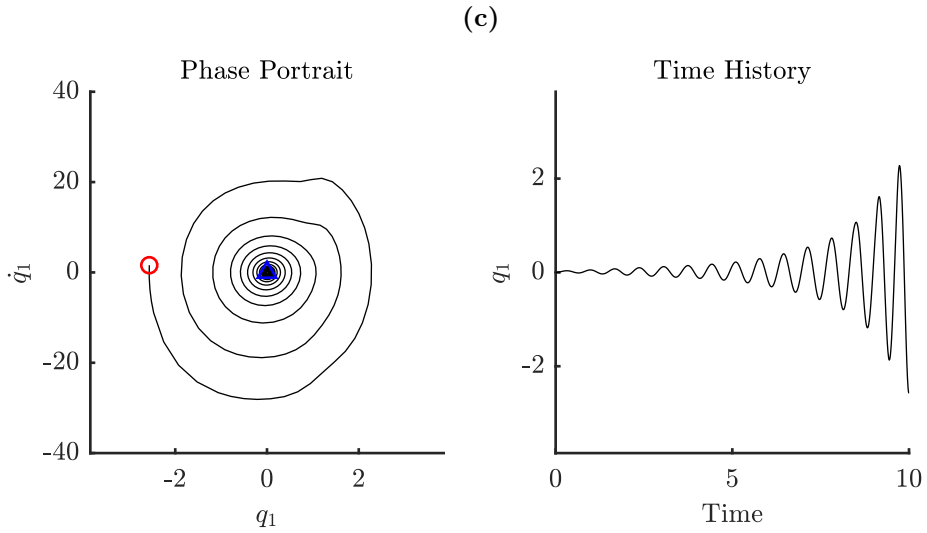

Figure 6.9 Phase portrait and time history at different axial speeds when $\theta = 0.0917°$. The applied DC and AC voltages are 20 V and 2 V, respectively. (a) $v = 0$, (b) $v = 0.5$ and (c) $v = 1$. The trajectories start from (△) and end at (○)

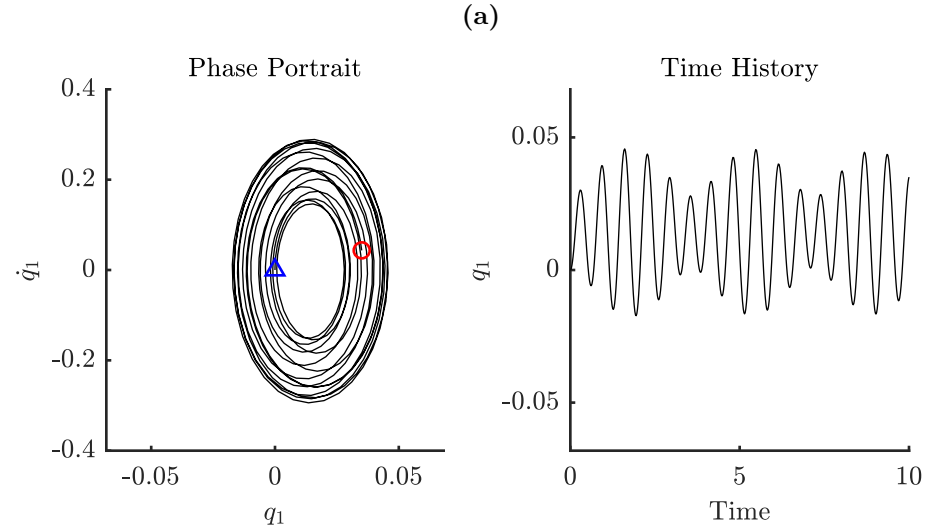

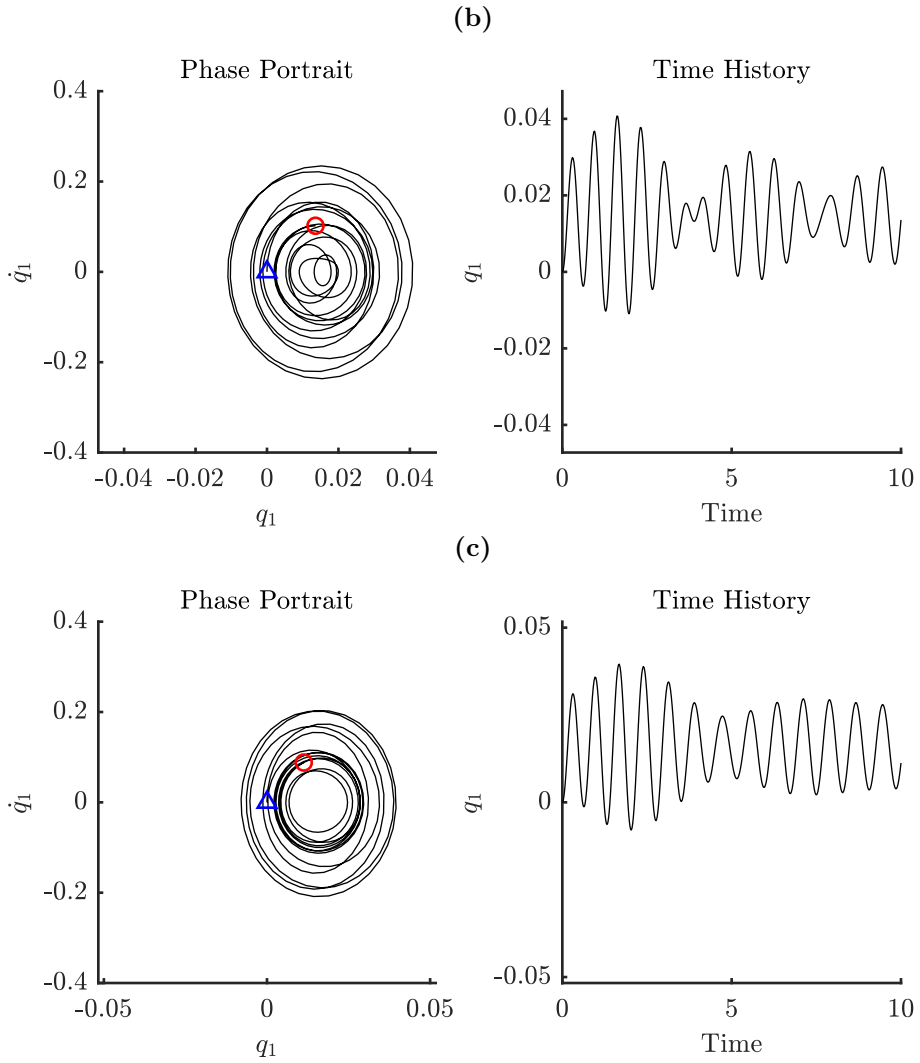

Figure 6.10 Phase portrait and time history at different axial speeds when $\theta = -0.0917°$. The applied DC and AC voltages are 20 V and 2 V, respectively. (a) $v = 0$, (b) $v = 0.5$ and (c) $v = 1$. The trajectories start from (△) and end at (○)

(a)

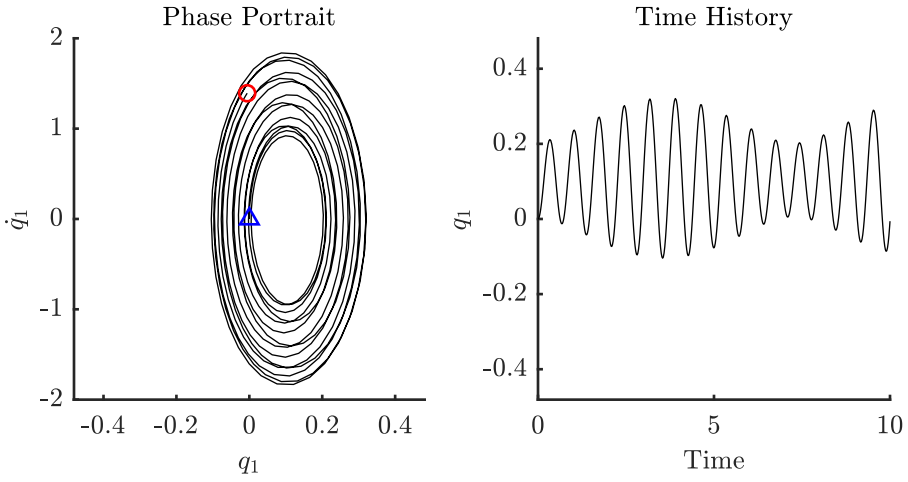
Phase Portrait
Time History
2
1
0
-1
-2
$\dot{q}_1$
-0.4
-0.2
0
0.2
0.4
q_1
0.4
0.2
0
-0.2
-0.4
q_1
0
5
10
Time

(b)

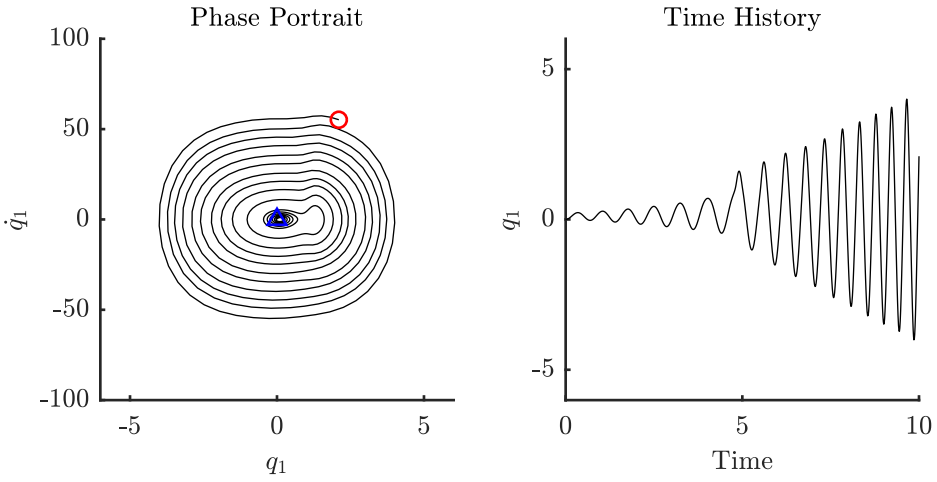
Phase Portrait
Time History
100
50
0
-50
-100
$\dot{q}_1$
-5
0
5
q_1
5
0
-5
q_1
0
5
10
Time

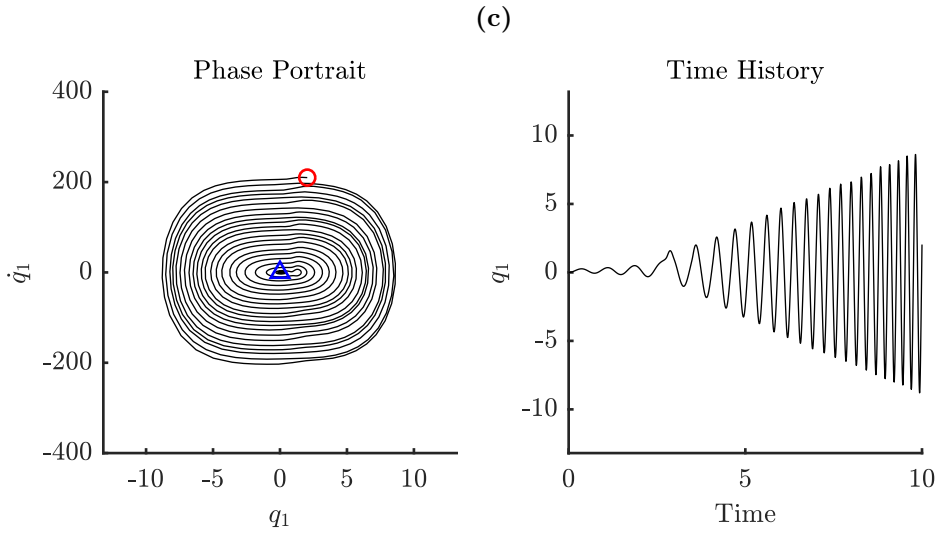

Figure 6.11 Phase portrait and time history at different axial speeds when $\theta = 0.0917°$. The applied DC and AC voltages are 50 V and 2 V, respectively. (a) $v = 0$, (b) $v = 0.5$ and (c) $v = 1$. The trajectories start from (△) and end at (○)

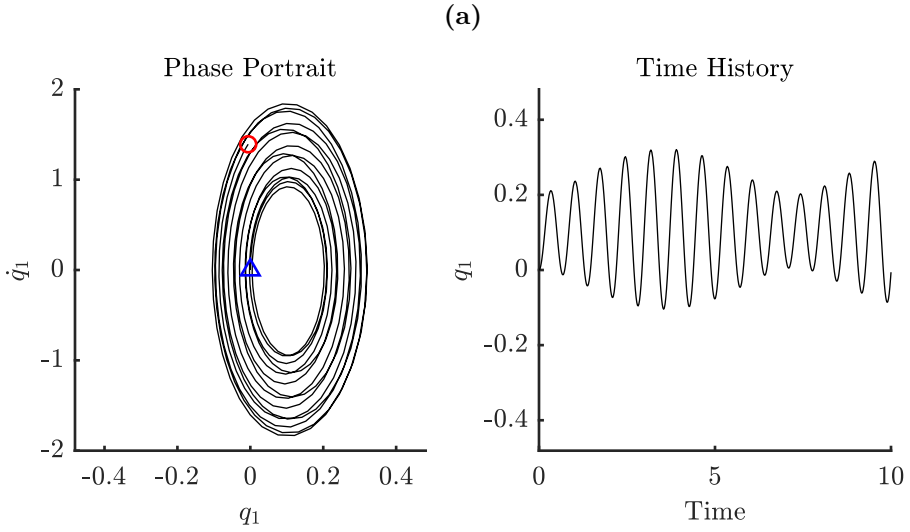

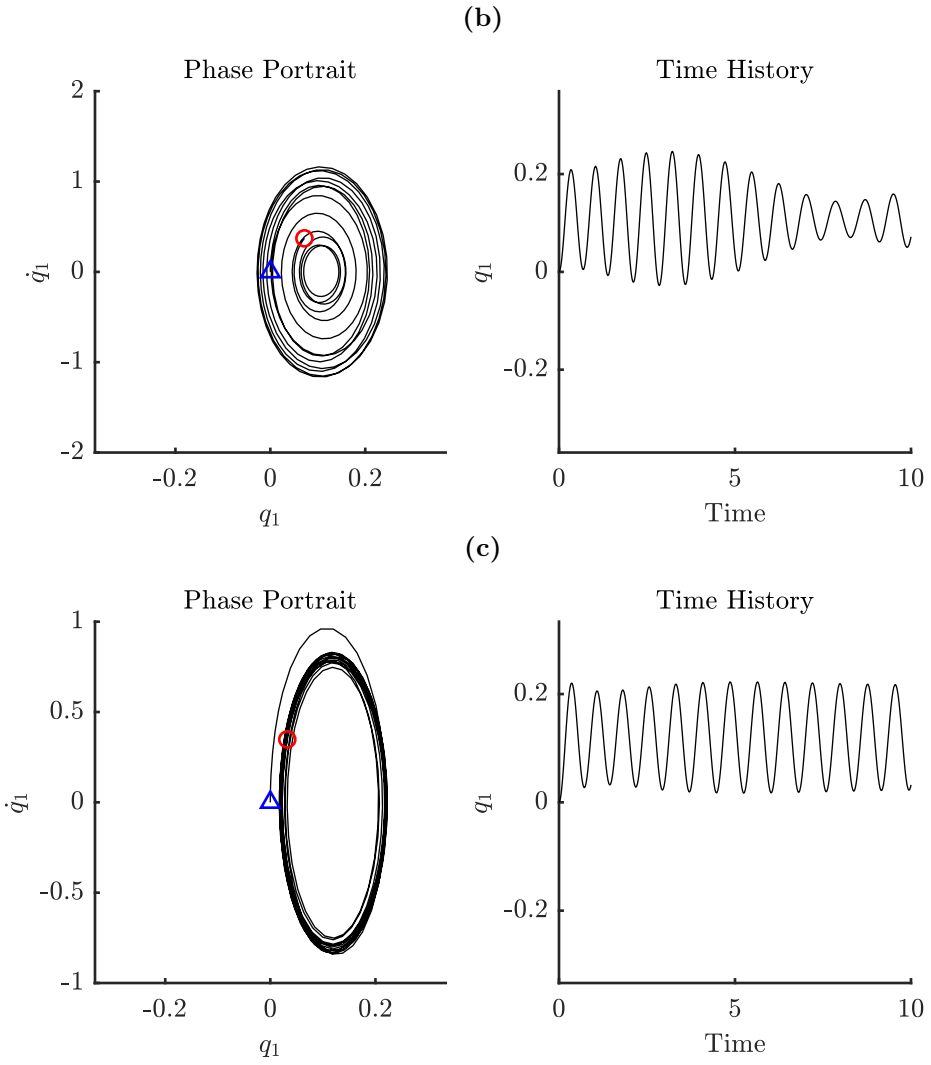

Figure 6.12 Phase portrait and time history at different axial speeds when $\theta = -0.0917°$. The applied DC and AC voltages are 50 V and 2 V, respectively. (a) $v = 0$, (b) $v = 0.5$ and (c) $v = 1$. The trajectories start from (△) and end at (○)

Chapter 7

Conclusion

The problem of the axially moving micro-beam over linearly varying electrostatic gap was analyzed within the framework of the modified couple stress theory. The mathematical model of the considered system included the internal material length parameter, which allowed the prediction of small-size effect. Relevant to mass production of MEMS / NEMS was the studying of the dynamic behavior of a small-size beam running over roller supports. The transverse vibration of a simply supported axially moving Euler-Bernoulli micro-beam was analytically modeled via Hamilton's principle. Galerkin method was then used to discretize the obtained partial differential equation into a set of ordinary differential equations. Nonlinear vibration characteristics of the axially moving micro-beam were consid-

ered for various axial velocities, different angles, and the representative applied voltages. Numerical results showed that:

1. The increase in axial speed had significantly decreased the pull-in voltage.

2. Increasing the axial speed changes the value of first saddle-node bifurcation point in the frequency response.

3. The slope of the electrode did not affect the pull-in voltage of the stationary micro-beam.

4. In the case of a linearly increasing gap, an increase in the micro-beam axial speed was found to increase the maximum deflection of the micro-beam, whereas in the case of a linearly decreasing gap, the increase of the micro-beam axial speed decreased the maximum deflection of the micro-beam.

References

[1] Robert Bogue. Recent developments in mems sensors: a review of applications, markets and technologies. *Sensor Review*, 33(4):300–304, 2013. 1

[2] R. Aitken, V. Chandra, J. Myers, B. Sandhu, L. Shifren, and G. Yeric. Device and technology implications of the internet of things. In *2014 Symposium on VLSI Technology (VLSI-Technology): Digest of Technical Papers*, pages 1–4, June 2014. 1

[3] Demand for MEMS Heats Up in 2016. `http://www.sourcetoday.com/buying-trends/demand-mems-heats-2016`, May 2017. 1

[4] IoT Needs New MEMS Approaches. `https://www.eetimes.com/author.asp?section_id=36&doc_id=1326768`, March 2015. 1

[5] James R. Sheats. Roll-to-roll manufacturing of thin film electronics. *Proc.SPIE*, 4688:4688 – 4688 – 9, 2002. 1

[6] Jehuda Greener, Glen Pearson, and Miko Cakmak. *Roll-to-roll Manufacturing: Process Elements and Recent Advances*. John Wiley & Sons, 2018. 1

[7] Ali H. Nayfeh, Mohammad I. Younis, and Eihab M. Abdel-Rahman. Dynamic pull-in phenomenon in MEMS resonators. *Nonlinear Dynamics*, 48(1-2):153–163, 2007. 3

[8] Ali N. Nayfeh and Perngjin Frank. Pai. *Linear and nonlinear structural mechanics*. Wiley-Interscience, 2004. 3

[9] Mohammad I. Younis. *Mems linear and nonlinear statics and dynamics*. Springer-Verlag New York, 2014. 3, 68

[10] N.A. Fleck, G.M. Muller, M.F. Ashby, and J.W. Hutchinson. Strain gradient plasticity: Theory and experiment. *Acta Metallurgica et Materialia*, 42(2):475 – 487, 1994. 4

[11] D.C.C. Lam, F. Yang, A.C.M. Chong, J. Wang, and P. Tong. Experiments and theory in strain gradient elasticity. *Journal of the Mechanics and Physics of Solids*, 51(8):1477 – 1508, 2003. 4

[12] Andrew W McFarland and Jonathan S Colton. Role of material microstructure in plate stiffness with relevance to microcantilever sensors. *Journal of Micromechanics and Microengineering*, 15(5):1060, 2005. 4

[13] J.S. Stölken and A.G. Evans. A microbend test method for measuring the plasticity length scale. *Acta Materialia*, 46(14):5109 – 5115, 1998. 4

[14] F Yang, A Chong, D Lam, and P Tong. Couple stress based strain gradient theory for elasticity. *International Journal of Solids and Structures*, 39(10):2731–2743, 2002. 4, 28, 32

[15] A. Cemal Eringen and D. G B Edelen. On nonlocal elasticity. *International Journal of Engineering Science*, 10(3):233–248, 1972. 4, 5

[16] A. Cemal Eringen. On differential equations of nonlocal elasticity and solutions of screw dislocation and surface waves. *Journal of Applied Physics*, 54(9):4703–4710, 1983. 4, 5

[17] R. D. Mindlin and H. F. Tiersten. Effects of couple-stresses in linear elasticity. *Archive for Rational Mechanics and Analysis*, 11(1):415–448, 1962. 4

[18] R. A. Toupin. Elastic materials with couple-stresses. *Archive for Rational Mechanics and Analysis*, 11(1):385–414, 1962. 4

[19] S K Park and X-L Gao. Bernoulli–Euler beam model based on a modified couple stress theory. *Journal of Micromechanics and Microengineering*, 16(11):2355–2359, 2006. 10, 11

[20] A G Evans and J S Sto. A MICROBEND TEST METHOD FOR MEASURING THE PLASTICITY LENGTH SCALE. 46(14), 1998. 10

[21] Ehsan Maani Miandoab, Hossein Nejat Pishkenari, Aghil Yousefi-Koma, and Hamid Hoorzad. Polysilicon nano-beam model based on modified couple stress and Eringen's nonlocal elasticity theories. *Physica E: Low-Dimensional Systems and Nanostructures*, 63:223–228, 2014. 10

[22] Masoud Rahaeifard, Mohammad Taghi Ahmadian, and Keikhosrow Firoozbakhsh. Size-dependent dynamic behavior of microcantilevers under suddenly applied DC voltage. *Proceedings of the Institution of Mechanical Engineers, Part C: Journal of Mechanical Engineering Science*, 228(5):896–906, 2014. 10

[23] M. Rahaeifard, M. H. Kahrobaiyan, M. T. Ahmadian, and K. Firoozbakhsh. Size-dependent pull-in phenomena in nonlinear microbridges. *International Journal of Mechanical Sciences*, 54(1):306–310, 2012. 11

[24] M. Mojahedi. Size dependent dynamic behavior of electrostatically actuated microbridges. *International Journal of Engineering Science*, 111:74–85, 2017. 11

[25] Hossein Rokni, Rudolf J. Seethaler, Abbas S. Milani, Shahrokh Hosseini-Hashemi, and Xian Fang Li. Analytical closed-form solutions for size-dependent static pull-in behavior in electrostatic micro-actuators via Fredholm integral equation. *Sensors and Actuators, A: Physical*, 190:32–43, 2013. 12

[26] M. Asghari, M. Rahaeifard, M. H. Kahrobaiyan, and M. T. Ahmadian. The modified couple stress functionally graded Timoshenko beam formulation. *Materials and Design*, 32(3):1435–1443, 2011. 12

[27] X. Chen and S. A. Meguid. Nonlinear vibration analysis of a microbeam subject to electrostatic force. *Acta Mechanica*, 228(4):1343–1361, 2017. 12, 22, 109

[28] C. Li, L. Chen, and J. P. Shen. Vibrational responses of micro/nanoscale beams: Size-dependent nonlocal model analysis and comparisons. *Journal of Mechanics*, 31(1):7–19, 2014. 13

[29] Bekir Akgöz and Ömer Civalek. Free vibration analysis of axially functionally graded tapered Bernoulli-Euler microbeams based on the modified couple stress theory. *Composite Structures*, 98:314–322, 2013. 14

[30] Hassen M. Ouakad, Muhammad A. Hawwa, and Hussain M. Al-Qahtani. Modeling the electrostatic deflection of a mems multilayers based actuator. *Mathematical Problems in Engineering*, 2013, 2013. 14

[31] J. N. Reddy. Nonlocal theories for bending, buckling and vibration of beams. *International Journal of Engineering Science*, 45(2-8):288–307, 2007. 15

[32] Cheng Li, C. W. Lim, Jilin Yu, and Qingchuan Zeng. Transverse vibration of pre-tensioned nonlocal nanobeams with precise internal axial loads. *Science China Technological Sciences*, 54(8):2007–2013, 2011. 15

[33] Bekir Akgoz and Omer Civalek. Free vibration analysis for single-layered graphene sheets in an elastic matrix via modified couple stress theory. *Materials and Design*, 42:164–171, 2012. 15

[34] Jinjian Liu, Ling Chen, Feng Xie, Xueliang Fan, and Cheng Li. On bending, buckling and vibration of graphene nanosheets based on the nonlocal theory. *Smart Structures and Systems*, 17(2):257–274, 2016. 16

[35] Maysam Naghinejad and Hamid Reza Ovesy. Free vibration characteristics of nanoscaled beams based on nonlocal integral elasticity theory. *Journal of Vibration and Control*, (February):107754631771786, 2017. 16

[36] Hamed Mobki, Morteza H. Sadeghi, Ghader Rezazadeh, Mohammad Fathalilou, and Ali asghar Keyvani-janbahan. Nonlinear behavior of a nano-scale beam considering length scale-parameter. *Applied Mathematical Modelling*, 38(5-6):1881–1895, 2014. 16

[37] Süleyman M. Badatli. Non-linear transverse vibrations of tensioned nanobeams using nonlocal beam theory. *Structural Engineering and Mechanics*, 55(2):281–298, 2015. 17

[38] Araz Rezaei Kivi, Saber Azizi, and Peyman Norouzi. Bifurcation Analysis of an Electrostatically Actuated Nano-Beam Based on Modified Couple Stress Theory. *Sensing and Imaging*, 18(1), 2017. 17

[39] J. a. Wickert and C. D. Mote. Classical Vibration Analysis of Axially Moving Continua. *Journal of Applied Mechanics*, 57(3):738, 1990. 17

[40] Wickert J. A. Non-Linear Vibration Of A Traveling Tensiod Beam. *International Journal of Non-Linear Mechanics*, 27(3):503–517, 1992. 18, 28, 39

[41] C.D. Mote. A study of band saw vibrations. *Journal of the Franklin Institute*, 279(6):430–444, 1965. 18

[42] Krzysztof Marynowski. Axially Moving Microscale Panel Model Based on Modified Couple Stress Theory. *Journal of Nanomechanics and Micromechanics*, 5(1):A4014002, 2015. 18

[43] Amir Mehdi Dehrouyeh-Semnani, Mohammad Dehrouyeh, Hamid Zafari-Koloukhi, and Mehdi Ghamami. Size-dependent frequency and stability characteristics of axially moving microbeams based on modified couple stress theory. *International Journal of Engineering Science*, 97:98–112, 2015. 19

[44] A.E. Abouelregal and A.M. Zenkour. Thermoelastic problem of an axially moving microbeam subjected to an external transverse excitation. *Journal of Theoretical and Applied Mechanics*, 53(1):167–178, 2015. 19

[45] C. W. Lim, C. Li, and Ji Lin Yu. Dynamic behaviour of axially moving nanobeams based on nonlocal elasticity approach. *Acta Mechanica Sinica/Lixue Xuebao*, 26(5):755–765, 2010. 20

[46] Cheng Li. Size-dependent thermal behaviors of axially traveling nanobeams based on a strain gradient theory. *Structural Engineering and Mechanics*, 48(3):415–434, 2013. 20, 21

[47] J. J. Liu, C. Li, X. L. Fan, and L. H. Tong. Transverse free vibration and stability of axially moving nanoplates based on nonlocal elasticity theory. *Applied Mathematical Modelling*, 45:65–84, 2016. 21

[48] Jinjian Liu, Cheng Li, Changjin Yang, Jiping Shen, and Feng Xie. Dynamical responses and stabilities of axially moving nanoscale beams with time-dependent velocity using a nonlocal stress gradient theory. *JVC/Journal of Vibration and Control*, 23(20):3327–3344, 2017. 22

[49] Ali Mokhtari, Hamid Reza Mirdamadi, Mostafa Ghayour, and Vahid Sarvestan. Time/wave domain analysis for axially moving pre-stressed nanobeam by wavelet-based spectral element method. *International Journal of Mechanical Sciences*, 105:58–69, 2016. 22

[50] Song Guo, Yuming He, Dabiao Liu, Jian Lei, and Zhenkun Li. Dynamic transverse vibration characteristics and vibro-buckling analyses of axially moving and rotating nanobeams based on nonlocal strain gradient theory. *Microsystem Technologies*, 24(2):963–977, 2018. 23

[51] Mousa Rezaee and Saeed Lotfan. Non-linear nonlocal vibration and stability analysis of axially moving nanoscale beams with time-dependent velocity.

International Journal of Mechanical Sciences, 96-97(October):36–46, 2015. 23

[52] Keivan Kiani. Longitudinal, transverse, and torsional vibrations and stabilities of axially moving single-walled carbon nanotubes. *Current Applied Physics*, 13(8):1651–1660, 2013. 23

[53] Keivan Kiani. Longitudinal and transverse instabilities of moving nanoscale beam-like structures made of functionally graded materials. *Composite Structures*, 107:610–619, 2014. 24

[54] Song Guo, Yuming He, Dabiao Liu, Jian Lei, Lei Shen, and Zhenkun Li. Torsional vibration of carbon nanotube with axial velocity and velocity gradient effect. *International Journal of Mechanical Sciences*, 119:88–96, 2016. 24

[55] M. R. Ilkhani and S. H. Hosseini-Hashemi. Size dependent vibro-buckling of rotating beam based on modified couple stress theory. *Composite Structures*, 143:75–83, 2016. 25

[56] JP Shen, C Li, XL Fan, and CM Jung. Dynamics of silicon nanobeams with axial motion subjected to transverse and longitudinal loads considering nonlocal and surface effects. 2017. 26

[57] Erwin Kreyszig. Advanced Engineering Mathematics, 2006. 30

[58] Jerry H. Ginsberg. *Advanced engineering dynamics*. Cambridge university press, 2 edition, 1995. 31, 32, 35

[59] Harlan B. Palmer. The Capacitance of a Parallel-Plate Capacitor by the Schwartz-Christoffel Transformation. *Transactions of the American Institute of Electrical Engineers*, 56(3):363–366, 1937. 38

[60] Sheng-Jiaw Hwang. Supercritical stability of axially moving materials, 1991. 54

[61] G. Taylor. The coalescence of closely spaced drops when they are at different electric potentials. *Proceedings of the Royal Society A: Mathematical, Physical and Engineering Sciences*, 306(1487):423–434, 1968. 70

[62] Harvey C. Nathanson, William E. Newell, Robert A. Wickstrom, and John Ransford Davis. The Resonant Gate Transistor. *IEEE Transactions on Electron Devices*, ED-14(3):117–133, 1967. 70

[63] Elmer S. Hung and Stephen D. Senturia. Extending the travel range of analog-tuned electrostatic actuators. *Journal of Microelectromechanical Systems*, 8(4):497–505, 1999. 71

[64] Rob Legtenberg and Harrie A.C. Tilmans. Electrostatically driven vacuum-encapsulated polysilicon resonators Part I. Design and fabrication. *Sensors and Actuators: A. Physical*, 45(1):57–66, 1994. 71

[65] Clark T C Nguyen, Linda P B Katehi, and Gabriel M. Rebeiz. Micromachined devices for wireless communications. *Proceedings of the IEEE*, 86(8):1756–1767, 1998. 71

[66] Ali Hasan Nayfeh. *Nonlinear interactions: analytical, computational and experimental methods*. Wiley, 2000. 105

Appendices

Appendix A

Coefficients

A.1 Coefficients of Equations (6.18)–(6.25)

$$
\begin{aligned}
A_1 &= \Big[g_1^2\gamma^2 + \gamma^2 m^2\Big(\frac{1}{3} - \frac{1}{2\pi^2}\Big) + g_1\gamma^2 m\Big] - \frac{8}{3\pi}\Big(2\gamma g_1 + \gamma m\Big)q + \frac{3}{4}q^2 \\
B_1 &= c\Big[g_1^2\gamma^2 + \gamma^2 m^2\Big(\frac{1}{3} - \frac{1}{2\pi^2}\Big) + g_1\gamma^2 m\Big] - vm\gamma\Big[2\gamma g_1 + \gamma m\Big] \\
&\quad - \Big[\frac{8c}{3\pi}\Big(2\gamma g_1 + \gamma m\Big) - \frac{32}{9\pi}\gamma m v\Big]q + \frac{3}{4}cq^2 \\
C_1 &= \pi^4(\zeta+1)\Big[g_1^2\gamma^2 + \gamma^2 m^2\Big(\frac{1}{3} - \frac{1}{2\pi^2}\Big) + g_1\gamma^2 m\Big] \\
&\quad + \pi^2(P - v^2)\Big[g_1^2\gamma^2 + \gamma^2 m^2\Big(\frac{1}{3} - \frac{1}{2\pi^2}\Big) + g_1\gamma^2 m\Big] \\
&\quad + \beta\Big[V_{\mathrm{DC}} + V_{\mathrm{AC}}\ \cos(\Omega t)\Big]^2 \\
D_1 &= -\frac{8}{3}\pi^3(\zeta+1)\Big[2g_1\gamma + \gamma m\Big] - \frac{8}{3}\pi(P - v^2)\Big[2g_1\gamma + \gamma m\Big] \\
E_1 &= \frac{3}{4}\pi^4(\zeta+1) + \frac{3}{4}\pi^2(P - v^2) + \\
&\quad + \frac{1}{2}\alpha\pi^4\Big[g_1^2\gamma^2 + \gamma^2 m^2\Big(\frac{1}{3} - \frac{1}{2\pi^2}\Big) + g_1\gamma^2 m\Big] \\
F_1 &= -\frac{4}{3}\pi^3\alpha\Big[2g_1\gamma + \gamma m\Big] \\
G_1 &= \frac{3}{8}\pi^4\alpha \\
H_1 &= -\frac{2}{\pi}\Big[2 + \beta\Big(2\gamma g_1 + \gamma m\Big)\Big]\Big[V_{\mathrm{DC}} + V_{\mathrm{AC}}\ \cos(\Omega t)\Big]^2
\end{aligned}
\tag{A.1}
$$

$$
\begin{aligned}
A_2 &= \Big[g_1^2\gamma^2 + \gamma^2 m^2(\frac{1}{3} - \frac{1}{8\pi^2}) + g_1\gamma^2 m\Big] + \frac{4}{3\pi}\gamma m q + \frac{3}{4}q^2 \\
B_2 &= c\Big[g_1^2\gamma^2 + \gamma^2 m^2(\frac{1}{3} - \frac{1}{8\pi^2}) + g_1\gamma^2 m\Big] - vm\gamma\Big[2\gamma g_1 + \gamma m\Big] \\
&\quad + \frac{4c}{3\pi}\gamma m q + \frac{3c}{4}q^2 \\
C_2 &= 16\pi^4(\zeta+1)\Big[g_1^2\gamma^2 + \gamma^2 m^2(\frac{1}{3} - \frac{1}{8\pi^2}) + g_1\gamma^2 m\Big] \\
&\quad + 4\pi^2(P - v^2)\Big[g_1^2\gamma^2 + \gamma^2 m^2(\frac{1}{3} - \frac{1}{8\pi^2}) + g_1\gamma^2 m\Big] \\
&\quad + \beta\Big[V_{\mathrm{DC}} + V_{\mathrm{AC}}\ \cos(\Omega t)\Big]^2 \\
D_2 &= \frac{64}{3}\gamma m\pi^3(\zeta+1) + \frac{16}{3}\gamma m\pi(P - v^2) \\
E_2 &= 8\pi^4\alpha\Big[g_1^2\gamma^2 + \gamma^2 m^2\Big(\frac{1}{3} - \frac{1}{8\pi^2}\Big) + g_1\gamma^2 m\Big] \\
&\quad + 12\pi^4(\zeta+1) + 3\pi^2(P - v^2) \\
F_2 &= \frac{32}{3}\pi^3\gamma m\alpha \\
G_2 &= 6\pi^4\alpha \\
H_2 &= \frac{\gamma m}{\pi}\beta\Big[V_{\mathrm{DC}} + V_{\mathrm{AC}}\ \cos(\Omega t)\Big]^2
\end{aligned}
\tag{A.2}
$$

$$
\begin{aligned}
A_3 &= \Big[g_1^2\gamma^2 + \gamma^2 m^2(\frac{1}{3} - \frac{1}{18\pi^2}) + g_1\gamma^2 m\Big] - \frac{8}{9\pi}\Big[2\gamma g_1 + \gamma m\Big]q + \frac{3}{4}q^2 \\
B_3 &= c\Big[g_1^2\gamma^2 + \gamma^2 m^2(\frac{1}{3} - \frac{1}{18\pi^2}) + g_1\gamma^2 m\Big] - vm\gamma\Big[2\gamma g_1 + \gamma m\Big] \\
&\quad - \Big[\frac{8c}{9\pi}\Big(2\gamma g_1 + \gamma m\Big) - \frac{32}{27\pi}\gamma m v\Big]q + \frac{3c}{4}q^2 \\
C_3 &= 81\pi^4(\zeta+1)\Big[g_1^2\gamma^2 + \gamma^2 m^2(\frac{1}{3} - \frac{1}{18\pi^2}) + g_1\gamma^2 m\Big] \\
&\quad + 9\pi^2(P - v^2)\Big[g_1^2\gamma^2 + \gamma^2 m^2(\frac{1}{3} - \frac{1}{18\pi^2}) + g_1\gamma^2 m\Big] \\
&\quad + \beta\Big[V_{\rm DC} + V_{\rm AC}\ \cos(\Omega t)\Big]^2 \\
D_3 &= -72\pi^3(\zeta+1)\Big[2\gamma g_1 + \gamma m\Big] - 8\pi(P - v^2)\Big[2\gamma g_1 + \gamma m\Big] \\
E_3 &= \frac{243}{4}\pi^4(\zeta+1) + \frac{27}{4}\pi^2(P - v^2) \\
&\quad + \frac{81}{2}\pi^4\alpha\Big[g_1^2\gamma^2 + \gamma^2 m^2(\frac{1}{3} - \frac{1}{18\pi^2}) + g_1\gamma^2 m\Big] \\
F_3 &= -36\pi^3\alpha\Big[2\gamma g_1 + \gamma m\Big] \\
G_3 &= \frac{243}{8}\pi^4\alpha \\
H_3 &= -\frac{2}{3\pi}\Big[2 + \beta\Big(2\gamma g_1 + \gamma m\Big)\Big]\Big[V_{\rm DC} + V_{\rm AC}\ \cos(\Omega t)\Big]^2
\end{aligned}
\tag{A.3}
$$

$$
\begin{aligned}
A_4 &= \Big[g_1^2\gamma^2 + \gamma^2 m^2(\frac{1}{3} - \frac{1}{32\pi^2}) + g_1\gamma^2 m\Big] + \frac{2}{3\pi}\gamma m q + \frac{3}{4}q^2 \\
B_4 &= c\Big[g_1^2\gamma^2 + \gamma^2 m^2(\frac{1}{3} - \frac{1}{32\pi^2}) + g_1\gamma^2 m\Big] - vm\gamma\Big[2\gamma g_1 + \gamma m\Big] \\
&\quad + \frac{2c}{3\pi}\gamma m q + \frac{3c}{4}q^2 \\
C_4 &= 256\pi^4(\zeta+1)\Big[g_1^2\gamma^2 + \gamma^2 m^2(\frac{1}{3} - \frac{1}{32\pi^2}) + g_1\gamma^2 m\Big] \\
&\quad + 16\pi^2(P - v^2)\Big[g_1^2\gamma^2 + \gamma^2 m^2(\frac{1}{3} - \frac{1}{32\pi^2}) + g_1\gamma^2 m\Big] \\
&\quad + \beta\Big[V_{\mathrm{DC}} + V_{\mathrm{AC}}\ \cos(\Omega t)\Big]^2 \\
D_4 &= \frac{512}{3}\gamma m\pi^3(\zeta+1) + \frac{32}{3}\gamma m\pi(P - v^2) \\
E_4 &= 192\pi^4(\zeta+1) + 12\pi^2(P - v^2) \\
&\quad + 128\pi^4\alpha\Big[g_1^2\gamma^2 + \gamma^2 m^2\Big(\frac{1}{3} - \frac{1}{32\pi^2}\Big) + g_1\gamma^2 m\Big] \\
F_4 &= \frac{256}{3}\pi^3\gamma m\alpha \\
G_4 &= 96\pi^4\alpha \\
H_4 &= \frac{\gamma m}{2\pi}\beta\Big[V_{\mathrm{DC}} + V_{\mathrm{AC}}\ \cos(\Omega t)\Big]^2
\end{aligned}
\tag{A.4}
$$

Vitae

Name: Mustafa Tahir Al Shaqaq

Nationality: Saudi

Date of Birth: 19/03/1992

Email: *alshaqaq.mustafa@gmail.com*

Permanent Address: Dammam 32433, Kingdom of Saudi Arabia

Academic Background:

- M.Sc. Mechanical Engineering: King Fahd University of Petroleum & Minerals (KFUPM), Dhahran, Saudi Arabia 2018
- B.S Mechanical Engineering King Fahd University of Petroleum & Minerals (KFUPM), Dhahran, Saudi Arabia 2015

Research Interests: Robotics, system dynamics and control, vibration and mechatronics.